2006

The ACS Virgo Cluster Survey. VIII. the Nuclei of Early-Type Galaxies

Patrick Côté
National Research Council of Canada

Slawomir Piatek
New Jersey Institute of Technology

Laura Ferrarese
National Research Council of Canada

Andrés Jordán
Oxford University

David Merritt
Rochester Institute of Technology

See next page for additional authors

Accepted for publication in the *Astrophysical Journal Supplement Series.*
Preprint typeset using LaTeX style emulateapj v. 10/10/03

THE ACS VIRGO CLUSTER SURVEY. VIII. THE NUCLEI OF EARLY-TYPE GALAXIES[1]

Patrick Côté[2], Slawomir Piatek[3], Laura Ferrarese[2], Andrés Jordán[4,5], David Merritt[6], Eric W. Peng[2], Monica Haşegan[7,8], John P. Blakeslee[9,10], Simona Mei[9], Michael J. West[11], Miloš Milosavljević[12,13], John L. Tonry[14]

Accepted for publication in the Astrophysical Journal Supplement Series.

ABSTRACT

The ACS Virgo Cluster Survey is a *Hubble Space Telescope* program to obtain high-resolution imaging, in widely separated bandpasses (F475W $\approx g$ and F850LP $\approx z$), for 100 early-type members of the Virgo Cluster, spanning a range of ≈ 460 in blue luminosity. We use this large, homogenous dataset to examine the innermost structure of these galaxies and to characterize the properties of their compact central nuclei. We present a sharp upward revision in the frequency of nucleation in early-type galaxies brighter than $M_B \approx -15$ ($66 \lesssim f_n \lesssim 82\%$) and show that ground-based surveys underestimated the number of nuclei due to surface brightness selection effects, limited sensitivity and poor spatial resolution. We speculate that previously reported claims that nucleated dwarfs are more concentrated to the center of Virgo than their non-nucleated counterparts may be an artifact of these selection effects. There is no clear evidence from the properties of the nuclei, or from the overall incidence of nucleation, for a change at $M_B \sim -17.6$, the traditional dividing point between dwarf and giant galaxies. There *does*, however, appear to be a fundamental transition at $M_B \sim -20.5$, in the sense that the brighter, "core-Sérsic" galaxies lack resolved (stellar) nuclei. A search for nuclei which may be offset from the photocenters of their host galaxies reveals only five candidates with displacements of more than $0\farcs5$, all of which are in dwarf galaxies. In each case, though, the evidence suggests that these "nuclei" are, in fact, globular clusters projected close to the galaxy photocenter. Working from a sample of 51 galaxies with prominent nuclei, we find a median half-light radius of $\langle r_h \rangle = 4.2$ pc, with the sizes of individual nuclei ranging from 62 pc down to ≤ 2 pc (i.e., unresolved in our images) in about a half dozen cases. Excluding these unresolved objects, the nuclei sizes are found to depend on nuclear luminosity according to the relation $r_h \propto \mathcal{L}^{0.50\pm0.03}$. Because the large majority of nuclei are resolved, we can rule out low-level AGN as an explanation for the central luminosity excess in almost all cases. On average, the nuclei are ≈ 3.5 mag brighter than a typical globular cluster. Based on their broadband colors, the nuclei appear to have old to intermediate-age stellar populations. The colors of the nuclei in galaxies fainter than $M_B \approx -17.6$ are tightly correlated with their luminosities, and less so with the luminosities of their host galaxies, suggesting that their chemical enrichment histories were governed by local or internal factors. Comparing the nuclei to the "nuclear clusters" found in late-type spiral galaxies reveals a close match in terms of size, luminosity and overall frequency. A formation mechanism that is rather insensitive to the detailed properties of the host galaxy is required to explain this ubiquity and homogeneity. The mean of the frequency function for the nucleus-to-galaxy luminosity ratio in our nucleated galaxies, $\langle \log_{10} \eta \rangle = -2.49 \pm 0.09$ dex ($\sigma = 0.59 \pm 0.10$), is indistinguishable from that of the SBH-to-bulge mass ratio, $\langle \log_{10} (\mathcal{M}_\bullet / \mathcal{M}_{gal}) \rangle = -2.61 \pm 0.07$ dex ($\sigma = 0.45 \pm 0.09$), calculated in 23 early-type galaxies with detected supermassive black holes (SBHs). We argue that the compact stellar nuclei found in many of our program galaxies are the low-mass counterparts of the SBHs detected in the bright galaxies. If this interpretation is correct, then one should think in terms of *Central Massive Objects* — either SBHs or compact stellar nuclei — that accompany the formation of almost all early-type galaxies and contain a mean fraction $\approx 0.3\%$ of the total bulge mass. In this view, SBHs would be the dominant formation mode above $M_B \approx -20.5$.

Subject headings: galaxies: clusters: individual (Virgo)–galaxies: elliptical and lenticular–galaxies: nuclei–galaxies: structure

[1] Based on observations with the NASA/ESA *Hubble Space Telescope* obtained at the Space Telescope Science Institute, which is operated by the association of Universities for Research in Astronomy, Inc., under NASA contract NAS 5-26555.

[2] Herzberg Institute of Astrophysics, National Research Council of Canada, 5071 West Saanich Road, Victoria, BC, V8X 4M6, Canada; patrick.cote@nrc-cnrc.gc.ca; laura.ferrarese@nrc-cnrc.gc.ca; eric.peng@nrc-cnrc.gc.ca

[3] Department of Physics, New Jersey Institute of Technology, Newark, NJ 07102; piatek@physics.rutgers.edu

[4] European Southern Observatory, Karl-Schwarzschild-Str. 2, 85748 Garching, Germany; ajordan@eso.org

[5] Astrophysics, Denys Wilkinson Building, University of Oxford, 1 Keble Road, Oxford, OX1 3RH, UK

[6] Department of Physics, Rochester Institute of Technology, 84 Lomb Memorial Drive, Rochester, NY 14623; merritt@astro.rit.edu

[7] Department of Physics and Astronomy, Rutgers University, New Brunswick, NJ 08854; mhasegan@physics.rutgers.edu

[8] Institute for Space Sciences, P.O.Box MG-23, Ro 77125, Bucharest-Magurele, Romania

[9] Department of Physics and Astronomy, The Johns Hopkins University, 3400 North Charles Street, Baltimore, MD 21218-2686; smei@pha.jhu.edu

[10] Department of Physics, Washington State University, Webster Hall 1245, Pullman, WA 99164-2814; jblakes@wsu.edu

[11] Department of Physics and Astronomy, University of Hawaii,

1. INTRODUCTION

Early-type galaxies are found in virtually all environments — from the field, to small groups, to rich clusters (Hubble & Humason 1931; Oemler 1974; Dressler 1980). In the highest density environments, ellipticals and lenticulars are known to dominate the overall fraction of bright galaxies, $f_{\rm E+S0} \sim 0.4 - 0.9$, with the precise contribution depending on local galaxy density and redshift (Smith et al. 2004; Postman et al. 2005). In the Virgo Cluster, the rich cluster nearest to our own Galaxy, $f_{\rm E+S0} \approx 0.44$ for galaxies brighter than $B \lesssim 13$ or $M_B \lesssim -18.1$ (Julian et al. 1997).[15] If one considers not just giant galaxies, but also the much more common dwarfs, then the dominance of early-type galaxies is even more pronounced: i.e., among the confirmed members of Virgo with unambiguous morphological classifications, the early-type fraction is ≈ 0.8 (Reaves 1983; Binggeli, Tammann & Sandage 1987, hereafter BTS87).

It has long been recognized that early-type galaxies, both in Virgo and elsewhere, often show compact nuclei near their centers. In their landmark study of the Virgo Cluster, BTS87 carried out a visual search for nuclei using wide-field, blue-sensitive photographic plates from the 2.5-m du Pont telescope. Of the 1277 members and 574 probable members in their Virgo Cluster Catalog (hereafter VCC), a total of 1192 were classified as non-nucleated dwarfs (dEs or dS0s) while an additional 415 dwarfs (predominantly dE,Ns) were found to be nucleated. Thus, roughly 25% of the dwarf galaxies in Virgo were found by BTS87 to have a discernible nucleus, although the precise fraction was also found to depend on galaxy luminosity and position within the cluster (see Figure 8 of Sandage, Binggeli & Tammann 1985 and Figure 19 of BTS87, respectively). Unfortunately, progress toward understanding the nature of these nuclei has been limited because of several factors: *e.g.*, ground-based studies must contend with the contamination from the underlying galaxy light, it is difficult to de-couple the brightness profiles of the nuclei from those of their host galaxies, and the nuclei are sufficiently compact that they appear unresolved in even the sharpest ground-based images (Caldwell 1983, 1987; Durrell 1997).

While the photographic survey of BTS87 remains a landmark study of nucleated galaxies in the local universe, there are reasons to believe that a modern survey of the nuclei belonging to early-type galaxies would be advisable — preferably one which capitalizes on the high angular resolution afforded by the *Hubble Space Telescope* (*HST*). First, *HST* imaging of late-type galaxies has revealed that 50–70% of these systems have compact stellar clusters at or near their photocenters (Phillips et al. 1996; Carollo, Stiavelli & Mack 1998; Matthews et al 1999; Böker et al. 2002; Böker et al. 2004). Second, if the early-type members of the Local Group are any guide, then one may expect estimates for the fraction of nucleated galaxies to increase as better imaging becomes available. For instance, in recent years a number of Local Group dwarfs have been found to contain previously unrecognized central substructures and/or nuclei, including Sagittarius (Layden & Sarajedini 2000; Monaco et al. 2005), Ursa Minor (Kleyna et al. 2003; Palma et al. 2003), Andromeda II (McConnachie & Irwin 2006) and Fornax (Coleman et al. 2004). Third, in their WFPC2 survey of dwarfs in the Virgo and Fornax Clusters, Lotz et al. (2004) found that six of the 30 "non-nucleated" dwarf ellipticals in their sample actually contained nuclei which had gone unnoticed in the ground-based surveys (Binggeli, Tammann & Sandage 1985, hereafter BTS85; BTS87; Ferguson 1989). Very recently, Grant, Kuipers & Phillipps (2005) used imaging from the Wide Field Camera on the Isaac Newton Telescope to show that faint nuclei in Virgo dwarfs were frequently missed in photographic surveys.

These results suggest that there may be significant incompleteness in our census of nuclei in early-type galaxies. Indeed, in their photographic study of Virgo, BTS87 cautioned that "most nuclei in the luminous E and S0 galaxies were probably missed due to [the] high surface brightness [of the underlying galaxy.]" In addition to this surface-brightness selection effect, BTS87 state explicitly that any nuclei with $B \gtrsim 23$ ($M_B \gtrsim -8$) would fall below their plate detection limits and hence be missing from their catalog.

The central regions of early-type galaxies have been favorite targets for *HST* since its launch in 1990. For the most part, such surveys have tended to focus on the core structure of the galaxies. However, several studies reported the discovery of compact nuclei in (predominantly bright) samples of early-type galaxies, beginning with pre-refurbishment (WFPC) imaging (Crane et al. 1993; Lauer et al. 1995) and continuing with imaging from WFPC2 (Rest et al. 2001; Lauer et al. 2005) and NICMOS (Ravindranath et al. 2001). These studies, which are primarily based on single-filter imaging of samples of (33–77) galaxies with distances between 1 and 100 Mpc, have confirmed that some early-type galaxies do contain compact nuclei, but there is disagreement over their overall frequency (with estimates ranging from 13% to $\approx$ 50%), whether or not they are resolved structures, and their classification as stellar or non-thermal (AGN) sources. A better understanding of the physical properties of these nuclei is important since they almost certainly hold clues to the violent processes that have shaped the central regions of galaxies, which could include star formation triggered by infalling gas, collisions and mergers of stars and star clusters, tidal disruption of clusters and the growth of stellar "cusps" by central black holes, and the mechanical and radiative feedback from accreting black holes or intense nuclear starbusts.

This paper presents a homogenous analysis of the nuclei belonging to a sample of 100 early-type galaxies in the Virgo Cluster. Our images, taken with the Advanced Camera for Surveys (ACS; Ford et al. 1998), form the basis of the ACS Virgo Cluster Survey (ACSVCS; Côté et al. 2004; hereafter Paper I). Other papers in this series have discussed the data reduction pipeline (Jordán et al. 2004a = Paper II), the connection between low-mass X-ray binaries in M87 (Jordán et al. 2004b = Paper III),

Hilo, HI 96720; westm@hawaii.edu
[12] Theoretical Astrophysics, California Institute of Technology, Mail Stop 130-33, Pasadena, CA 91125; milos@tapir.caltech.edu
[13] Sherman M. Fairchild Fellow
[14] Institute for Astronomy, University of Hawaii, 2680 Woodlawn Drive, Honolulu, HI 96822; jt@ifa.hawaii.edu
[15] Throughout this paper, we adopt a Virgo distance modulus of $(m - M)_0 = 31.09$ mag (Tonry et al. 2001; Mei et al. 2005b).

the measurement and calibration of surface brightness fluctuation magnitudes (Mei et al. 2005ab = Papers IV and V), the morphology, isophotal parameters and surface brightness profiles for early-type galaxies (Ferrarese et al. 2006a = Paper VI), the connection between globular clusters and ultra-compact dwarf galaxies (Haşegan et al. 2005 = Paper VII), the color distributions of globular clusters (Peng et al. 2006a = Paper IX), the half light radii of globular clusters and their use as a distance indicator (Jordán et al. 2006 = Paper X) and the discovery of diffuse star clusters in early-type galaxies (Peng et al. 2006b = Paper XI).

There are several features of the ACS Virgo Cluster Survey which make it uniquely suited to the study of nuclei in early-type galaxies. First, the survey itself targets a large sample of 100 early-type galaxies lying at a common distance of about 16.5 Mpc so that the $\approx 0\farcs1$ FWHM of the ACS point-spread function (PSF) corresponds to a small, and nearly constant, physical scale of ≈ 8 pc. This excellent spatial resolution, coupled with the fine plate scale of $0\farcs049$ pix^{-1}, makes it possible to measure structural parameters for any nuclei larger than a few parsecs in size. Second, with blue magnitudes in the range $9.31 \lesssim B_T \lesssim 15.97$ ($-21.88 \lesssim M_B \lesssim -15.21$), our program galaxies span a wide range in luminosity so it is possible to study the phenomenon of nucleation in giant and dwarf galaxies simultaneously. Third, the images are sufficiently deep that they reveal not only the nuclei, but also the many globular clusters belonging to our program galaxies; thus, the same images which provide information on the nucleus and host galaxy can also be used to study the associated globular cluster systems and to explore possible evolutionary links between the clusters and nuclei. And finally, because multi-band imaging is available in two widely-separated bandpasses (F475W and F850LP) for each object in the survey, it is possible to use broadband colors to place rough constraints on the star formation and chemical enrichment histories of the nuclei and their host galaxies.

The organization of this article is as follows. §2 gives a brief summary of the observational material used in our analysis. A description of the galaxy brightness profiles and the method of their analysis is presented in §3. §4 contains a discussion of the empirical properties of the nuclei in our survey, such as their overall numbers, possible displacements from the galaxy photocenters, luminosities, colors, surface brightnesses and half-light radii. In §5 we discuss the implications of our findings for various formation scenarios. The article concludes with a summary of the main results in §6. A future paper in this series will discuss the broader implications of our findings for models of nucleus formation in early-type galaxies (Merritt et al. 2006).

2. OBSERVATIONS AND DATA REDUCTIONS

Our analysis is based on *HST* imaging for 100 early-type galaxies having morphological types E, S0, dE, dE,N and dS0. All are confirmed members of the Virgo Cluster based on radial velocity measurements. Images were taken with the ACS instrument used in Wide Field Channel (WFC) mode with the F475W and F850LP filter combination, which are roughly equivalent to the g and z bands, respectively, in the Sloan Digital Sky Survey photometric system. These images form the basis of the ACS Virgo Cluster Survey, a complete description of which may be found in Paper I. Note that the 26 brightest galaxies in this survey constitute a complete sample of early-type members of Virgo with $B_T \leq 12.15$, and that the full sample represents 44% of all early-type members of Virgo spanning the magnitude range $9.3 \lesssim B_T \lesssim 16$. A customized data pipeline (described in detail in Paper II) produces geometrically-corrected, flux-calibrated, cosmic-ray-free images in the F475W and F850LP bandpasses.

Table 1 gives some basic information about the target galaxies, tabulated in order of increasing blue magnitude (decreasing luminosity). An identification number for each galaxy is given in the first column, followed by the identification from the VCC (BST85) and other names for the galaxy in the Messier, NGC, UGC or IC catlogs. Blue magnitudes, B_T, from BST85 are presented in column 4, while the fifth column records the adopted Galactic reddening from Schlegel, Finkbeiner & Davis (1998). Columns 6 and 7 record the surface brightness of each galaxy, in both the g and z bandpasses, measured via spline interpolation at a geometric mean radius[16] of $r = 1''$ (≈ 80 pc). This model-independent choice of surface brightness should closely approximate the galaxy's *central* surface brightness, but is measured at a radius large enough to ensure negligible contamination from any central nucleus.

The remaining columns of Table 1 will be described below. Coordinates, morphological classifications and other information on the program galaxies may be found in Papers I and VI.

3. ANALYSIS

Our goals in this paper include the measurement of the structural and photometric properties of the nuclei in our program galaxies, and an investigation into the relationship between these nuclei and their host galaxies. Additionally, we wish to compare the properties of the nuclei to those of the globular clusters in the program galaxies and, more generally, to the Virgo ultra-compact dwarf (UCD) galaxies (e.g., Drinkwater et al. 1999; Hilker et al. 1999; Drinkwater et al. 2000; Phillipps et al. 2001) identified in the course of this survey and described in Haşegan et al. (2005; hereafter Paper VII) and Haşegan et al. (2006). A companion paper in this series (Paper VI) presents an analysis of the surface brightness profiles of the program galaxies along with a tabulation of the best-fit structural parameters, while two other articles examine the photometric (Paper IX) and structural (Paper X) parameters of the globular clusters. As we make use of several results from these studies, the reader is referred to these papers for complete details.

3.1. *Parameterization of the Surface Brightness Profiles*

Because the nuclei are always superimposed on the light of the underlying galaxy, measuring their photometric and structural properties requires a model for the galaxy surface brightness profile. For each galaxy

[16] The geometric mean radius is defined as $r \equiv a\sqrt{(1-\epsilon)}$ where a is the semi-major axis and ϵ is the ellipticity.

in our survey, g- and z-band azimuthally-averaged radial surface brightness profiles are available from Paper VI. These profiles were derived by fitting the isophotes with the ELLIPSE task in IRAF which, in turn, is based on the algorithm of Jedrzejewski (1987). The g- and z-band brightness profiles were parameterized with a standard Sérsic (1968) model,

$$I_g(r) \;=\; I_0 \exp[-b_n(r/r_e)^{1/n}], \qquad (1)$$

where I_0 is the central intensity and n is a shape parameter which yields an $R^{1/4}$-law profile for $n = 4$ (de Vaucouleurs 1948) and an exponential profile for $n = 1$. The parameter b_n is defined such that $\Gamma(2n) = 2\Gamma_1(2n, b_n)$, where Γ and Γ_1 are the complete and incomplete gamma functions, respectively (e.g., Graham & Driver 2005). As shown by Caon, Capaccioli & D'Onofrio (1993), a convenient approximation relating b_n to the shape parameter n is $b_n \approx 1.9992n - 0.3271$ for $1 \lesssim n \lesssim 10$. Given this definition of b_n, r_e is the effective radius of the galaxy.

The g- and z-band brightness profiles for each galaxy were also fit with a "core-Sérsic" model,

$$I(r) = I'\left[1 + \left(\frac{r_b}{r}\right)^{\alpha}\right]^{\gamma/\alpha} \exp\left[-b_n\left(\frac{r^{\alpha}+r_b^{\alpha}}{r_e^{\alpha}}\right)^{1/(\alpha n)}\right], \qquad (2)$$

where

$$I' = I_b 2^{-\gamma/\alpha} \exp\left[b_n\left(2^{1/\alpha} r_b/r_e\right)^{1/n}\right] \qquad (3)$$

This model, which was first proposed by Graham et al. (2003), consists of a power-law component in the inner region of a galaxy, which "breaks" to a traditional Sèrsic profile beyond some radius, r_b. The model has a total of six free parameters: the logarithmic slope of the inner power-law (γ); the shape of the Sérsic function (n); the break radius (r_b); the effective half-light radius of the Sérsic profile (r_e); the intensity at the break radius (I_b) and a parameter (α) which governs the sharpness of the transition between the inner power law and the outer Sérsic function. After some experimentation, it was decided to use the modified parametrization of Trujillo et al. (2004),

$$I_g(r) = I_b\Big[(r_b/r)^{\gamma} u(r_b - r) + \\ + e^{b_n(r_b/r_e)^{1/n}} e^{-b_n(r/r_e)^{1/n}} u(r - r_b)\Big] \qquad (4)$$

in which $\alpha \to \infty$ and $u(x - z)$ is the Heaviside step function. This model produced more stable fits, with better consistency between the five remaining parameters (I_b, γ, n, r_e and r_b) measured in the g and z bandpasses.

Equations (1) and (4) are intended to describe the profiles of galaxies which have no central nucleus. However, it is obvious that many galaxies in our sample do indeed have compact sources at or near their centers. For such nucleated galaxies, a single-component King model (Michie 1963; King 1966) was used to represent this central component. This introduces three additional parameters to the fit: the total intensity of the nucleus (I); the projected half-light radius (r_h); and the King concentration index (c). In other words, for *nucleated galaxies*, the fitted model, $I(r)$, takes the form

$$I(r) \;=\; I_g(r) + I_k(r), \qquad (5)$$

where $I_g(r)$ is either a pure Sérsic model (Equation 1) or a core-Sérsic model (Equation 4), depending on the galaxy in question, and $I_k(r)$ is the central King model component. For non-nucleated galaxies, the profiles are fit simply with models of the form of Equations (1) or (4). A detailed justification for the choice of galaxy model (i.e., Sérsic vs. core-Sérsic) is given on a case-by-case basis in Paper VI. We adopt these classifications verbatim, with the exception of three intermediate-luminosity galaxies: VCC543 (UGC7436), VCC1528 (IC3501) and VCC1695 (IC3586).[17] While the *global* brightness profiles of these galaxies are adequately represented by Sérsic models, such models overpredict the amount of galaxy light on subarcsecond scales. For the purposes of measuring photometric and structural properties for the nuclei in these galaxies, we parameterize the galaxy profiles with core-Sérsic models in all three cases.

We note that the definition of a "nucleus" invariably hinges on some assumption — explicit or otherwise — about the intrinsic brightness profile of the host galaxy. Our study is no exception in this regard. Choices for the galaxy profiles made by previous workers have included King models (Binggeli & Cameron 1993), pure exponentials (Binggeli & Cameron 1993; Stiavelli et al. 2001), Nuker laws (Rest et al. 2001; Ravindranath et al. 2001; Lauer et al. 2005) and Sersic profiles (Durrell 1997; Stiavelli et al. 2001). After considerable experimentation (Paper IV), we opted to use the family of models represented by Equations (1) and (2) because they have the great advantage they are flexible enough to provide accurate fits to the brightness profiles of both giant and dwarf galaxies (see Paper VI). The use of a single (Sérsic) model to describe the full sample of galaxies also seems advisable in light of mounting evidence that, at least in terms of their *structural parameters*, the longstanding perception of a fundamental dichotomy between giant and dwarf ellipticals (e.g., Kormendy 1985) may be incorrect (see, e.g., Jerjen & Binggeli 1997; Graham & Guzman 2003; Paper VI). From a theoretical perspective, the choice of Equations (1) and (4) also seems reasonable given recent findings that the Sérsic law provides an accurate representation of the spatial and surface density profiles of dark matter halos in high-resolution ΛCDM simulations (Navarro et al. 2004; Merritt et al. 2005).

At the same time, our decision to parameterize the central nuclei with King models is motivated by high-resolution observations of the nuclei in nearby galaxies. In nucleated Local Group galaxies such as NGC205 and Sagittarius, King models are found to provide accurate representations of the central components (e.g., Djorgovski et al. 1992; Butler & Martínez-Delgado 2005; Monaco et al. 2005). Nevertheless, for galaxies at the distance of the Virgo Cluster, we are working close to the limits of resolvability, so we caution that our choice of King models to parameterize the central components may not be unique, particularly for faint nuclei in the highest surface brightness galaxies. Alternative parameterizations of the central brightness "cusps" in our sample galaxies will be

[17] Note that $r_b >> r_h$ for all nucleated (Type Ia) core-Sérsic galaxies; $\langle r_b/r_h \rangle = 74$ for the four galaxies in this category.

explored in a future paper in this series (Merritt et al. 2006).

3.2. *Choice of Drizzling Kernel, PSF Determination and Fitting Procedure*

As described in Paper II, our analysis of the nuclei, brightness profiles, and isophotal structure of the galaxies is based on F475W and F850LP images in which a *Gaussian* kernel is used to distribute flux onto the output (drizzled) images. This choice of kernel has the advantage that, relative to *Lanczos3* kernel, bad pixels can be repaired more effectively, albeit with the penalty of a slight reduction in angular resolution.[18] Due to the compact nature of the nuclei (even the most extended objects have effective radii $\lesssim 1''$), it is important that the effects of the PSF are taken into account when fitting models to the observed brightness profiles.

PSFs in the F475W and F850LP filters, varying quadratically with CCD position, were derived using DAOPHOT II as described in Paper II. Briefly, archival images of the Galactic globular cluster NGC104 (47 Tucanae) taken during programs G0-9656 and GO-9018 were used to construct empirical PSFs in the two bandpasses. These archival images were drizzled in the same manner as the images for the program galaxies. A total of ≈ 200 stars in each filter were used to construct the PSFs, which extend to a radius of $0\farcs5$ in both bandpasses. To follow the behavior of the PSFs to still larger radii, we matched our empirical PSFs at a radius of $0\farcs3$ to those measured for high-S/N composite stars by Sirianni et al. (2005). These latter PSFs extend to radii of $3''$, and were constructed from images of 47 Tuc fields taken as part of the photometric calibration of ACS. Figure 1 shows azimuthally averaged PSFs for the F475W and F850LP filters measured at the position of the nucleus in VCC1303 (NGC4483) — the program galaxy whose center is nearest to the mean position for the full sample of program galaxies.

A χ^2 minimization scheme was used to find the models which best fit the azimuthally-averaged, one-dimensional intensity profiles for each galaxy. Minimizations were carried out using the `Minuit` package in the CERN program library; initial determinations of the minima, obtained using a Simplex minimization algorithm (Nelder & Mead 1965), were later refined using a variable metric method with inexact line search (MIGRAD). Following Byun et al. (1996), all points in the profile were assigned equal weight. For both nucleated and non-nucleated galaxies, the PSFs at the location of the galaxy's center were convolved with the models before fitting to the intensity profiles. Customized PSFs were created for each galaxy in the survey, centered at the exact (sub-pixel) location of the nucleus. While, in practice, the PSF convolution has little impact on the fitted Sérsic or core-Sérsic model parameters, with the exception of γ, this step is critically important when evaluating accurate structural parameters for the central nucleus.

[18] Using the *Lanczos3* kernel produces images with better noise characteristics and a somewhat sharper PSF ($0\farcs09$ versus $0\farcs1$), so this kernel was used for both the surface brightness fluctuation measurements and the determination of the globular cluster photometric and structural parameters.

Profile fits are carried out independently in the two bandpasses, with the exception of the 11 nucleated galaxies brighter than $B_T = 13.5$ (i.e., Type Ia galaxies; see §4). Our numerical experiments suggest that in this high surface brightness regime, the profile of the underlying galaxy makes the measurement of nuclei half-light radii and total magnitudes extremely challenging (see Appendix A). For these galaxies, the composite g- and z-band profiles were first fitted simultaneously and the individual fits constrained so that the galaxy shape index parameter, nucleus concentration index and half-light radius were the same in the two bandpasses. When dust is present (see below), the models are fitted to the dust-corrected surface brightness profiles if $\geq 50\%$ of the points along a given isophote are affected; otherwise the dust affected regions are masked. More details on the correction for dust obscuration are given in Paper VI.

Sufficiently compact nuclei will appear unresolved even in our ACS images. To estimate the resolution limit of our observations, we constructed brightness profiles for a number of likely stars which appear in our images. These candidate stars were classified as unresolved in the object catalogs produced by KINGPHOT, the reduction package used to measure structural and photometric parameters for the globular clusters in these fields (see Papers II and X). Fitting King models to the brightness profiles of these objects gives median half-light radii of $0\farcs011\pm0\farcs004$ and $0\farcs018\pm0\farcs005$ in the F475W and F850LP bandpasses, respectively. As an additional test, we may make use of the fact that VCC1316 (M87 = NGC4486), one of the AGN galaxies in our survey (see below), contains a prominent non-thermal central point source. Although this source is saturated in our F475W images, a King model fitted to the central source in the z-band brightness profile gives $r_h = 0\farcs021$. In what follows, we adopt a conservative upper limit of $0\farcs025 \approx 2$ pc for the resolution limit in both bandpasses.

Before proceeding, we pause to demonstrate that the vast majority of the nuclei belonging to our program galaxies are indeed more extended than point sources. In Figure 2, we show g-band surface brightness profiles for a representative sample of nine nucleated galaxies, chosen to span the full range in fitted half-light radius (with $\langle r_h \rangle$ decreasing from left to right and from top to bottom). In each panel, the red curves show the results of fitting the nuclear component with a King model, while the blue curves show the results of fitting a central point source; residuals from both fits are shown in the lower panel. With the exception of VCC1528 (IC3501), the central nucleus is resolved for all of the galaxies in Figure 2. In total, six galaxies in our sample — VCC1883 (NGC4612), VCC140 (IC3065), VCC1528, VCC1695 (IC3586), VCC1895 (UGC7854) and VCC1826 (IC3633) — have best-fit half-light radii, measured in at least one bandpasses, that fall below our nominal resolution limit of $0\farcs025$. These half-light radii are given in parantheses in Table 1. They have been included in the following analysis, but we caution that they are formally unresolved in our ACS images. We shall return to the issue of these compact nuclei in §5.2. Additional tests on the resolution limits, possible biases in the derived photometric and structural parameters, and a discussion of measurement errors, are given in §4.1 and Appendix A.

4. RESULTS

As many as eighteen of the 100 galaxies in Table 1 show evidence for dust — either as isolated patches and filaments, or in the form of disks having varying degrees of regularity (see Paper VI). For the most part, this dust has no impact on the identification of possible nuclei. However, for four galaxies in our sample (i.e., VCC1535 = NGC4526, VCC1030 = NGC4435, VCC685 = NGC4350 and VCC571) the central dust obscuration is severe enough to make a reliable classification of these galaxies as nucleated or non-nucleated impossible. Moreover, for VCC1535 and VCC1030, both of which harbour massive, kpc-scale dust disks, the surface brightness profiles are themselves so limited that it is not even possible to place the galaxies in the appropriate Sérsic or core-Sérsic categories.

In general, the census of active galactic nuclei (AGN) in intrinsically faint galaxies — and in the ACS Virgo Cluster Survey galaxies in particular — is far from complete. However, two of the brighter galaxies in our sample (VCC1316 = NGC4486, M87, 3C 274 and VCC763 = NGC4374, M84, 3C 272.1) are known to host AGNs with strongly non-thermal spectral energy distributions (e.g., Wrobel 1991; Ho 1999; Chiaberge, Capetti & Celotti 1999). In both cases, the unresolved non-thermal nucleus is clearly seen in the ACS images; in neither instance, however, does there appear to be a resolved stellar nucleus. A third galaxy (VCC1619 = NGC4550), is classified as a LINER by Ho et al. (1997). This galaxy contains some dust within the central $\sim 25''$, but there is clear evidence for a resolved stellar nucleus.

Wrobel (1991) detected nuclear radio emission in three other galaxies in our survey (VCC1226 = NGC4472, M49; VCC1632 = NGC4552, M89; and VCC1978 = NGC4649, M60). In both VCC1226 and VCC1632, the innermost $\sim 1''$ are slightly obscured by dust (see Paper VI), but once a correction for dust obscuration is performed, there is no evidence of a stellar nucleus in either case. We see no sign of a nucleus in VCC1978.

A search for low-level AGN in our program galaxies is now underway using low- to intermediate-resolution ground-based optical spectra, the results of which will be presented in a future paper in this series. These spectroscopic data will be useful in establishing the extent to which non-thermal sources are responsible for, or contribute to, the central luminosity excesses observed in a number of these galaxies. For the time being, Table 2 summarizes our classifications for the program galaxies, as discussed in the next section. We begin by defining a class of galaxies (Type 0) in which dust obscuration (four galaxies) or AGN emission (two galaxies) renders a reliable classification as nucleated or non-nucleated impossible. In what follows, we shall limit our analysis to the remaining 94 galaxies.

4.1. *Identification and Classification of the Nuclei*

As a first step in the identification of nuclei in our program galaxies, the g- and z-band surface brightness profiles were each fitted with the appropriate galaxy model (i.e., either a pure Sérsic or core-Sérsic model) outside a geometric mean radius of $0\farcs5$. Those galaxies with brightness profiles which lay systematically above the inward extrapolation of fitted model for $\lesssim 0\farcs5$ were considered to be nucleated. Because many of the nuclei are somewhat bluer than the underlying galaxies, a central excess was often more apparent in the g-band profile than in the redder bandpass. In addition to classifying the galaxies on the basis of their brightness profiles, the F475W and F850LP images for each galaxy were carefully inspected for the presence of a distinct central excess. Using these two criteria, a total of 62 galaxies were found to show clear evidence for a central nucleus; such galaxies are classified as Type Ia or Ib.

Unfortunately, for 11 of these 62 galaxies, although the presence of a faint central component could be established from the images themselves or from the brightness profiles, the nucleus itself was too faint to allow us to recover trustworthy photometric or structural parameters from the surface brightness profiles. Such galaxies are referred to as Type Ib in Tables 1 and 2. Our analysis of the structural and photometric properties of the nuclei is therefore based on the subset of 51 nucleated galaxies for which it was possible to obtain a reliable fit to the central brightness profiles: i.e., Type Ia galaxies. The Type Ib galaxies are classified as nucleated for the purposes of computing the overall frequency of nucleation, but their nuclei are omitted from the analysis in §4.4 to 4.8.

Of the remaining 94–62 = 32 galaxies, five may have nuclei which are offset by $\approx 0\farcs5$ or more from the centers of the isophotes (Type Ie galaxies). We consider these five galaxies in more detail in §4.3. The remaining 94–62–5 = 27 objects consist of galaxies which are either unquestionably non-nucleated, or galaxies with uncertain classifications. As described in Appendix A, we have carried out a series of experiments in which simulated nuclei having sizes and luminosities that obey the empirical scaling relations found in §4, are added to — and removed from — the observed brightness profiles. By re-fitting the brightness profiles obtained in this way, we aim to refine the nuclear classifications of these galaxies. To summarize our conclusions from these simulations, we classify 12 of these 27 galaxies as *certainly non-nucleated* (Type II), 11 as *possibly nucleated* (Type Id) and four others as *likely nucleated* (Type Ic). These classifications are reported on a case-by-case basis in Table 1, and summarized for the entire sample in Table 2.

Figure 3 shows F475W images for the central $10''\times10''$ regions ($\approx$ 800×800 pc) of all 100 galaxies in the survey. Each galaxy is labelled according to the classifications from Table 1. Azimuthally-averaged surface brightness profiles in the g-band for all 100 galaxies are shown in Figure 4. For the 51 Type Ia galaxies shown in this figure, the dashed and dotted curves indicate the best-fit models for the nucleus and galaxy, while the combined profile is shown by the solid curve. For all remaining galaxies, the solid curve simply shows the best-fit Sérsic or core-Sérsic model. Note that no fit was possible for either VCC1535 or VCC1030, the two galaxies with the most severe dust obscuration. Open symbols in Figure 4 denote datapoints that were omitted when fitting the galaxy profile (e.g., the innermost datapoints for galaxies which contain nuclei too faint to be fit reliably, outer datapoints for the close companions of luminous giant galaxies, and, occasionally, datapoints correspond-

ing to pronounced rings, shells, or other morphological peculiarities).

4.2. *Errors on Fitted Parameters*

Given that independent fits of the g- and z-band brightness profiles are performed for the Type Ia galaxies, it is natural to ask how well the photometric and structural parameters of the nuclei measured in the two bands agree. The first two panels of Figure 5 compare the King model half-light radii, r_h, and total magnitudes, $g_{\rm AB}$ and $z_{\rm AB}$, measured from the separate profiles (filled circles). Note that for 11 of these 51 galaxies (i.e., those objects with $B_T \lesssim 13.5$), the King concentration index and half-light radii of the nuclei were constrained to be the same in the two bandpasses; these nuclei are plotted as open stars in the first panel of Figure 5. In addition, we include in this figure the five galaxies with possible offset nuclei, bearing in mind that in these cases, the r_h, $g_{\rm AB}$ and $z_{\rm AB}$ measurements were carried out in a rather different way (see §4.3 for details). The open circles show the nuclei of these five galaxies.

The third panel of Figure 5 compares two estimates for the color of the nuclei: i.e., that obtained by integrating the best-fit g- and z-band King models, $(g-z)_{AB}$, and an aperture color, $(g-z)^a_{AB}$, obtained using a circular aperture of radius 4 pixels ($0\farcs20 \approx 16$ pc) applied to the nucleus of the galaxy-subtracted image. The mean difference between the total and aperture colors is 0.018 mag, in the sense that the aperture colors are slightly redder. The *rms* scatter in the measured radii and colors is found to be $\langle\sigma(r_h)\rangle \sim 0\farcs007$ and $\langle\sigma(g-z)\rangle \sim 0.059$ mag, respectively. Assuming the latter uncertainty arises equally from errors in the g and z bands, we find $\langle\sigma(g)\rangle = \langle\sigma(z)\rangle \sim 0.041$ mag for the nuclei magnitudes. We adopt these values for the typical uncertainties on the fitted radii, colors and magnitudes, bearing in mind that additional systematic errors (e.g., in the photometric zeropoints or in the construction of the PSFs) may affect the measurements. In any case, we conclude from Figure 5 that there is excellent internal agreement between the measured sizes, colors and magnitudes.

4.3. *Frequency of Nucleation*

VCC classifications for our program galaxies are given in Table 1 where column (8) reports the classification from BST85: `Y` means nucleated, `N` means non-nucleated. Our new classifications are given in column (9). Column 10 indicates which type of model was used to represent the galaxy: "`S`" = Sérsic or "`cS`" = core-Sérsic.

The most basic property of the nuclei which might serve as a constraint on theories for their origin is the overall frequency, f_n, with which they are found in our program galaxies. Among the 94 galaxies which can be reliably classified as either nucleated or non-nucleated, we find 62 galaxies, or $f_n = 62/94 \approx 66\%$ of the sample to show clear evidence for a central nucleus (Types Ia and Ib). However, we believe this estimate should be considered a firm lower limit on the frequency. Including the Type Ic galaxies (which are very likely to be nucleated but could not be classified as such unambiguously), gives $f_n = 66/94 \approx 70\%$. If one also includes the Type Id galaxies, which *may* be nucleated, one then finds $f_n = 77/94 \approx 82\%$. Finally, if all five galaxies with possible offset nuclei are included (although we caution in §4.3 that the weight of evidence argues against doing so), the percentage of nucleated galaxies could be as high as $f_n = 82/94 \approx 87\%$. While the true frequency probably lies between these extremes, it is nevertheless striking to think that, among our sample of 94 classifiable galaxies, in only 12 cases can the *absence* of a nucleus be established with any degree of certainty.

4.3.1 Comparison with Ground-Based Studies

Among the 100 elliptical, lenticular and dwarf galaxies in the ACS Virgo Cluster Survey, 24 dwarf galaxies (dE,Ns) and one E galaxy were classified as nucleated in the original VCC (BST85; see also Table 1 of Paper I).[19] The frequency of nucleation which we derive here, $f_n \approx$ 66–87%, is much higher than the value of $f_n \approx 25\%$ found using the classifications of BST85, and represents a sharp upward revision of the nucleation frequency for early-type galaxies in this luminosity range.

There are several reasons why such a discrepancy should come as no surprise. To the best of our knowledge, ours is the first systematic census of nuclei in early-type galaxies that includes both dwarf and giant galaxies (spanning a factor of ~ 460 in blue luminosity). More importantly, the studies of BST85 and BTS87, along with most of the major subsequent studies of dwarf galaxies and their nuclei (e.g., Binggeli & Cameron 1991; 1993), were based on visual inspection of photographic plates. As pointed out in §1 and stressed by BST85 themselves, the VCC classifications are known to be incomplete fainter than $B \gtrsim 23$ ($M_B \gtrsim -8$) and to suffer from surface brightness selection effects for the luminous E and S0 galaxies. Clearly, selection effects of this sort are less of an issue for our survey, where the identification of the nuclei is relatively straightforward thanks to the depth and high spatial resolution of the ACS images.

In any case, care must be taken when comparing our measurement to previous estimates since the frequency of nucleation is known to depend on the luminosities of the galaxies under consideration (e.g., Sandage, Binggeli & Tammann 1985). Figure 6 shows the luminosity functions for our sample of 62 nucleated galaxies (Types Ia and Ib) as the double-hatched histogram; the hatched histogram shows this same sample plus the 15 likely or possibly nucleated galaxies of Types Ic and Id (i.e., 77 galaxies in total). For comparison, the 25 galaxies classified as nucleated by BST85 are shown by the filled histogram, and the open histogram shows the distribution of the 94 classifiable galaxies from the ACS Virgo Cluster Survey. As expected, the disagreement between our classifications and that of BST85 is quite dramatic for galaxies brighter than $B_T \approx 13.7$. This happens to be the approximate dividing point between dwarf and giant galaxies in the VCC, which strongly suggests that the disagreement is the result of selection effects that made it difficult or impossible for BST85 to identify nuclei in

[19] The lone elliptical in our sample which was classified as nucleated by BST85 is VCC1422 = IC3468 (E1,N:). However, Binggeli & Cameron (1991) argue that this galaxy is in fact a misclassified *dwarf*. In what follows, we take the total number of nucleated dwarf galaxies in our sample, estimated from the BTS87 classifications, to be 25.

bright, high-surface-brightness galaxies. For $B_T \gtrsim 13.7$, there is better agreement although we still find significantly more nuclei even among these faint galaxies: i.e., we classify 46 of 53 galaxies, or 87%, of this subsample as nucleated, compared to just 25/56 ($\approx 47\%$) using the BST85 classifications. The luminosity dependence of f_n is shown explicitly in the lower panel of Figure 6.

A vivid demonstration of the importance of surface brightness selection effects when classifying nuclei is shown in Figures 7 and 8. The first of these figures compares the distribution of galaxy surface brightnesses, measured at a geometric mean radius of 1″, for the same four samples shown in the Figure 6. By contrast, Figure 8 shows nucleus magnitude as a function of galaxy surface brightness measured at a geometric mean radius of 1″. Filled symbols show the 51 Type Ia galaxies in our sample, while the open squares show the 25 galaxies classified as nucleated by BST85. Open circles in this figure denote the five galaxies with possible offset nuclei.

Figures 7 and 8 leave little doubt that the survey of BST85 preferentially missed nuclei in the bright, high-surface-brightness galaxies. We further note that a recent survey of 156 Virgo dwarfs with the Wide Field Camera on the Isaac Newton Telescope uncovered faint nuclei in 50 galaxies previously classified as non-nucleated, consistent with our upward revision for frequency of nucleation (Grant, Kuipers & Phillipps 2005). Of course, it is conceivable we *too* may be missing faint nuclei in the highest surface brightness galaxies; it is certainly true that the 11 galaxies for which we are unable to measure reliable photometric or structural parameters for the nuclei are among the highest surface brightness galaxies in our survey. Accordingly, we stress once again that the estimate of $f_n \approx 66\%$ from §4.1, which is based on galaxies with unambiguous nuclei, *is certainly a lower limit to the true frequency of nucleation among our sample of early-type galaxies*. We shall return to this point in §5.2 (see also Appendix A).

Figures 9 and 10 illustrate the importance of *HST* imaging for the identification of nuclei in these galaxies. In Figure 9 we show a comparison between the co-added F475W image for VCC2048 (IC3773) — a Type Ia galaxy — with three simulated ground-based images for this same galaxy. In these three cases, the co-added F475W frame has been binned 4×4 and convolved with Gaussians having dispersions of 1, 2 and 3 pixels, corresponding to FWHM of 0.″5, 0.″9 and 1.″4. It is clear that seeing effects alone make the detection of faint, compact nuclei challenging under normal conditions of ground-based seeing. This finding is all the more sobering when one considers that VCC2048, classified as dS0(9) in the VCC, was thought on the basis of the original BST85 classifications to be the brightest non-nucleated dwarf galaxy in our sample.

The first two panels of Figure 10 compare the F475W image for VCC784 (NGC4379) with a V-band image taken with the 2.4m Hiltner MDM telescope on 21 April, 1993 in conditions of 1.″14 seeing. This galaxy, one of the brightest Type Ia galaxies in our survey, was also classified as non-nucleated in the study of BST85. As the third panel of Figure 10 demonstrates, there is no hint of a central nucleus in the ground-based surface brightness profile, despite the fact that the nucleus, which is clearly visible in the ACS brightness profile, is among the brightest and largest in our sample.

4.3.2 Comparison with Previous HST Studies

As noted in §1, a few *HST* studies had previously revealed the presence of compact nuclei in bright early-type galaxies (e.g., Rest et al. 2001; Ravindranath et al. 2001; Lauer et al. 2005). While these programs preferentially focussed on distant, high-luminosity ellipticals and lenticulars — with 80% of the galaxies in these respective surveys having absolute magnitudes brighter than $M_V \sim -20, -20$ and -20.8, compared to $M_V \sim -16$ for the present survey — there is nevertheless some overlap with our sample at the bright end due to the large number of luminous E and S0 galaxies in the Virgo Cluster. In this section, we compare our nuclear classifications with those reported in these previous surveys, limiting the comparison to those galaxies in our survey which have unambiguous classifications (i.e., Types Ia, Ib and II). For completeness, we also compare our classifications for three faint galaxies to those of Lotz et al. (2004) who carried out a WFPC2 snapshot survey of early-type dwarf galaxies in the Virgo and Fornax Clusters. Table 3 summarizes the nuclear classifications for galaxies in common with the surveys of Rest et al. (2001), Ravindranath et al. (2001), Lauer et al. (2005) and Lotz et al. (2004).

The Rest et al. (2001) study presented WFPC2 (F702W $\approx R$) imaging for 67 early-type galaxies between 6 and 54 Mpc, with a mean distance of $\langle d \rangle = 28 \pm 9$ Mpc. To minimize spurious detections, Rest et al. (2001) adopted rather conservative criteria in their search for nuclei, identifying nucleated galaxies as those objects which showed a central excess, along both the major and minor axes, over the best-fit "Nuker" model inside a radius of 0.″15. Based on these criteria, they identified nuclei in 9 of their 67 galaxies (13%). No structural and photometric parameters were measured for the nuclei. There are six galaxies in common between their survey and ours. We find reasonable agreement between the two studies, with the exception of VCC731 (NGC4365): Rest et al. (2001) report no nucleus in this galaxy, whereas we find a small, but definite, central brightness excess. Accordingly, we classify this galaxy as Type Ib (i.e., certainly nucleated).

The NICMOS study of Ravindranath et al. (2001) was carried out using F160W ($\approx H$) images from the NIC2 (FWHM = 0.″17, scale = 0.″076) and NIC3 (FWHM = 0.″22, scale = 0.″2) cameras. For 33 galaxies with distances in the range 7 to 69 Mpc and $\langle d \rangle = 21 \pm 14$ Mpc, these authors fitted two-dimensional, PSF-convolved "Nuker" models to their NICMOS images. Compact sources — consisting of narrow, PSF-convolved Gaussians — were then included for those galaxies whose one-dimensional surface brightness profiles showed evidence for a central excess (14 of their 33 galaxies). FWHMs and magnitudes for the nuclei were then obtained by χ^2 minimization. We find good agreement with the Ravindranath et al. (2001) classifications. Specifically, we confirm the absence of nuclei in VCC1226 and VCC881 (M86 = NGC4406). For VCC763 (M84 = NGC4374), which is classified as nucleated by these authors, we confirm the presence of a central point source, although the galaxy

is classified as Type 0 in Table 1 due to the presence of strong AGN activity. All of the nuclei in the study of Ravindranath et al. (2001) were found to be unresolved point sources, although this is probably a consequence of the relatively poor resolution of their images: i.e., at the mean distance of their sample galaxies, the NICMOS FWHM corresponds to ~ 20 pc.

The WFPC2 study of Lauer et al. (2005) was based on F555W or F606W ($\approx V$) imaging for 77 galaxies; a little more than half of their galaxies (45) were also imaged in the F814W ($\approx I$) bandpass. The galaxies have distances in the range 10 to 97 Mpc, with mean $\langle d \rangle = 33 \pm 21$, so the $0\farcs07$ FWHM for the PC1 CCD corresponds to a physical scale of 11 pc for the typical galaxy. Magnitudes and colors for the nuclei in their sample — identified as an excess above the "Nuker" model which best fits the observed brightness profile — were derived by direct integration of the model residuals. In only two of their 25 nucleated galaxies did the nucleus appear resolved. There are seven ACSVCS galaxies having unambiguous nuclear classifications which are in common with Lauer et al. (2005). The classifications are in agreement in three cases: VCC1978, VCC731 and VCC1903 (M59 = NGC4621). For VCC1146 (NGC4458), which Lauer et al. (2005) classify as non-nucleated, we believe the discrepancy may be due to the highly extended nature of the nucleus. With $r_h \approx 0\farcs8 = 62$ pc, it is largest nucleus in our sample, and would be difficult to distinguish from the underlying galaxy profile in brightness profiles of limited radial extent; the Lauer et al. (2005) brightness profile for this galaxy covers just the inner $5''$.

The three remaining galaxies — VCC1226, VCC881 and VCC1632 — are listed as nucleated in Lauer et al. (2005), but we classify each of these galaxies as Type II (non-nucleated). We speculate that the detection of nuclei in VCC1226 and VCC1632 is an artifact resulting from the presence of dust in both galaxies, which partly obscures the innermost $\sim 1''$. Lauer et al. (2005) do not correct their images for dust obscuration; once such a correction is performed, we find no indication of a central nucleus in either galaxy (see also Paper VI).

In the case of VCC881, which is classified as nucleated by Lauer et al. (2005), a faint continuum enhancement is indeed detected in both the g and z bands at the central location. This feature would certainly be enhanced by the deconvolution procedure applied by Lauer et al. (2005) to their data. However, it is unclear whether this corresponds to a stellar nucleus. If one assumes that VCC881 follows the scaling relation between nucleus and galaxy luminosity obeyed by the rest of the sample, then the putative nucleus would be underluminous by a factor of ~ 250. Furthermore, starting around $0\farcs4$, the surface brightness profile of VCC881 *decreases* towards the center (Carollo et al. 1997). The origin of this central surface brightness depression is unclear (Lauer et al. 2002; Paper VI): e.g., an intrinsic decrease in the luminosity (or mass) density, or perhaps obscuration by gray dust, might be responsible. Since either processes could produce a modest and localized continuum enhancement such as the one seen at the nuclear location, we believe this galaxy is best classifed as non-nucleated (Type II). We further note that there is no evidence of nuclear activity in VCC881 from its optical, radio and X-ray properties (Ho et al. 1997; Rangarajan et al. 1995; Fabbiano et al. 1989).

Lotz et al. (2004) carried out WFPC2 (F555W $\approx V$ and F814W $\approx I$) imaging for 69 dEs and dE,Ns, mostly belonging to the Virgo and Fornax Clusters. In their analysis, a nucleus was identified as a bright compact object within $1\farcs5$ of the galaxy photocenter. While the Lotz et al. (2004) survey tended to focus on fainter galaxies than does our survey (i.e., their program galaxies have absolute blue magnitudes in the range $-17 \lesssim M_V \lesssim -11.7$ mag, with mean $\langle M_V \rangle = -14.2$ mag), there are three galaxies which appear in both studies: VCC9 (IC3019), VCC543 and VCC1948. In the case of VCC9 and VCC1948, the two studies agree in finding no evidence of a nucleus at the position of the galaxy photocenter. However, we have identified both of these galaxies as possible examples of galaxies with offset nuclei (see §4.4). Although Lotz et al. (2004) do not comment on a possible offset nucleus in the case of VCC1948, they state that: "VCC9 was originally classified as nucleated by Binggeli et al. (1985), but its brightest globular cluster candidate is $1\farcs8$ from its center". For comparison, we measure an offset of $1\farcs91 \pm 0\farcs07$ for this object and, like Lotz et al. (2004), conclude that it is probably a star cluster projected close to the galaxy photocenter, rather than a *bonafide* nucleus. The remaining galaxy, VCC543, appears in the list of non-nucleated galaxies in Table 3 of Lotz et al. (2004), although we find unmistakable evidence for a nucleus in this object (see Figures 3 and 4) that is offset by no more than $0\farcs07 \pm 0\farcs12$ from the galaxy photocenter.

Finally, we note that two recent papers (de Propris et al. 2005; Strader et al. 2006) have examined the properties of nuclei belonging to subsets of the galaxies from the ACS Virgo Cluster Survey, based on the same observational material used in this paper. A detailed comparison of the sizes, magnitudes and colors we measure for the nuclei with those reported by de Propris et al. (2005) and Strader et al. (2006) is given in Appendix B.

4.4. *Possible Offset Nuclei*

Before proceeding, we pause to consider those galaxies that may have offset nuclei. Nuclei displaced from the photocenters of their host galaxies are potentially interesting since they may hold clues to the general processes which trigger and/or regulate the formation of nuclei in general. For instance, offsets may arise through the ongoing merging of globular clusters through dynamical friction (Tremaine, Ostriker & Spitzer 1975; Miller & Smith 1992), the fading of stellar populations in dwarf irregular or blue compact dwarf galaxies as they evolve into dwarf ellipticals (e.g., Davies & Phillips 1988), recoil events following the ejection of a supermassive black hole from the nucleus (Merritt et al. 2004) or counter-streaming instabilities that develop in flat and/or non-rotating systems (Zang & Hohl 1978; De Rijcke & Debattista 2004).

From an observational perspective, the identification of such nuclei is a complicated problem. They are prone to confusion with globular clusters, foreground stars or background galaxies — difficulties that are particularly serious in ground-based imaging, where the nuclei and contaminants will appear unresolved. The most ambi-

tious study of offset nuclei undertaken to date is that of Binggeli, Barazza & Jerjen (2000), who measured offsets for a sample of 78 nucleated dwarf galaxies in the Virgo Cluster using digitized images of blue photographic plates obtained in conditions of FWHM $\approx 1\farcs2$ seeing. They found offset nuclei to be commonplace, with $\delta r_n \gtrsim 0\farcs5$ in 45 (58%) and $\delta r_n \gtrsim 1''$ in 14 of the objects (18%). It is of interest to check these results given the small sizes of the measured offsets relative to the ground-based seeing disk, the absence of color information that might be used to identify contaminants, and the possibility of confusion with Galactic stars, globular clusters and, to a lesser extent, background galaxies.

We have used our ACS images to measure offsets for the nuclei of the 62 Type Ia and Ib galaxies in our sample. In both the F475W and F850LP images for each galaxy, we first calculate the centroid of the nucleus and its corresponding uncertainty. The location of the galaxy photocenter is then found by averaging the centers of ellipses fitted to the galaxy isophotes over the range $1'' \leq r \leq r_e$ (Paper VI). The uncertainty on the position of the photocenter is taken to be the standard deviation about the mean ellipse center. Adding in quadrature the uncertainties for the position of the nucleus and photocenter then yields the uncertainties for the offset. The results reported in column 17 of Table 1 are averages of the offsets measured from the F475W and F850LP images.

Figure 11 shows the measured offsets for the 62 galaxies. Offsets are shown both in arcseconds (upper panel) and in units of the effective radius of the galaxy, $\langle r_e \rangle$, taken from Paper VI (lower panel). In only three galaxies do we see evidence for an offset as large as $1''$. Using a less restrictive criterion of $\delta r_n \gtrsim 0\farcs5$, we find only five galaxies that may have offset nuclei (i.e., Type Ie galaxies). These galaxies, which are shown as the open circles in Figure 11, are:

VCC9. This very low surface brightness galaxy has multiple bright sources near its photocenter; it may be a dIrr/dE transition object and seems to contain a rich population of "diffuse star clusters" (Paper XI). In addition to the presumed nucleus, there is a second source about two magnitudes fainter which is located $\approx 1\farcs5$ from the photocenter (and a similar distance from the presumed nucleus). Both the color and the half-light radius of the presumed nucleus are similar to those of metal-poor globular clusters in our dwarf galaxies. Thus, it is conceivable that this galaxy has no nucleus at all.

VCC21 (IC3025). More than a dozen bright sources are found in the inner regions of this very low surface brightness galaxy. Based on its mottled appearance, this galaxy too should be re-classified as a dIrr/dE transition object. The presumed nucleus is located $\approx 0\farcs76 \pm 0\farcs07$ from the galaxy photocenter, the smallest offset in our sample of five candidates. There are, however, two fainter sources close by, and given the large number of sources in this galaxy, its transitional morphology, and the fact that the presumed nucleus has a very blue color of $(g-z) \approx 0.3$, we believe the evidence indicates that the "nucleus" in VCC21 is probably a young star cluster.

VCC1779 (IC3612). This highly flattened galaxy ($\epsilon \simeq 0.5$) is noteworthy in that it contains dust filaments — unusual for low- and intermediate-luminosity galaxies in our sample (see Paper VI). Like VCC9 and VCC21, this galaxy may be a dIrr/dE transition object. The ACS images reveal four bright sources, all of which may be globular clusters, near the galaxy center. We identify the brightest of these sources, which is *not* the nearest to the center, as the putative nucleus. If the nearest (and second brightest) source is instead identified as the nucleus, then the offset would be $\approx 0\farcs4$ rather than $\approx 0\farcs5$.

VCC1857 (IC3647). This galaxy, another very low surface brightness object, has a very bright source located $\approx 7''$from its center. This is by far the largest offset for any galaxy in our sample, so the identification of this source as a nucleus should be viewed with some caution. The color and half-light radius of the presumed nucleus are consistent with those expected for an otherwise normal (metal-poor) globular cluster.

VCC1948. The presumed nucleus in this galaxy, another very low surface brightness object, is located $\approx 1\farcs4$ from the galaxy photocenter. It is the brightest of several sources in the inner few arcseconds. There also appears to be a very faint surface brightness "excess" that is nearly coincident with the galaxy photocenter. It is therefore possible that this galaxy may be a normal (Type Ib) nucleated galaxy, albeit one with an unusually faint nucleus. If so, then the source identified as the possible nucleus may be a globular cluster.

We conclude that in every case there is considerable uncertainty regarding the nature of the presumed offset nucleus. It is possible — and we consider it likely — that the "offset nuclei" in all five of these galaxies are merely globular clusters residing in non- or weakly-nucleated galaxies.

Are there nuclei with even smaller offsets? The nuclei of four other galaxies (VCC1539, VCC2019, VCC1895 and VCC1695) have offsets $0\farcs1 \lesssim \delta_{r_n} \lesssim 0\farcs5$ and, in fractional terms, there are four other galaxies that have nuclei offset by more than 1% of the galaxy effective radius (VCC2019, VCC1199, VCC1695 and VCC1895). We remind the reader, however, that these offsets correspond to just two ACS/WFC pixels, and should be confirmed using deeper, higher resolution imaging. Our only secure conclusion is that, *at most*, only five of the nucleated galaxies in our survey, or $\approx 7\%$ of the sample, have nuclei that are offset by more than $0\farcs5$ from their photocenters — at least three times smaller than the value of $\sim 20\%$ found by Binggeli et al. (2001). Moreover, we believe that most — and perhaps *all* — of the "nuclei" in the Type Ie galaxies are probably globular clusters, so this should be considered a firm upper limit on the percentage of galaxies with nuclei offset by more than $0\farcs5$. The actual percentage may in fact be zero.

4.5. *The Spatial Distribution of Nucleated and Non-Nucleated Galaxies*

A key result to emerge from the survey of BTS87 was the discovery of a spatial segregration between nucleated and non-nucleated dwarf galaxies in Virgo: the dE,Ns are more strongly concentrated to the cluster center than the dEs (see, e.g., Figure 9 of BTS87). A similar trend was later reported for the Fornax Cluster by Ferguson & Sandage (1989). Our discovery of nuclei in many of the galaxies classified as non-nucleated by BST85 suggests that it is worth reconsidering this important issue.

To facilitate comparison with the BTS87 and BST85 results, we limit our analysis in this section to those galaxies fainter than $B_T \gtrsim 13.7$, the approximate dividing point between dwarfs and giants in the VCC. As it happens, this magnitude also divides the ACS Virgo Cluster Survey equally into two samples of 50 galaxies.

In the left panel of Figure 12, the heavy solid curve shows the cumulative distribution of projected distances from the center of the Virgo Cluster for the 50 galaxies with $B_T \gtrsim 13.7$.[20] Using the VCC classifications, one finds this sample to be composed predominantly of dwarfs (i.e., 33 of 50 galaxies according to Table 1 of Paper I). The dotted and dashed curves show the corresponding distributions for the nucleated (23) and non-nucleated (27) galaxies in this sample, once again using the VCC classifications. A KS test confirms the visual impression from this figure that the nucleated galaxies in our survey exhibit the same trend noted by BTS87 for the full sample of nucleated dwarfs in the VCC: i.e., the dE,N galaxies are more centrally concentrated than their non-nucleated counterparts.

In the right panel of this figure, we show the sample of 49 galaxies with $B_T \gtrsim 13.7$ which we are able to classify as nucleated or non-nucleated from our ACS images (heavy solid curve).[21] Excluding for the moment the five galaxies with possible offset nuclei, whose true nature is uncertain, we find 40 of 44 remaining galaxies to be nucleated (dotted curve). Given the preponderance of nucleated galaxies, it is not surprising to see that a systematic difference in central concentration between the two populations is no longer apparent. Of course, with just four non-nucleated galaxies in this regime, the sample falls below the minimum size needed for statistically reliable results using a KS test, but our point in showing this comparison is to stress again that the overwhelming majority of program galaxies with $B_T \leq 13.7$ contain nuclei.

A definitive investigation into the spatial distribution of nucleated and non-nucleated galaxies in the Virgo Cluster would require ACS imaging for many hundreds of galaxies. Nevertheless, we can speculate on the origin of the trend noted by BTS87. It has long been known that galaxies in Virgo show some segregation in terms of luminosity and morphology. Ichikawa et al. (1988) noted that the dwarf elliptical galaxies in the central regions of Virgo appear to be larger and brighter than those in the cluster outskirts. At the same time, BTS87 showed that the bright early-type galaxies (E+S0) are less strongly concentrated to the cluster center than the faint (dE) early-type galaxies (see their Figures 7 and 8). Since central surface brightness is proportional to total luminosity for early-type galaxies, the BTS87 finding implies that bright, high-surface-brightness dwarfs (HSBDs) in Virgo are more spatially extended than low-surface-brightness dwarfs (LSBDs). Because the original BTS87 classifications suffer from a serious surface brightness selection effect — in the sense that nuclei belonging to galaxies with central surface brightnesses $\mu_g(1'') \lesssim 20$ mag arcsec^{-2} will go undetected; see Figure 8 — the observed trend may simply be a consequence of this surface brightness selection effect.

To put this claim on a more quantitative footing, we have calculated the density profiles for HSBD and LSBD early-type galaxies in Virgo, using a surface brightness of $\mu_g(1'') \approx 20$ mag arcsec^{-2} as a dividing point between the two subgroups. As shown in Figure 8, BTS87 would have tended to classify LSBDs as nucleated, while the HSBDs would have been preferentially classified as non-nucleated. A least-squares fit to our sample galaxies gives $\mu_g(1'') = 1.139 B_T + 3.44$, so that $\mu_g(1'') \lesssim 20$ mag arcsec^{-2} corresponds to a total galaxy magnitude of $B_T \approx 14.55$. Restricting ourselves to the early-type members of Virgo with $13.7 \lesssim B_T \lesssim 18$, this leaves us with a total of 448 galaxies. The upper limit of $B_T = 13.7$ represents the approximate transition between dwarfs and giants in Virgo, while the lower limit reflects the completeness limit of the BTS87 survey. Among this sample of 448 galaxies, there are 42 HSBDs with $13.7 \lesssim B_T \lesssim 14.55$, and 406 LSBDs with $14.55 \lesssim B_T \lesssim 18$.

Figure 13 shows the density profiles, $\Sigma(r)$, for these two populations. In calculating the profiles, we have excluded galaxies belonging to the M and W Clouds, and discarded galaxies with declinations less than 9° to guard against contamination from the Virgo B subgroup centered on VCC1226 (M49). Fitting exponentials of the form $\Sigma(R) \propto e^{-\alpha R}$ gives scalelengths of $\alpha = 0.49 \pm 0.06$ and 0.36 ± 0.06 deg^{-1} for the LSBD and HSBD populations, respectively. In other words, there is a statistically significant tendency for the HSBD early-type galaxies — the same galaxies which would preferentially be misclassified as non-nucleated in the VCC because of their high central surface brightnesses — to be more spatially extended. This is consistent with the interpretation that the differing spatial distributions for dE and dE,N galaxies noted by BTS87 is, in fact, a consequence of their survey's surface brightness limit.

4.6. *The Nucleus-to-Galaxy Luminosity Ratio*

Lotz et al. (2004) and Grant, Kuipers & Phillipps (2005) found that brighter galaxies tend to contain brighter nuclei. The upper panels of Figure 14 plot the magnitudes of the nuclei against those of the host galaxies; results for the g and z bandpasses are shown in the left and right panels, respectively. Filled and open symbols show the results for 51 Type Ia and five Type Ie galaxies. The dashed lines in these panels show the least-squares lines of best fit: $g'_n = (0.90 \pm 0.18) g'_g + (7.59 \pm 2.50)$ and $z'_n = (1.05 \pm 0.18) z'_g + (5.77 \pm 2.19)$. For comparison, the solid lines show the best-fit relations, with

[20] The cluster center is taken to be the position of M87: α(J2000) = 12:30:49.4 and δ(J2000) = 12:23:28.

[21] One galaxy in this magnitude range, VCC571, is excluded because of an irregular dust lane which obscures the nucleus and makes a definitive classification impossible.

(fixed) unity slope:

$$\begin{aligned} g'_n &= g'_g + (6.25 \pm 0.21) \\ z'_n &= z'_g + (6.37 \pm 0.22) \end{aligned} \quad (6)$$

The lower panels of Figure 14 show these same data in a slightly different form. In these panels, we plot the ratio of nucleus luminosity, $\mathcal{L}_n$, to host galaxy luminosity, $\mathcal{L}_g$,

$$\eta = \mathcal{L}_n/\mathcal{L}_g, \quad (7)$$

as a function of galaxy magnitude. Total luminosities for the nuclei were obtained by integrating the brightness profiles of the best-fit King model components (see §3). These magnitudes are recorded in columns (11) and (12) of Table 1. Galaxy luminosities are taken from Paper VI, in which the best-fit galaxy model — either Sérsic or core-Sérsic, as specified in column (10) of Table 1 — was integrated over all radii to obtain the total luminosity. The contribution of the nucleus itself was excluded in the calculation of $\mathcal{L}_g$.

The primary conclusion to be drawn from Figure 14 is that the nucleus-to-galaxy luminosity ratio does not vary with galaxy luminosity, although there is considerable scatter about the mean value. In terms of η, the relations in equation 6 are equivalent to

$$\begin{aligned} \langle \eta_g \rangle &= 0.32 \pm 0.06 \ \% \\ \langle \eta_z \rangle &= 0.28 \pm 0.06 \ \% \end{aligned} \quad (8)$$

for the two bands, where the quoted uncertainties refer to the mean errors. Our best estimate for the mean nucleus-to-galaxy luminosity ratio is then

$$\langle \eta \rangle = 0.30 \pm 0.04 \ \%. \quad (9)$$

This is well below previous estimates: only 5 of the 51 nucleated galaxies in Figure 9 of Binggeli, Barazza & Jerjen (2000) have nuclei with fractional luminosities smaller than this. While the discrepancy may partly be the result of different choices for the models used to parameterize the galaxy brightness profiles (e.g., Binggeli et al. 2000 use King models for the galaxy when calculating the luminosity of the central excess), it is also true that the greater depth and sensitivity of the ACS imaging allows us to identify fainter nuclei than is possible from the ground, while the high spatial resolution allows a more accurate subtraction of the underlying galaxy light.

4.7. *Luminosity Functions*

The luminosity function of nuclei is one of the most powerful observational constraints on models for their formation. For instance, one theory involves the growth of a central nucleus through mergers of globular clusters whose orbits have decayed because of dynamical friction (Tremaine, Ostriker & Spitzer 1975; Tremaine 1976; Lotz et al. 2001). While this scenario is consistent with the well known fact that the brightest nuclei have luminosities that exceed those of the brightest globular clusters (e.g., Durrell et al. 1996; Durrell 1997), a reliable measurement for the luminosity function of the nuclei has been hard to come by due to the lack of high-resolution CCD imaging for large, homogenous samples of early-type galaxies. The need for *HST* imaging in this instance is clear, since subtle differences in the subtraction of the galaxy light (particularly the choice of model to represent the galaxy) can lead to large differences in the inferred luminosities of the nuclei (see, e.g., section 5 of Binggeli & Cameron 1991).

In Figure 15, we plot the luminosity functions, in g and z, for the sample of 51 Type Ia nuclei given in Table 1. A Gaussian distribution,

$$\Phi(m_n^0) \propto A_n e^{-(m_n^0 - \overline{m}_n^0)^2/2\sigma_n^2} \quad (10)$$

provides an adequate representation of the luminosity functions, although there is no physical justification for this particular choice of fitting function (and it is likely that the luminosity function suffers from some degree of incompleteness at both the bright and faint ends). Moreover, if the mean luminosity of nuclei in early-type galaxies is indeed a roughly constant fraction, $\eta \approx 0.3\%$, of that of their host (§4.6), then the distribution shown in Figure 14 may largely be a reflection of the luminosities of the program galaxies. With these caveats in mind, we overlay the best-fitting Gaussian distributions in Figure 15 as the dotted curves. Fitted parameters and their uncertainties are recorded in Table 4.

A core objective of the ACS Virgo Cluster Survey is a study of the globular cluster populations associated with early-type galaxies. Since many thousands of Virgo globular cluster candidates have been identified in the course of the survey (e.g., Papers IX, X and XI), it is possible to compare directly the luminosity functions of the nuclei with those of the globular clusters. Figure 15 shows the g- and z-band luminosity functions for $\approx$ 11,000 high-probability globular cluster candidates from the survey. These objects were chosen to have globular cluster probability indices, $\mathcal{P}_{\rm gc}$, in the range $0.5 \leq \mathcal{P}_{\rm gc} \leq 1$ (see Jordán et al. 2006 for details). A complete discussion of the globular cluster luminosity function is beyond the scope of this paper and will be presented in a future article. For the time being, we simply note that, brighter than the 90% completeness limits of $g_{\rm lim} \sim 26.1$ mag and $z_{\rm lim} \sim 25.1$ mag, the luminosity functions of the globular clusters in Virgo (which are dominated by the contributions from the brightest galaxies) are well described by Gaussian distributions with $\sigma = 1.3$ mag and reddening-corrected turnover magnitudes of $g_{\rm to} \approx 23.9$ mag and $z_{\rm to} \approx 22.8$ mag. These Gaussians are shown as the upper dotted curves in each panel of Figure 15.

It is apparent that the luminosity function of the nuclei extends to higher luminosities than that of the globular clusters and that, irrespective of the functional form used to parameterize the luminosity function of the nuclei, their distribution is significantly broader than that of the globular clusters. In addition, their distribution is displaced to higher luminosities than that of the globular clusters. We measure this offset to be $\Delta g = 3.52$ mag and $\Delta z = 3.63$ mag in the two bands. Thus, on average, the nuclei are ~ 25 times brighter than a typical globular cluster. We shall return to this point in §5.2.

Also shown in Figure 15 are seven probable UCD galaxies in the Virgo Cluster, drawn from Paper VII and from Haşegan et al. (2006). These objects were identified on the basis of magnitude and half-light radius from the same images used to study the nuclei and globular clusters. Although the UCD sample is limited in size, membership in Virgo has been established for each object through radial velocity measurements, surface brightness

fluctuation distances, or both. Furthermore, the mass-to-light ratios presented in Paper VII demonstrate that at least some of these objects appear genuinely distinct from globular clusters. Several explanations for their origin have been proposed; according to what is probably the leading formation scenario, they are the surviving nuclei of dwarf galaxies which have been extensively stripped by gravitational tidal fields in the host cluster (e.g., Bassino et al. 1994; Bekki et al. 2001). The UCDs shown in Figure 15 have luminosities which coincide with the peak of the nuclei luminosity function, which is certainly consistent with this "threshing" scenario. However, it is important to bear in mind that the luminosities of the UCDs shown in Figure 15 are entirely due to the construction of the sample: i.e., candidates from Paper VII and Haşegan et al. (2006) were *selected* to have $18 \leq g \leq 21$ mag and $17 \leq z \leq 20$ mag.

4.8. *Structural Properties*

Prior to the launch of *HST*, virtually nothing was known about the sizes of the nuclei in dwarf galaxies. A notable exception was the compact, low-luminosity nucleus of the Local Group dwarf elliptical galaxy NGC205, which was measured to have $r_h \sim 0\farcs4 = 1.4$ pc by Djorgovski et al. (1992). This early estimate, which was based on deconvolved ground-based images, is in good agreement with more recent values obtained using ACS surface brightness profiles (e.g., Merritt et al. 2006). However, measuring half-light radii for nuclei at the distance of Virgo using ground-based images is impossible (e.g., Caldwell 1983; Sandage, Binggeli & Tammann 1985; Caldwell & Bothun 1987). For instance, using high-resolution CFHT images for ten Virgo dwarfs, Durrell (1997) was only able to place an upper limit of $r_h \lesssim 0\farcs4$–$0\farcs5$ (30–40 pc) on the sizes of the nuclei.

Even with the excellent angular resolution and spatial sampling afforded by *HST*/ACS, the measurement of structural parameters for the nuclei is challenging — more so than for a typical Virgo globular cluster because the nuclei are observed on a bright background which is varying rapidly in both the radial and azimuthal spatial directions. In their WFPC2 snapshot survey of dwarf galaxies in the Virgo and Fornax clusters, Stiavelli et al. (2001) and Lotz et al. (2004) did not attempt to measure half-light radii for the nuclei, but they noted that these nuclei have "sizes" less than $0\farcs13$ (10 pc). Working from the same WFPC2 data for a subset of five nucleated dwarfs, Geha, Guhathakurta & van der Marel (2002) derived half-light radii in the range 9–14 pc ($0\farcs11$–$0\farcs18$).

With their greater depth and superior sampling of the instrumental PSF, our ACS images are better suited to the measurement of half-light radii than any previous dataset, including the WFPC2 imaging. Moreover, images are available in two filters, so it is also possible to carry out independent size measurements and identify possible systematic errors arising from uncertainties in the F475W and F850LP PSFs. As shown in Figure 5, we have made such a comparison and find good agreement between the half-light radii measured in the different bandpasses, with a typical *random* measurement error of $\sigma(r_h) \sim 0\farcs007$. We note that half-light radii measured for the nuclei of approximately two dozen of our program galaxies have recently been reported by de Propris et al. (2005) and Strader et al. (2006). Appendix B presents a comparison of our structural and photometric parameters with those measured in these studies.

Figure 16 shows the distribution of half-light radii for the nuclei of Type Ia galaxies from Table 1. The distribution is evidently quite broad, with a peak at $r_h \lesssim 0\farcs05$ (4 pc) and an extended tail to much larger radii ($0\farcs83 \approx 62$ pc). The dashed line at $0\farcs025$ (≈ 2 pc) in each panel shows our estimate for the resolution limit of the images used to characterize the properties of the nuclei.[22] In both bandpasses, the median half-light of the nuclei in our sample is found to be $0\farcs05$ (4 pc). Clearly, the nuclei have a size distribution that is different from that of the globular clusters. In the latter case, the distribution is sharply peaked, with a typical (and nearly constant; Paper X) half-light radius of $\langle r_h \rangle = 0\farcs033 \approx 2.7$ pc (i.e., $\sim 30\%$ larger than the resolution limit for the nuclei). It is clear that the nuclei are not only *brighter* than typical globular clusters (§4.5) but they are also, on average, larger. There is, however, considerable overlap between the two distributions, and the most compact nuclei have half-light radii that are indistinguishable from those of globular clusters. The UCDs, on the other hand, have half-light radii which resemble those of the nuclei. As with the luminosity functions, this agreement may be a consequence of the selection process: i.e., UCD candidates were identified from the sample of sources with sizes in the range $0\farcs17$–$0\farcs5$ (14–40 pc).

Figure 17 shows that there is a clear correlation between size and luminosity for the nuclei, in the sense that the brighter objects have larger half-light radii. We have fit relations of the form $r_h \propto \mathcal{L}^\beta$ to the data in Figure 17, excluding both the offset nuclei and the 5–6 nuclei which fall below the nominal resolution limit of $0\farcs025$ (shown by the dashed lines in the two panels). The solid lines in the two panels show the relations:

$$\begin{aligned} r_{h,g} &\propto \mathcal{L}_g^{0.505\pm0.042} \\ r_{h,z} &\propto \mathcal{L}_z^{0.503\pm0.039} \end{aligned} \tag{11}$$

This luminosity dependence constitutes another clear point of distinction between nuclei and globular clusters: the latter, both in the Milky Way (van den Bergh et al. 1991; Paper VII) and in our program galaxies (Paper X), have a near-constant size of $\langle r_h \rangle = 2.7$ pc. This value is indicated by the arrows in Figure 17. Nuclei fainter than $g \sim 19$ mag and $z \sim 18$ mag have typical half-light radii of $0\farcs04$ (3.2 pc), or about 20% larger than a typical globular cluster; the brightest nuclei are an order of magnitude larger still. Given their uncertain nature, it is worth noting that all five of the candidate offset nuclei from §4.3 have half-light radii close to the mean of the globular clusters.

It is interesting to see that the UCDs — which in Figure 16 were found to have half-light radii comparable to those of the largest nuclei — are outliers in this

[22] Note that this resolution limit applies only to those images which were drizzled with a *Gaussian* kernel. In Paper X, we estimated from numerical simulations that the half-light radii of globular clusters — which are measured using the KINGPHOT software package directly from 2D images generated with a *Lanczos3* kernel — are largely unbiased for $r_h \gtrsim 0\farcs0125 \approx 1$ pc. However, the negative lobes of this kernel makes it difficult to repair bad pixels, so the *Gaussian* kernel is preferred for the analysis of the galaxy/nucleus surface brightness profiles.

size-luminosity plane. Compared to nuclei of comparable luminosity, the UCDs are nearly three times larger, with $r_h \approx 0\farcs2$–$0\farcs5$. Alternatively, one might consider the UCDs to be ~ 2 mag underluminous for their size. In any event, the fact that UCD candidates from Paper VII were chosen to lie within a specific range of magnitude and half-light radius suggests that a general conclusion about systematic size differences between the two populations would be premature.

Figure 18 shows that there also exists a difference in surface brightness between the globular clusters and nuclei. This figure plots the average surface brightness within the half-light radius,

$$\langle \mu'_h \rangle \ = m' + 0.7526 + 2.5 \log (\pi {r_h}^2), \qquad (12)$$

for these two populations. Because of their near-constant size, the globular clusters fall along a diagonal swath in this diagram. Note that the dashed line in Figure 18 is *not* a fit to the globular clusters, but simply the expected relation for clusters which obey Equation 11 and have a constant half-light radius of $r_h \equiv 2.7$ pc. Although there is sizeable scatter, The nuclei have a mean surface brightness of $\langle \mu_h \rangle = 16.5$ mag arcsec^{-2} in g and 15.2 mag arcsec^{-2} in z, although there is considerable scatter ($\sigma \approx 1.5$ mag) about these values. The basic properties for the UCDs and nuclei in Virgo are compared in Table 5.

By virtue of their larger radii at fixed luminosity, the Virgo UCDs have surface brightnesses that are lower than those of comparably bright nuclei. This is opposite to the claim of de Propris et al. (2005) who argued that Fornax UCDs have *higher* surface brightness than the Virgo nuclei. However, these authors seem to base this conclusion on a visual comparison of the nuclei brightness profiles with that for their "mean UCD". We have calculated the average surface brightness within the half-light radius for the four Fornax UCDs which have absolute magnitudes and half-light radii reported in their Table 2. In doing so, we have transformed their V-band magnitudes into the g and z bandpasses using assumed colors of $(g - V) = 0.48$ and $(V - z) = 0.76$, which are appropriate for old, intermediate-metallicity populations (see Table 3 of Paper III). Their radii have been converted from parsecs to arcseconds using their adopted Fornax distance modulus of $(m - M)_0 = 31.39$. The resulting surface brightnesses for these four UCDs are shown as the open squares in Figure 18. We find that the Fornax and Virgo UCDs occupy similar locations in the diagram, and that both populations have *lower* surface brightness (by ~ 2.5 mag arcsec^{-2} in both bandpasses) than comparably bright nuclei, contrary to the claims of de Propris et al. (2005).

Finally, we note that the five candidate offset nuclei are observed to fall along the diagonal swath defined by the globular clusters in Figure 18. This strengthens the conclusion from §4.3 that these objects are globular clusters, rather than *bonafide* nuclei.

4.9. *Nuclei Colors*

The first comprehensive investigation into the colors of nuclei in dwarf galaxies was the series of papers by Caldwell (1983; 1987) and Caldwell & Bothun (1987). Based on imaging of 30 dwarfs in the Fornax Cluster, Caldwell & Bothun (1987) found no evidence for a color difference between the nuclei and their host galaxies. They did, however, find a correlation between nuclei luminosity and galaxy color, in the sense that the reddest galaxies tended to harbor the brightest nuclei. At a given luminosity the nucleated galaxies were also found to be slightly redder than their non-nucleated counterparts. A decade later, high-resolution CFHT imaging for two Virgo dwarfs (Durrell 1997) hinted at an apparent diversity in nuclei colors: in one galaxy (VCC1254), the nucleus was found to be significantly bluer than the galaxy, while in the case (VCC1386), the colors were indistinguishable.

Recently, Lotz et al. (2004) have carried out aperture photometry for the nuclei of 45 dE,N galaxies in the Virgo and Fornax Clusters using VI images from three WFPC2 snapshot programs. They find that: (1) the nuclei are consistently bluer than the underlying galaxy light, with offset $\Delta(V - I) = 0.1$–0.15 mag; (2) the nuclei colors correlate with galaxy colors and luminosities, in the sense that the redder nuclei are found in the redder and brighter galaxies; (3) and the nuclei are slightly redder than the globular clusters associated with the host galaxy.

Our examination of the nuclei colors begins with Figure 19. The left panel of this figure shows the color-magnitude diagram for the nuclei of the 51 Type Ia galaxies (filled circles) and the five galaxies with possible offset nuclei (open circles). For the Type Ia galaxies, the symbol size is proportional to the blue luminosity of the host galaxy. For reference, 11 galaxies with nuclei redder than $(g - z)'_{AB} = 1.35$ have been labeled.[23] Note that one other galaxy, VCC21, has a very blue nucleus with $(g - z)'_{AB} \approx 0.30$. Although it is listed in Table 1 as a possible example of a galaxy with an offset nucleus, we have argued in §4.3, §4.6 and §4.7 that such offset "nuclei" are likely to be misclassified star clusters. In the case of VCC21, the blue color of the object points to a young age (i.e., ≤ 1 Gyr for virtually any choice of metallicity; see Figure 6 of Paper I). This interpretation is consistent with the galaxy's dIrr/dE transitional morphology.

There are a number of noteworthy features in the color-magnitude diagram shown in Figure 19. First, both the colors and luminosities of the nuclei are seen to correlate with host galaxy luminosity, in the sense that the nuclei belonging to the most luminous galaxies are the brightest and reddest objects in our sample. This finding is consistent with the trend noted by Lotz et al. (2004). Even more striking, though, is the tendency for *the nuclei themselves to follow a clear color-luminosity relation.* To the best of our knowledge, this is the first time such a trend has been detected. The dashed line in Figure 19 shows the relation

$$(g - z)'_{AB} \ = \ -0.095(\pm 0.015) g'_{AB} \ + \ 2.98(\pm 0.30), \qquad (13)$$

obtained from a least-squares fit to the 37 nuclei belonging to galaxies with $B_T \leq 13.5$. While this relation pro-

[23] These galaxies are VCC1146, VCC1619, VCC1630, VCC1913, VCC784, VCC1720, VCC828, VCC1627, VCC1250, VCC1242 and VCC1283.

vides an excellent description of the color-magnitude relation for the nuclei in faint galaxies, it appears to break down for brighter galaxies: in this regime, the nuclei not only show considerable scatter, but they lie systematically to the faint/red side of the extrapolated relation. These red nuclei cause the histogram of nuclei colors to have secondary peak at $(g-z)'_{AB} \approx 1.5$ (see the right panel of Figure 19). They are found exclusively in high-surface-brightness environments, which raises the possibility of a bias in the measured colors. However, the simulations described in Appendix A — in which artificial nuclei of known size, magnitude and color are added to the non-nucleated galaxy VCC1833 and their properties measured in the same way as the actual nuclei — show no evidence for a significant color bias for such bright nuclei. In addition, the colors for most of these nuclei are actually redder than the galaxies themselves, by ~ 0.1 mag, so it seems unlikely that contamination from the host galaxy can entirely explain their red colors.

For comparison, the open stars in Figure 19 show the sample of Virgo UCDs from Paper VII and Haşegan et al. (2006). The agreement with the nuclei is striking: i.e., with a mean color of $\langle (g-z)'_{AB} \rangle = 1.03 \pm 0.06$ mag, the UCDs have colors that are virtually identical to those of comparably bright nuclei. This constitutes yet another piece of evidence for a link between UCDs and the nuclei of early-type galaxies.

To better visualize how the properties of the host galaxy may affect the relationship between nuclei color and magnitude, Figure 20 divides the sample by host galaxy magnitude into four subgroups. These subsamples are shown in the four separate panels, with the color-magnitude relation given by Equation (13) repeated in each case (the dashed line). Also included in each panel are the globular clusters (small points) belonging to the galaxies in each of these magnitude intervals; to reduce contamination from stars and compact galaxies, we plot only those sources with "globular cluster probabilities" (see Paper IX for details) in the range $0.5 \leq \mathcal{P}_{\rm gc} \leq 1$. Note the clear bimodality in the colors of globular clusters belonging to these galaxies (Paper IX). With the exception of the very red nuclei noted above, we conclude that the nuclei in our Type Ia galaxies have colors which fall within the range spanned by the bulk of the globular clusters in these same galaxies: $0.7 \lesssim (g-z)'_{AB} \lesssim 1.4$ mag. Comparing the globular cluster colors to those of the UCDs from Figure 19, we see that the UCDs are $\approx$ 0.1–0.2 mag redder than the population of blue globular clusters, but $\approx$ 0.2–0.3 mag bluer than the red clusters. This may be a point of distinction with the UCDs in Fornax, which Mieske et al. (2006) find to have colors similar to the red globular clusters.

Figure 21 shows how the colors of the galaxies, nuclei and globular clusters depend on the galaxy luminosity. Results are shown for the g and z bands in the left and right panels, respectively. A common distance of 16.5 Mpc has been assumed for all galaxies (Mei et al. 2005). Galaxy colors are taken from Paper VI and represent the average color in the range $1'' \leq r \leq r_e$, subject to the ACS/WFC field view and excluding those regions with surface brightnesses 1 mag arcsec^{-2} or more below the sky. The majority of our galaxies show no evidence for strong color gradients, so these colors should accurately reflect their integrated colors. For the globular clusters, we plots colors for the red and blue subpopulations, as determined in Paper IX, along with that of the composite cluster system. To highlight the subtle trends exhibited by these various samples, we show mean colors for the nuclei, globular clusters and galaxies in four broad bins of approximately equal width in galaxy magnitude ($\sim$ 2 mag). Results for the nuclei are shown for three bins containing an equal number of objects.

This figure reveals a correlation between nucleus color and galaxy luminosity that is broadly consistent with the finding of Lotz et al. (2004) for fainter galaxies. However, the trend is relatively weak and is in fact due mainly to the $\sim$ one dozen galaxies noted above that have very red nuclei. These galaxies make up most of the objects in the bins at $M_g \approx -18.6$, $(g-z)'_{AB} \approx 1.4$ and $M_z \approx -19.6$, $(g-z)'_{AB} \approx 1.35$. In the fainter galaxies, the nuclei colors show essentially no correlation with galaxy luminosity. For galaxies fainter than $M_g = -17$, the nuclei have $\langle (g-z)_{AB} \rangle \approx 1.02$ — intermediate in color to the globular clusters and stars in galaxies in this luminosity regime.

5. DISCUSSION

In the preceding sections we have focussed on the observed properties of the nuclei found in our program galaxies. We now turn to the broader question of what these observations may be telling us about the origin and evolution of galactic nuclei. Before doing so, we pause to briefly review some of the scenarios that have been proposed as possible explanations for stellar nuclei in early-type galaxies. A more complete discussion of the theoretical implications of our findings will be given in Merritt et al. (2006).

5.1. *A Review of Formation Models*

Tremaine, Ostriker & Spitzer (1975) were the first to suggest that galactic nuclei may be the remains of merged globular clusters, which were driven inward to the galactic center by dynamical friction (Chandrasekhar 1943). According to this "merger model", the metallicity and luminosity of the nucleus should be a superposition of the metallicity and luminosity of the progenitor clusters. Because dynamical friction causes the orbits of most massive globular clusters to decay most rapidly, a nucleated galaxy would be expect to show a selective depletion of *bright* globular clusters, at least in the inner regions where the dynamical friction timescale is short compared to a Hubble Time. The contribution of globular clusters mergers to the growth of central black holes and galactic nuclei has been explored in a series of papers by Capuzzo-Dolcetta and coworkers (e.g., Capuzzo-Dolcetta 1993; Capuzzo-Dolcetta & Tesseri 1999). Recently, Bekki et al. (2004) have used numerical simulations to examine the physical properties (e.g., half-light radii, central velocity dispersion, mean density) of nuclei that form in such mergers.

Motivated by the discovery that the dE galaxies in Virgo are less centrally concentrated than the dE,N galaxies (c.f. §4.4), Oh & Lin (2000) revisited the question of how the tidal field from the Virgo cluster affects the evolution of globular cluster orbits within dE galaxies. They found that tidal perturbations acting on galaxies near the center of the cluster tend to be compressive,

and have little net effect on the rate of decay of the globular cluster orbits. In the outer regions of the Virgo cluster, tidal forces tend to disrupt galaxies, and the resulting decrease in density leads to longer time scales for dynamical friction. Thus, tidal forces favor the formation of nuclei in galaxies which are located in the cluster core, and suppress the formation in more distant galaxies. Clearly, this will cause the relative number of nucleated and non-nucleated galaxies to vary within the cluster, with the highest fraction of nucleated galaxies in the core.

A second, broad category of models focuses on a dissipational origin for the nuclei. Noting that galaxies with nuclei are typically rounder than those without, van den Bergh (1986) speculated that nuclei form from the gas which collects more easily in the centers of slowly-rotating galaxies. Silk, Wyse & Shields (1987) argued that dwarf galaxies experience late accretion of cool gas from the intergalactic medium, leading to star formation and the growth of compact central nuclei. In a similar vein, Davies & Phillips (1988) proposed that early-type dwarfs result from the fading of stellar populations in dwarf irregular or blue compact dwarf galaxies. In this scenario, intermittent bursts of central star formation — driven by the infalling gas — continue until the gas reservoir is depleted. According to this scenario, the final star-forming event gives rise to the nucleation observed today.

Babul & Rees (1992) examined the impact of the local intergalactic medium on the evolution of a low-mass galaxy. They argued that the pressure of the intergalactic medium acts as a confining agent: in a high-pressure environment, early-type dwarfs are able to retain more gas and produce a nucleus from the gas that has been prevented from escaping by the intergalactic medium. Since the external pressure acting on galaxies decreases with increasing distance from the cluster center, some properties of the nuclei (such as their luminosity and color) should also depend on position within the cluster, with the highest frequency of nucleation in the central regions of a cluster.

Gas inflow models have also been explored within the context of disk galaxy mergers. Mihos & Hernquist (1994) used N-body/hydrodynamical simulations to show that such mergers are accompanied by gas dissipation and central star formation which may result in the formation of a dense stellar core, or the fueling of a pre-existing AGN. Following Weedman (1983), Mihos & Hernquist (1994) further note that the dense stellar core may itself collapse to form a supermassive black hole (SBH). The observational evidence for a possible link between such SBHs and the stellar nuclei of early-type galaxies is examined in §5.2.0.

5.2. *Implications for Nucleus Formation*

5.2.1 Connection to Nuclear Star Clusters in Late-Type Galaxies

High-resolution *HST* imaging for Sa-Sd galaxies has shown that these objects frequently contain compact nuclear clusters near their photocenters (e.g. Phillips et al. 1996; Carollo, Stiavelli & Mack 1998; Matthews et al 1999; Böker et al. 2002; Böker et al. 2004). Figure 22 compares the sample of nuclear clusters from Böker et al. (2004) to our sample of early-type nuclei. In the upper panel, we plot the physical sizes for both samples, where we have assumed a common distance of 16.5 Mpc for the Virgo galaxies (Tonry et al. 2001; Paper V). It is clear that the nuclear clusters of Böker et al. (2004) have sizes similar to the early-type nuclei.

The lower panel of Figure 22 compares the absolute magnitudes of the two samples. Note that the observations of Böker et al. (2004) were carried out in the F814W (I) bandpass. Comparing the means of the samples, we find the two populations to be comparably bright, with $\langle M_g \rangle = -10.9$ and $\langle M_z \rangle = -12.0$ for the early-type nuclei, and $\langle M_I \rangle = -11.7$ for the nuclear clusters. Böker et al. (2002) further report that 59 of 77 late-type spirals in their survey contain a nuclear cluster close to the galaxy photocenter, giving an overall frequency of nucleation of $f_n \approx 77\%$. For comparison, in §4.2 we estimated $66 \lesssim f_n \lesssim 82\%$ for our sample of early-type galaxies, counting galaxies with possible offset nuclei as non-nucleated. Thus, in all these respects, the nuclear clusters found in late-type galaxies are nearly identical to the nuclei studied here. The lone point of distinction between the nuclear clusters and the early-type nuclei seems to be one of age: the majority of the nuclear clusters appear to have $\tau \lesssim 10^8$ yr (Walcher et al. 2005 and references therein), while the broadband colors rule out such young ages for *all* of the Type Ia nuclei, irrespective of metallicity (see §5.2.0 and Figure 6 of Paper I). This difference notwithstanding, the similar properties of the nuclei and nuclear clusters — and their appearance in galaxies of such disparate morphology — clearly points to a rather generic formation mechanism: e.g., one which is largely independent of local or global environmental factors, such as the gas content and present-day morphology of the host galaxy, or the density of neighboring galaxies.

5.2.2 A Fundamental Division Between Sérsic and core-Sérsic Galaxies

The above conclusion applies equally well to the luminosity of the host galaxy: i.e., the nuclei are not confined to just the dwarfs, but are also found with regularity in many of the giants. In fact, half (21/42) of the galaxies brighter than $B_T = 13.6$ or $M_B \approx -17.6$ (the approximate division between dwarfs and giants in the VCC) have classifications of Type Ia or Ib.[24] The fact that nuclei are common above and below the canonical dwarf-giant boundary suggests that, at least in terms of their *nuclear* properties, there is no evidence for a fundamental change in galaxies at this magnitude. This is consistent with the mounting evidence from photometric scaling relations that the "dichotomy" between normal and dwarf ellipticals, as originally envisioned by Kormendy (1985) and others, may not be real (e.g., Jerjen & Binggeli 1997; Graham & Guzmán 2003; Paper VI).

On the other hand, there *does* appear to be a fundamental transition at $M_B \approx -20.5$ in terms of nuclear properties. Brighter than this, we measure $f_n \sim 0$ and, in almost all cases, the presence of a nucleus can be ruled out with some confidence (see Appendix A). Fainter

[24] Excluding the five Type 0 galaxies in this luminosity range.

than $M_B \approx -20.5$, the fraction of nucleated galaxies rises sharply, as shown in the lower panel of Figure 6. It has been argued (Graham & Guzmán 2003; Trujillo et al. 2004; Graham 2004; Paper VI) that this magnitude marks a transition from faint, Sérsic-law galaxies to bright, core-Sérsic-law galaxies, whose flat "cores" are presumed to result from core depletion by coalescing of supermassive black holes (Ebisuzaki et al. 1991; Quinlan & Hernquist 1997; Faber et al. 1997; Milosavljević & Merritt 2001). The absence of nuclei in galaxies brighter than $M_B \approx -20.5$ is consistent with this scenario. Of course, it is equally possible that these "missing" nuclei are absent in the bright galaxies not because of the disruptive effects of mergers and black hole coalescence, but because they failed to form in such galaxies in the first place. Discriminating between these competing scenarios should prove to be a fruitful area for future theoretical study.

5.2.3 Coincidence of Nuclei with Galaxy Photocenters

In almost all cases, the nuclei are found to be coincident with the photocenters of their host galaxies. In only five cases does there appear to be a statistically significant offset of $\delta r_n/\langle r_e\rangle \geq 0.04$. The bulk of the evidence, however, favors the view that these "nuclei" are, in actuality, star clusters projected close to the galaxy photocenters. That is to say, the sizes, surface brightnesses and colors of the five possible offset nuclei more closely resemble those of globular clusters than those of the other nuclei in our sample. Interestingly, all five of the host galaxies show some characteristics of dIrr/dE transition objects, including blue colors, low central surface brightnesses, the presence of dust, and a mottled or irregular appearance. This suggests that if dwarf ellipticals represent an evolutionary stage that follows gas exhaustion and stellar fading (Davies & Phillips 1988), ram pressure stripping (Mori & Burkert 2000) or harrassment (Moore, Lake & Katz 1998) of gas-rich dIrr/disk galaxies, then the formation of a central nucleus is not an immediate or inevitable consequence. Additional time seems to be required to "grow" a central nucleus.

5.2.4 Nucleus Formation through Globular Clusters Mergers?

Because the theoretical framework for the globular cluster merger model is at a more mature stage than for any other model, we now turn our attention to the question of whether this scenario is consistent with our new observations for the nuclei. We note that Lotz et al. (2001) have previously examined the viability of the merger hypothesis on the basis of data collected for nuclei and globular clusters in their WFPC2 snaphot survey of dwarf galaxies. Apart from identifying a possible depletion of bright clusters in the innermost regions of the galaxies, they could find no strong evidence for a merger origin of the nuclei, either from the spatial distribution of the clusters or from the measured luminosities of the nuclei.

As pointed out in §4.6, a comparison of the luminosity functions of nuclei and globular clusters in these galaxies shows that the *typical* nucleus is ≈ 3.5 magnitudes brighter than a typical globular cluster. If cluster mergers are responsible for the formation of a central nucleus, then one might expect an average of ~ 25 mergers would be needed to assemble a nucleus from typical clusters. Of course, as Figure 20 shows, a single number does not tell the whole story. The four panels of this figure plot the distribution of nuclei and globular clusters in the color-magnitude diagram. For the brightest galaxies (shown in the first panel), the nuclei have a median luminosity $\approx 125\times$ that of globular clusters at the peak of the cluster luminosity function. For the fainter galaxies (shown in the three remaining panels), the nuclei are brighter than a typical globular clusters by factors of 29, 15 and 17, respectively.

Are these numbers feasible? In Figure 23 we attempt to answer this question by plotting the integrated luminosity in globular clusters against the luminosity of the nucleus for Type Ia galaxies in our survey. Results are shown in the upper panels, with measurements made in the g and z bands given in the left and right panels, respectively. As in Figures 19 and 20, symbol type indicates the magnitude of the host galaxy. In calculating the total luminosity in globular clusters for these galaxies, we have simply summed the luminosities of globular cluster candidates with probabilities in the range $\mathcal{P}_{\rm gc} \geq 0.5$. Although this approach will obviously miss any globular clusters located outside the ACS field, the correction should be small for the Type Ia galaxies in our survey which, with $M_B \lesssim -19$, have $\langle R_e\rangle \sim 15''$ or less (Paper VI). The correlations apparent in these panels are a consequence of the fact that both the total number of globular clusters, and the luminosity of the nucleus, scale with host galaxy luminosity.

The lower panels of Figure 23 plot the ratio of globular-to-nucleus luminosities, κ, in the two bandpasses. In both cases, the ratio is near unity. This should perhaps come as no surprise since the mean nucleus-to-galaxy luminosity ratio, $\eta = 0.30 \pm 0.04\%$, found in §4.5 is nearly identical to the globular cluster formation efficiency of $\epsilon = 0.26 \pm 0.05\%$ measured by McLaughlin (1999) for early-type galaxies. This latter measurement is in turn based on observations of 97 early-type galaxies and represents the total mass in globular clusters normalized to the total baryonic (stellar + gas) mass. While the agreement may be purely coincidental, it is a remarkable empirical result that the formation of early-type galaxies results in a nearly constant fraction of the initial baryonic mass, $\sim 0.3\%$, being deposited into both globular clusters and, in many cases, a central nucleus. Of course, this conclusion appears *not* to apply to galaxies brighter than $M_B \approx -20.5$, which lack nuclei either because they did not form in the first place or because they were subsequently destroyed by some as-yet-unidentified process.

In any case, galaxies which lie below the dashed line at $\kappa = 1$ in Figure 23 pose a clear challenge to the merger model for the obvious reason that they simply have too few clusters to explain the luminosity of the nucleus. The difficulty is most severe for the dozen or so red nuclei associated with the brightest Type Ia galaxies. Of course, this argument is based on the number of clusters contained by the host galaxy *at the present time*. If the observed clusters are the rare "survivors" descended from a much larger initial cluster population, then it may be possible to circumvent this problem.

An additional test of the merger model is possible. If

the mergers were dissipationless so that star formation and chemical enrichment can be ignored, then we can use the observed colors of globular clusters to predict colors for the nuclei. Since both globular cluster color and the fraction of red globular clusters are increasing functions of host galaxy luminosity (Paper IX), we expect the nuclei in this model to become progressively redder in brighter galaxies. The heavy solid curve shown in the four panels of Figure 20 shows the predicted color magnitude relation for nuclei which grow through globular cluster mergers. This curve is based on Monte Carlo experiments in which the color evolution of the nuclei is followed using the observed colors of the globular clusters in these galaxies. The thin curves show the 95% confidence limits on the relation. Although these simulations do indeed predict redder colors for the brighter nuclei (which are found preferentially in the brighter galaxies containing a larger proportion of red clusters), the predicted scaling is much milder than what is observed.

Bekki et al. (2004) have used numerical simulations to investigate the physical properties of nuclei which form through repeated mergers of globular clusters. Their predicted scaling relation between half-light radius and luminosity, $r_h \propto \mathcal{L}^{0.38}$, is shown by the dotted line in Figure 17. The relation has a somewhat milder luminosity dependence than the observed relation, $r_h \propto \mathcal{L}^{0.50\pm0.03}$, but is nevertheless in reasonable agreement. A similar conclusion applies to the luminosity dependence of surface brightness averaged within the half-light radius. We find no strong correlation between $\langle\mu_h\rangle$ and $\mathcal{L}$, but the predicted relation, $r_h \propto \mathcal{L}^{0.23}$ (shown as the dotted line in Figure 18), is reasonably consistent with the observations, having only a weak luminosity dependence. In the future, it will be of interest to compare the predicted and observed relationship between luminosity and central velocity dispersion. Spectra for most of our program galaxies are now in hand and such a comparison will be the subject of a future paper in this series.

5.2.5 Stellar Populations in the Nuclei: Clues from Colors

Ground-based spectroscopy will also be useful for investigating the history of star formation and chemical enrichment in the nuclei, although care must be exercised when decoupling the contributions from the galaxy and nucleus. This separation is more straightforward in the *ACS* imaging, although in this case we are limited in our ability to measure ages and metallicities because of the well known age-metallicity degeneracy of broadband colors. The upper panel of Figure 24 shows linear interpolations of the [Fe/H]-$(g-z)'_{AB}$ relation for simple stellar populations from the models of Bruzual & Charlot (2003). The four relations show color-metallicity relation for ages of τ = 1, 2, 5 and 10 Gyr, although it is, needless to say, quite unlikely that a single age is appropriate for all of the nuclei in our sample. For comparison, the heavy dashed curve in black shows the color-metallicity relation derived from globular clusters in the Milky Way, M49 and M87 (Paper IX). If it is assumed that the nuclei have ages similar to the globular clusters, then this empirical relation may be used to derive metallicities for the nuclei.

Converting from colors to metallicities with these relations, we find the five metallicity distributions shown in the lower panel of Figure 24. The results are summarized in Table 6. Not suprisingly, the metallicity distributions derived from the models depend sensitively on the assumed age. For τ = 10 Gyr, the colors of the bluest nuclei, with $(g-z)_{AB} \sim 0.8$ mag, would require very low metallicities: i.e., [Fe/H] ~ -2 or less. By the same token, the reddest nuclei in our sample would require metallicities 1-100$\times$ solar for an assumed age of 1 Gyr. For ages as young as $\tau \lesssim 10^8$ yr, which is appropriate for many of the nuclear clusters in late-type galaxies (see §5.2.0) no reasonable choice of metallicity can explain the colors of $\approx$ 0.8–1.5 that are observed. Thus, to the extent that the nuclei can be characterized by a single formation epoch, they show evidence for an old to intermediate age: i.e., $\tau > 1$ Gyr. Using the globular cluster color metallicity relation gives a mean metallicity of $\langle$[Fe/H]$\rangle = -0.88 \pm 0.79$ dex. Firmer conclusions on the ages and metallicities of the nuclei must await the spectroscopic analysis.

Spectroscopic constraints on the mix of stellar populations in the nuclei should also shed some light on what may be the most serious challenge facing the merger model: the existence of a tight correlation between nucleus luminosity and color (Figures 19-20). Such a correlation is generally thought to be a signature of self enrichment in stellar systems, and is reminiscent of the color-magnitude relation for dwarf and giant galaxies (e.g., Bower, Lucey & Ellis 1992; Caldwell et al. 1992). That the colors correlate tightly with the luminosities of the nuclei, and less so with those of the host galaxies, suggests that the chemical enrichment process was governed primarily by local/internal factors. The existence of a tight color-magnitude relation for the nuclei is a difficulty for the merger model as envisioned by Tremaine et al. (1975) since the clusters from which the nuclei are assembled show no color-magnitude relation themselves, and our Monte-Carlo experiments reveal the slope of the observed color-magnitude relation is steeper than that predicted in dissipationless cluster mergers.

We speculate that the merger model in its original form (i.e., "dry" mergers of stellar clusters) is an oversimplication of a process that almost certainly involves some gas dissipation. In fact, if nuclei do indeed have stellar ages of a few Gyr old or more, then they were assembled during the earliest, most gas-rich stage of galaxy evolution. It would be interesting to revisit the merger model with the benefit of numerical simulations that include the effects of not just dark matter and stars, but also gas, to see if star formation and chemical enrichment caused by mergers/inflows are capable of producing a color-magnitude relation consistent with that shown in Figure 19. In a number of respects, the dozen or so bright nuclei labelled in Figure 19 appear to form a population distinct from their faint counterparts, most notably in their integrated colors (which appear redder than the galaxies themselves). These nuclei may be candidates for the "dense stellar cores" which form in numerical simulations (Mihos & Hernquist 1994) when (chemically-enriched) gas is driven inward, perhaps as a result of mergers.

5.2.6 Ultra-Compact Dwarfs, Nuclei and Galaxy Threshing

Our ACS observations may also provide some clues to the origin of UCD galaxies. In terms of color, luminosity and size, the UCDs from Paper VII bear a strong resemblance to many of the nuclei studied here, leading credence to the galaxy threshing scenario (Bassino et al. 1994; Bekki et al. 2001). However, these UCDs were selected for study on the basis of luminosity and half-light radius, so it is unclear to what extent these conclusions may apply to the population of UCDs as a whole. An unbiased survey of the UCD population in Virgo should be undertaken to clarify this issue, although this will be a difficult and time-consuming task as it requires high-resolution spectroscopy and HST imaging to distinguish true UCDs from bright globular clusters (see §7 of Paper VII). Jones et al. (2006) have recently reported the first results from a program to search for UCDs in Virgo using radial velocities for ~ 1300 faint, star-like sources in the direction of the cluster. However, lacking structural and internal dynamical information for UCD candidates found in this way, it is impossible to know to what extent their sample has been "polluted" by globular clusters: either those associated with galaxies or intergalactic in nature (e.g., West et al. 1995).

For the time being, we may use the existing sample of Virgo UCDs from Paper VII and Haşegan et al. (2006) to re-examine the threshing model in light of our findings for the Virgo nuclei. Specifically, we may estimate the luminosities of the UCD progenitor galaxies within the context of the threshing model: for the typical ratio of nucleus-to-galaxy luminosity found in §4.5, $\langle\eta\rangle \approx 0.3\%$, we expect the progenitors to have $-18.2 \lesssim M_B \lesssim -16.6$, with a value mean of $\langle M_B\rangle = -17.3 \pm 0.6$. If the threshing scenario is correct, then we might expect the surviving analogs of the UCD progenitors to resemble galaxies #40–69 in Table 1. It is interesting to note that only about half (16/30) of these galaxies were classified as dwarfs by BST85, meaning that a significant fraction of *bright* galaxies may need to have been "threshed" to explain the UCD luminosity function within the context of this model. Photometric, dynamical and structural parameters for these candidate UCD progenitor galaxies may serve as useful constraints for self-consistent numerical simulations of galaxy threshing and UCD formation.

5.2.7 Connection to Supermassive Black Holes

A large body of literature now exists on the SBHs that reside in the centers of many galaxies (see, e.g., the review of Ferrarese & Ford 2005). While it had been known for some time that SBH masses, $\mathcal{M}_\bullet$, correlate with the bulge masses, $\mathcal{M}_{gal}$, of their host galaxies (Kormendy & Richstone 1995), it was only after the discovery of a tight relation between $\mathcal{M}_\bullet$ and bulge velocity dispersion (Ferrarese & Merritt 2001; Gebhardt et al. 2001) that Merritt & Ferrarese (2001) were able to show that the frequency function for galaxies with SBHs has a roughly normal distribution in $\log_{10}(\mathcal{M}_\bullet/\mathcal{M}_{gal})$. Fitting to the data available at that time, Merritt & Ferrarese (2001) found a mean of value of -2.90 (0.13%) and a standard deviation of 0.45 dex.

Remarkably, this mean value is, to within a factor of $\approx$ two, identical to the mean fractional luminosity contributed by nuclei to their host galaxies (§4.6). In fact, the nuclei and SBHs share a number of other key similarities that are highly suggestive of a direct connection: e.g., they share a common location at the bottom of the gravitational potential wells defined by their parent galaxies and dark matter halos, and both are probably old components that formed during the earliest stages of galaxy evolution (§5.2.0; Haehnelt et al. 1998; Silk & Rees 1998; Wyithe & Loeb 2002). Could it be that the compact nuclei which are found so frequently in the low- and intermediate-luminosity early-type galaxies are related in some way to SBHs dectected in the brighter galaxies?

Figure 25 examines the connection between nuclei and SBHs in more detail. In the upper panel, we show the distribution of absolute blue magnitudes, M_B, for the 51 galaxies in our survey that contain Type Ia nuclei (solid histogram). This distribution should be compared to that for the early-type galaxies having SBH detections (open squares and dotted histogram). This latter sample is based on data from Table II of Ferrarese & Ford (2005), which reports SBH mass measurements from resolved dynamical studies for 30 galaxies. Among this sample, there are 23 early-type galaxies with measured SBH masses (all based on stellar and/or gas dynamical methods). It is clear from Figure 25 that the two samples have very different distributions. With the exception of M32 (with $M_B = -15.76$ mag and $\mathcal{M}_\bullet = 2.5 \times 10^6$ solar masses), the SBH galaxies are all brighter than $M_B \approx -18$, a cutoff that is thought to reflect the formidable technical challenges involved in detecting smaller SBHs in fainter early-type galaxies.

By contrast, the Type Ia galaxies have $M_B \gtrsim -18.9$ mag. Note that this does *not* reflect the true upper boundary for nucleated galaxies, since nuclei definitely exist in galaxies brighter than this — Table 1 lists 14 galaxies with certain or suspected nuclei (i.e., Types Ib, Ic or Id) having $M_B \lesssim -18.9$ mag — but the high surface brightness of the host galaxies do not allow a reliable measurement of the nuclei luminosities or sizes. As we have argued in §5.2.0, the more fundamental cutoff seems to occur at $M_B \sim -20.5$ mag since we find no nucleated galaxies brighter than this.

Before moving on, we note that four of the galaxies with SBH masses in Table II of Ferrarese & Ford (2005) appear in our survey. In two cases — VCC1978 (NGC4649) and VCC1231 (NGC4473) — there is no evidence for a nucleus so we classify the galaxies as Type II. In a third case, VCC763 (NGC4374), the center of the galaxy is partly obscured by an AGN (Type O) but we see no evidence of a resolved stellar nucleus (§4). The fourth and final galaxy, VCC1664 (NGC4564), has a reported SBH mass of $5.6\times10^7\mathcal{M}_\odot$ (Gebhardt et al. 2003). We classify this object as Type Ic, meaning that we see evidence for a resolved nucleus but are unable to measure its properties owing to the high surface of the galaxy.

In the lower panel of Figure 25, we compare the frequency functions of SBHs and Type Ia nuclei. Bulge masses for the SBH galaxies were found by assuming a constant bulge color of $(B-V) = 0.9$ mag and combining the magnitudes from Ferrarese & Ford (2005) with the mass-to-light ratio relation $\Upsilon_V = 6.3(L_V/10^{11})^{0.3}$ from

Paper VII. For the SBH sample, we find

$$\begin{aligned} \langle \log_{10}(\mathcal{M}_\bullet/\mathcal{M}_{gal}) \rangle &= -2.61 \pm 0.07 \text{ dex} \\ &= 0.25 \pm 0.04 \text{ \%} \\ \sigma(\log_{10} \mathcal{M}_\bullet/\mathcal{M}_{gal}) &= 0.45 \pm 0.09 \text{ dex} \end{aligned} \quad (14)$$

whereas for the nuclei, we find

$$\begin{aligned} \langle \log_{10} \eta \rangle &= -2.49 \pm 0.09 \text{ dex } (= 0.32 \pm 0.07\%) \\ \sigma(\log_{10} \eta) &= 0.59 \pm 0.10 \text{ dex} \end{aligned} \quad (15)$$

For comparison, Gaussian distributions with these parameters are shown in the lower panel of Figure 25.

In our view, the available evidence favors the view that the compact stellar nuclei found in many of the fainter galaxies may indeed be the counterparts of SBHs in the brighter galaxies. If this speculation is correct, then it might be more appropriate to think in terms of *Central Massive Objects* — either SBHs or compact stellar nuclei — that accompany the formation of almost all early-type galaxies and contain a mean fraction $\approx 0.3\%$ of the total bulge mass. We note that a similar conclusion has been reached independently by Wehner & Harris (2006). Models for the formation of SBHs in massive galaxies would then be confronted with the additional challenge of explaining the different manifestations of Central Massive Object formation along the galaxy luminosity function, with an apparent preference for SBH formation above $-20.5 \lesssim M_B \sim -18$ mag. These issues are explored in more detail in Ferrarese et al. (2006b).

6. SUMMARY

Using multi-color ACS imaging from the *Hubble Space Telescope*, we have carefully examined the central structure of the 100 early-type galaxies which make up the ACS Virgo Cluster Survey. In this paper, we have focussed on the compact nuclei which are commonly found at, or close to, the photocenters of many of the galaxies. Our main conclusions are as follows:

1. Nuclei in early-type galaxies are more common than previously believed. Excluding the six galaxies for which the presence of a nucleus could not be established, either because of dust obscuration or the presence of an AGN, and counting the five galaxies with possible offset nuclei as non-nucleated, we find the frequency of nucleation to fall in the range $66\% \lesssim f_n \lesssim 82\%$ for early-type galaxies brighter than $M_B \approx -15$.

2. Nuclei are found in galaxies both above and below the canonical dividing line for dwarfs and giants ($M_B \approx -17.6$). Half (21/42) of the galaxies brighter than $M_B \approx -17.6$ are found to contain nuclei. This is almost certainly a lower limit on the true frequency of nucleation because of incompleteness and surface brightness selection effects in these bright galaxies.

3. On the other hand, galaxies brighter than $M_B \approx -20.5$ appear to be distinct in that they do *not* contain nuclei — at least, not those of the kind expected from upward extrapolations of the scaling relations obeyed by nuclei in fainter galaxies. Whether this means that nuclei never formed in these "core-Sérsic" galaxies (see Paper VI and references therein), or were instead subsequently destroyed by violent mergers and core evacuation due to coalescing supermassive black holes, is unclear. The absence of nuclei in galaxies brighter than $M_B \approx -20.5$ adds to the mounting evidence for a fundamental transition in the structural properties of early-type galaxies at this magnitude.

4. Few, if any, of the nuclei are found to be significantly offset from the photocenters of their host galaxies. In only five galaxies do we measure offsets $\delta r_n \gtrsim 0\farcs5$ or $\delta r_n/\langle r_e \rangle \gtrsim 0.04$. In all fives cases, however, the available evidence (i.e., magnitudes, colors, half-light radii and surface brightness measurements) suggests that such "nuclei" are probably star clusters projected close to the galaxy photocenters.

5. The central nuclei are *resolved*, with a few notable exceptions: such as the two AGN galaxies, M87 and M84, which have prominent non-thermal nuclei, and a half dozen of the faintest galaxies with very compact, but presumably stellar, nuclei. This observation rules out low-level AGN as an explanation for the central luminosity excess in the vast majority of the galaxies. Excluding those galaxies with faint, unresolved nuclei, we find the half-light radii of the nuclei to vary with luminosity according to the relation $r_h \propto \mathcal{L}^{0.50\pm0.03}$.

6. A Gaussian distribution provides an adequate, though by no means unique, description of the luminosity function for the nuclei. The peak of the luminosity function occurs at $\langle M_g \rangle = -11.2 \pm 0.6$ and $\langle M_z \rangle = -12.2 \pm 0.6$, or roughly $25\times$ brighter than the peak of the globular cluster luminosity functions in these same galaxies. We find the ratio of nucleus-to-galaxy luminosities to be $\eta \approx 0.3\%$, independent of galaxy luminosity but with significant scatter.

7. A comparison of the nuclei to the nuclear star clusters in late-type galaxies shows a remarkable similarity in luminosity, size and overall frequency. This suggests that a quite generic formation mechanism is required to explain the nuclei: one which is largely independent of local or global environmental factors, such as the gas content and present-day morphology of the host galaxy, or the density of neighboring galaxies.

8. In terms of color, luminosity and size, the UCDs from Paper VII bear a strong resemblance to the compact nuclei in a number of these galaxies, leading credence to the "threshing" scenario in which UCDs are assumed to be the tidally stripped remains of nucleated galaxies. If this model is correct, then we argue that the UCD progenitor galaxies would — if they avoided "threshing" — now resemble galaxies with magnitudes in the range $-18.2 \lesssim M_B \lesssim -16.6$. Simulations to test the viability of the threshing mechanism for such galaxies are advisable.

9. The colors of the nuclei are tighly correlated with their total luminosities, but only weakly with those of their host galaxies. This may suggest that the history of chemical enrichment in the nuclei was governed by local or internal factors.

10. The mean of the frequency function for the nucleus-to-galaxy luminosity ratio in our nucleated galaxies, $\langle \log_{10} \eta \rangle = -2.49 \pm 0.09$ dex ($\sigma = 0.59 \pm 0.10$), is indistinguishable from that of the SBH-to-bulge mass ratio, $\langle \log_{10} (\mathcal{M}_\bullet / \mathcal{M}_{gal}) \rangle = -2.61 \pm 0.07$ dex ($\sigma = 0.45 \pm 0.09$), calculated in 23 early-type galaxies with detected SBHs.

11. We argue that the compact stellar nuclei found in many of our program galaxies may be the low-mass counterparts of SBHs detected in the bright galaxies, a conclusion reached independently by Wehner & Harris (2006). If this view is correct, then one should think in terms of *Central Massive Objects (CMOs)* — either SBHs or compact stellar nuclei — that accompany the formation of almost all early-type galaxies and contain a mean fraction $\approx 0.3\%$ of the total bulge mass. In this view, SBHs would be the dominant mode of CMO formation above $M_B \approx -20.5$.

As the nearest large collection of early-type galaxies, the Virgo cluster is likely to remain, for the forseeable future, at the center of efforts to understand the physical processes that drive nucleus formation. Unfortunately, exploring the stellar dynamics of the most compact nuclei — and modeling the mass distribution within the central few parsecs of the host galaxies — requires integrated-light spectra with an angular resolution of $\sim 0\farcs1$ or better. Thus, the Virgo nuclei are obvious targets for diffraction-limited, near-IR spectrographs on 8m-class ground-based telescopes, particularly since the demise of the *Space Telescope Imaging Spectrograph* on *HST*. For the time being, though, ACS imaging of the nuclei should serve to guide models of their formation and evolution. This will be the subject of a future paper in this series, in which we will examine the implications of these observations for theories of nucleus formation (Merritt et al. 2006).

We thank Peter Stetson for assistance with the construction of the PSFs used in this study. Support for program GO-9401 was provided through a grant from the Space Telescope Science Institute, which is operated by the Association of Universities for Research in Astronomy, Inc., under NASA contract NAS5-26555. P.C. acknowledges additional support provided by NASA LTSA grant NAG5-11714. M.M. acknowledges additional financial support provided by the Sherman M. Fairchild foundation. D.M. is supported by NSF grant AST-020631, NASA grant NAG5-9046, and grant HST-AR-09519.01-A from STScI. M.J.W. acknowledges support through NSF grant AST-0205960. This research has made use of the NASA/IPAC Extragalactic Database (NED) which is operated by the Jet Propulsion Laboratory, California Institute of Technology, under contract with NASA.

APPENDIX

TESTS FOR COMPLETENESS, RESOLVABILITY AND BIAS

The approach used to classify galaxies according to the presence or absence of a central nucleus has been described in §4. Briefly, the classification procedure relies on both a visual inspection of the ACS images and the detection of a central "excess" in the brightness profile relative to the fitted Sérsic or core-Sérsic galaxy model. The results are summarized in Table 2. We find a total of 62 galaxies in which the presence of a nucleus could be established with a high level of confidence (i.e., the Type Ia and Ib galaxies). Five more galaxies (Type Ie) *may* contain an offset nucleus but, as we have argued above, the weight of evidence favors the view that these "nuclei" are actually globular clusters. Six other galaxies (Type 0) contain either an AGN or dust at the photocenters, making the identification of a nucleus difficult or impossible.

This leaves us with a sample of 100 – 62 – 5 – 6 = 27 galaxies which may be classified provisionally as non-nucleated. Of course, the faintest, most extended nuclei will go undetected in any survey, especially when superimposed on a bright galaxy background. It therefore seems likely that at least some of these galaxies may, in fact, be nucleated. In this Appendix, we attempt to elucidate the nature of these galaxies with the aid of numerical simulations guided by our findings from §4.

For the 27 galaxies in question, Figure 26 plots residuals, over the innermost $10''$, between the *observed* brightness profile and the fitted models shown in Figure 4. Because a few of these galaxies contain multiple components (e.g., rings, bars or shells), or have outer brightness profiles that are contaminated by the light of nearby giant galaxies, the profiles were sometimes fit over a restricted range in radius. In two cases where this outer fitting radius is $\leq 10''$ (VCC778 = NGC4377 and VCC575 = NGC4318), an upward arrow shows the adopted limit. Likewise, six galaxies (VCC1664 = NGC4564, VCC944 = NGC4417, VCC1279 = NGC4478, VCC355 = NGC4262, VCC1025 = NGC4434 and VCC575) in which the presence of a faint central nucleus was suspected on the basis of an upturn in the central brightness profile, an upward arrow at $0\farcs2$–$0\farcs3$ shows the inner limit used to avoid biasing the fitted galaxy parameters. Note that in most cases, the fitted Sérsic or core-Sérsic model provides a reasonably accurate match to the central brightness profile, meaning that any nuclei which may be hiding in these galaxies have had only a minor impact on the observed profiles.

Of course, two possibilities exist for any given galaxy: either it contains a nucleus or it does not. To test the first possibility, we use the scaling relation from §4 which links the luminosity of the galaxy to that of its nucleus (Equation

6). Meanwhile, Equation 11 provides a link between galaxy luminosity and nucleus size (half-light radius). For each of the 27 galaxies in Figure 26, we then subtract a nucleus of the expected size and luminosity based on the magnitude of the galaxy itself. If the nucleus-subtracted profile of the galaxy is better represented by a Sersic or core-Sérsic model than the original profile, this would be (circumstantial) evidence for the presence of a faint nucleus.

The alternative possibility is that the galaxy is truly non-nucleated. In this case, we can *add* a simulated nucleus of the appropriate size and magnitude to see if it would be detectable from the images and/or the surface brightness profile. Taken together, these two experiments allow us to crudely estimate the overall completeness of our survey and to refine the provisional classifications for these 27 galaxies. We caution, however, that the approach of adding and subtracting nuclei not only assumes that the scaling relations found in §4 are valid for all galaxies in the survey, but it ignores the significant scatter about the fitted relations.

With these caveats in mind, we present the results of this exercise in Figure 26. In each panel, the small blue squares show the residuals profile obtained after adding a simulated nucleus to the image and recalculating the brightness profile. Small red squares show the profile obtained if this nucleus is instead subtracted. For four galaxies (VCC1692, 1664, 944 and 1025), the best-fit Sérsic/core-Sérsic model for the subtracted profile provides some improvement over the original fit. We therefore classify these four as galaxies as Type Ic systems.

At the same time, we identify 12 other galaxies which can be classified unambiguously as non-nucleated (Type II). In these galaxies, the subtracted brightness profiles show strong inward gradients in their central regions: an obviously non-physical result. Interestingly, these 12 galaxies fall into two rather distinct categories: (1) *bright giants* which have shallow "cores" in the central few arcseconds and thus are best fit with core-Sérsic models; and (2) *faint dwarfs* which are best fit with pure Sérsic models. The common feature linking these two populations is the presence of a low-surface brightness core that facilitates the detection of a central nucleus. For this reason, we can say with some confidence that these 12 galaxies do *not* contain nuclei that follow the scaling relations observed in §4 for the Type Ia galaxies. The final 11 galaxies remain elusive since we can neither confirm nor rule out the presence of a nucleus in these cases. We classify these objects as possibly nucleated (Type Id).

Figures 6-7 clearly demonstrate that it is possible to detect nuclei in galaxies that span a wide range in luminosity and central surface brightness. But to what extent is our ability to detect nuclei — and to measure their sizes and magnitudes — affected by the surface brightness of the underlying galaxy and their own luminosity or size? Needless to say, a complete characterization of the biases and incompleteness affecting the nuclei requires *a priori* knowledge of their intrinsic properties: information that we are obviously lacking. Nevertheless, we may take a first step towards answering these questions by adding simulated nuclei of known size and magnitude to the center of a non-nucleated galaxy. For these experiments, we focus on a single non-nucleated galaxy, VCC1833, which, as a Sérsic-law galaxy with a central surface brightness of $\mu_g(1'') \approx 19.3$ and $\mu_z(1'') \approx 18.1$ mag arcsec^{-2}, is representative of the Type Ia galaxies in our survey.

Nuclei that span a range in both magnitude and size were added to the galaxy photocenter. Input magnitudes covered the intervals $16 \leq g \leq 25$ and $16 \leq z \leq 24$ in 1 mag increments; at each magnitude, nuclei were added with half-light radii of 0.″00, 0.″02, 0.″03, 0.″04, 0.″1, 0.″05, 0.″1, 0.″15 and 0.″2. Simulations were carried out independently for the F475W and F850LP images, and for each simulation, the surface brightness profile was measured from the artificial image using the same procedure as for the real galaxy. A nucleated Sérsic model was then fitted to the profile of the simulated galaxy+nucleus and the best-fit parameters for the nucleus recorded.

The results of these simulations are shown in Figure 27. The upper panel of this figure shows the difference between the recovered and input half-light radius, Δr_h, as a function of input radius. The lower panel plots the difference between the recovered and input magnitude, Δm, as a function of input magnitude. In both panels, results are shown for the separate F475W and F850LP bandpasses (blue and red squares, respectively). The symbol size is proportional to either input magnitude (as in the upper panel, where larger symbols correspond to brighter nuclei) or input radius (as in the lower panel, where larger symbols correspond to more compact nuclei).

There are several conclusions which may be drawn from this figure, although sweeping claims must be avoided because the results of the simulations will almost certainly depend on the central surface brightness of the galaxy, the steepness of its brightness profile, etc, so the findings are not generalizable to the other program galaxies in any straightforward way. With these caveats in mind, we note that nuclei brighter than $g \approx 19$ mag or $z \approx 18$ mag in this particular galaxy would be detected for any choice of r_h in the range 0-0.″2. Conversely, nuclei fainter than $g \approx 23$ mag or $z \approx 24$ mag would never be detected. There appears to be no serious bias affecting the r_h measurements for nuclei with $r_h \leq 0.''05$, at least for nuclei brighter than $g \sim 20$–21 mag. In this size regime — a range which encompasses half of the nuclei in Table 1 — the input half-light radii are recovered to a precision of $\sim 15\%$ or better. For larger nuclei, with $r_h \gtrsim 0.''05$, there is a bias which ranges from $\lesssim 10\%$ for the brightest nuclei, to nearly a factor of two for the faintest detectable nuclei, in the sense that the recovered nuclei are smaller. Unfortunately, the intrinsic distribution of nuclei sizes is unknown, so it is not possible to apply an *a posteriori* correction to the measured sizes. In any case, we note that the result from §4 that would be most directly affected by a bias of this sort is the observed scaling between nucleus and luminosity (Figure 17), where it was found $\mathcal{L} \propto r^{\beta}$ with $\beta = 0.50 \pm 0.03$. If we make the admittedly dubious assumption that the luminosity dependence of the bias found in the case of VCC1833 is representative of the full sample of Type Ia galaxies, then we would expect the exponent in Equation 11 to fall to $\beta \sim 0.4$.

For the faintest nuclei, the simulations reveal that completeness is a function of surface brightness, in the expected

sense that, at fixed luminosity, more compact nuclei (i.e., higher surface brightness) are more likely to be detected. As the lower panel of Figure 27 shows, there is also a tendency to measure fainter magnitudes for the simulated nuclei, at least in this galaxy. Not surprisingly, the importance of this bias depends sensitively on the input magnitude; for the brightest nuclei, the bias is less than 0.1 mag in both filters, irrespective of the input r_h. For the fainter nuclei, the bias can be as large as ~ 0.5 mag, and is slightly worse in the F850LP filter. To the extent that the simulations for VCC1833 are applicable to other galaxies in the survey, this means that the faintest Type Ia nuclei may have measured colors that are systematically too blue by ~ 0.1 mag.

COMPARISON WITH DE PROPRIS ET AL. (2005) AND STRADER ET AL. (2006)

Two recent papers, de Propris et al. (2005) and Strader et al. (2006), have presented magnitudes, colors and half-light radii for the nuclei belonging to a subset of our program galaxies. Since the same observational material that forms the basis of our analysis was used in each of these studies, it is of interest to compare the various measurements.

Based on the VCC classifications that were available when the ACS Virgo Cluster Survey was begun, 25 of the 100 program galaxies were thought to contain nuclei (see Table 1 of Paper I). As we have shown in §4, the actual number of nucleated galaxies in our survey is about three times larger than this, although in a number of cases the nuclei were too faint to determine reliable photometric or structural parameters; in the final analysis, magnitudes, colors and sizes could be measured for 51 (Type Ia) nuclei.

We first consider the results of de Propris et al. (2005), who studied 18 of the 25 galaxies originally classified as nucleated dwarfs. These authors parameterized the underlying galaxies as Sérsic models. After subtracting this Sérsic component, colors and magnitudes for the nuclei were determined by summing the light within a $1''$ aperture, while half-light radii for the nuclei were measured with the ISHAPE software package (Larsen 1999) for a circular Plummer profile and Tiny Tim PSF. We have transformed the de Propris et al. (2005) VEGAMAG photometry onto the AB system using the zeropoints given in Table 11 of Sirianni et al. (2005). Their half-light radii were converted from parsecs to arcseconds using their adopted Virgo distance of 15.3 Mpc. Extinction corrections, which in both studies are based on the DIRBE maps of Schlegel et al. (1998), were applied to our photometry as described in Paper II.

The two upper panels of Figure 28 compare our magnitudes with those of de Propris et al. (2005) (filled circles), where the dashed lines show the one-to-one relations. There is only fair agreement between the measured magnitudes (the *rms* scatter is ≈ 0.30 mag in both bands). In the lower left panel of Figure 28, we compare our two estimates for the nuclei colors with those of de Propris et al. (2005). Whether one uses integrated or aperture colors, the agreement is fair at best (*rms* scatter ≈ 0.17 mag in either case). As discussed in §4.1, an internal comparison of our color measurements shows a an *rms* scatter of 0.059 mag between the integrated and aperture colors. In any case, the scatter in the comparison with the de Propris et al. (2005) colors is largely driven by three galaxies — VCC200, VCC1826 and VCC2050 (IC3779) — which de Propris et al. (2005) find to host exeptionally blue nuclei, $(g-z)_{AB} \lesssim 0.75$ mag. For single burst stellar populations, such colors would require ages $\lesssim 3$ Gyr for virtually any choice of metallicity (see Figure 6 of Paper I). By contrast, we measure colors in the range 0.8–1.2 for these three nuclei.

In addition, we find poor agreement (*rms* scatter = $0\farcs056$) between the half-light radii measured in the two studies. In the lower right panel of Figure 28, we plot the de Propris et al. (2005) half-light radii against the mean of our measurements in the g and z bandpasses. An internal comparison of our $g-$ and z-band measurements shows good agreement, with an *rms* scatter of $\sim 0\farcs01$ (§4.1). Unfortunately, an internal comparison of the de Propris et al. (2005) is not possible since they report a single value of the half-light radius for each nucleus, and it is not clear if this value refers to a measurement made in a single bandpass, or the average of measurements in the g and z bandpasses.

Figure 28 also shows a comparison of our magnitudes, colors and half-light radii for 25 nuclei to those of Strader et al. (2006) (open squares). The Strader et al. (2006) measurements were also determined using the ISHAPE package (Larsen 1999), although these authors used an empirical PSF and assumed a King model nucleus of fixed concentration index $c \equiv \log(r_t/r_c) = 1.477$. Although there is no discussion of how the contribution from the underlying galaxy was modeled in their analysis of the nuclei, the authors do state that photometry and size measurements for the nuclei were carried out using procedures identical to the globular clusters, in which the background is usually modeled as a constant or a plane. However, near the photocenter where the nuclei are found, the galaxy light is varying rapidly in both the radial and azimuthal directions, and since the galaxy brightness profiles nearly always exhibit an inward rise, this procedure will lead to overestimates of the nuclei luminosities and sizes.

From the upper panels of Figure 28, we see that the Strader et al. (2006) magnitudes are, on average, ~ 0.4 mag brighter than ours. In addition, the discrepancy rises to $\gtrsim 1$ mag for the faintest nuclei — those which should be most prone to errors in modeling the underlying galaxy light. There is better agreement between the measured colors from the two studies, as the lower left panel shows (*rms* scatter = 0.098 and 0.072 mag for the integrated and aperture colors, respectively). At the same time, however, there is poor agreement between the measured half-light radii (*rms* scatter = $0\farcs055$), where their radii are $\sim 80\%$ larger than ours. Unfortunately, Strader et al. (2006) tabulate a single value of the radius for each nucleus, so no internal comparison of their size measurements is possible.

REFERENCES

Babul, A., & Rees, M.J. 1992, MNRAS, 255, 346

Bassino, L.P., Muzzio, J.C., & Rabolli, M. 1994, ApJ, 431, 634

Bekki, K., Couch, W.J., & Drinkwater, M.J. 2001, ApJ, 552, L105
Bekki, K., Couch, W.J., Drinkwater, M.J., & Shioya, Y. 2004, ApJ, 610, L13
Benítez, N., et al. 2002, Bull.. Am. Astron. Soc., 34, 1236
Binggeli, B., Barazza, F., & Jerjen, H. 2000, A&A, 359, 447
Binggeli, B., & Cameron, L.M. 1991, A&A, 252, 27
Binggeli, B., & Cameron, L.M. 1993, A&ASS, 98, 297
Binggeli, B., Sandage, A., & Tammann, G.A. 1985, AJ, 90, 1681 (BST85)
Binggeli, B., Tammann, G.A., & Sandage, A. 1987, AJ, 94, 251 (BTS87)
Böker, T., Laine, S., van der Marel, R.P., Sarzi, M., Rix, H.-W., Ho, L., & Shields, J.C. 2002, AJ, 123, 1389
Böker, T., Sarzi, M., McLaughlin, D.E., van der Marel, R.P., Rix, H.-W., Ho, L.C., & Shields, J.C. 2004, AJ, 127, 105
Bower, R.G., Lucey, J.R., & Ellis, R.S. 1992, MNRAS, 254, 601
Butler, D. J., & Martínez-Delgado, D. 2005, AJ, 129, 2217
Byun, Y.I., et al. 1996, AJ, 111, 1889
Caldwell, N. 1983, AJ, 88, 808
Caldwell, N. 1987, AJ, 94, 1116
Caldwell, N., & Bothun, G. D. 1987, AJ, 94, 1126
Caldwell, N., Armandroff, T.E., Seitzer, P., & Da Costa, G.S. 1992, AJ, 103, 840
Caon, N., Capaccioli, M., & D'Onofrio, M. 1993, MNRAS, 265, 1013
Capuzzo-Dolcetta, R. 1993, ApJ, 415, 616
Capuzzo-Dolcetta, R., & Tesseri, A. 1999, MNRAS, 308, 961
Carollo, C.M., Franx, M., Illingworth, G.D., & Forbes, D.A. 1997, ApJ, 481, 710
Carollo, C.M., Stiavelli, M., & Mack, J. 1998, AJ, 116, 68
Chabrier, G. 2003, PASP, 115, 763
Chandrasekhar, S. 1943, ApJ, 97, 255
Chiaberge, M., Capetti, A., & Celotti, A. 1999, A&A, 349, 77
Coleman, M., Da Costa, G.S., Bland-Hawthorn, J., Martínez-Delgado, Freeman, K.C. & Malin, D. 2004, AJ, 127, 832
Côté, P., Blakeslee, J.P., Ferrarese, L., Jordán, A., Mei, S., Merritt, D., Milosavljević, M., Peng, E.W., Tonry, J.L., & West, M.J. 2004, ApJS, 153, 223 (Paper I)
Crane, P., et al. 1993, AJ, 106, 1371
Davies, J.I., & Phillipps, S. 1988, MNRAS, 233, 553
de Propris, R., Phillipps, S., Drinkwater, M.J., Gregg, M.D., Jones, J.B., Evstigneeva, E., & Bekki, K. 2005, ApJ, 623, 105
De Rijcke, S., & Debattista, V.P. 2004, ApJ, 603, L25
de Vaucouleurs, G. 1948, Ann. d'Astrophys., 11, 247
Djorgovski, S., Bendinelli, O., Parmeggiani, G., & Zavatti, F. 1992, in Morphological and Physical Classification of Galaxies, ed. G. Longo, M. Capaccioli, & G. Busarello (Kluwer, Dordrecht), p. 439
Dressler, A. 1980, ApJ, 236, 351
Drinkwater, M.J., Phillipps, S., Gregg, M.D., Parker, Q.A., Smith, R.M., Davies, J.I., Jones, J.B., Sadler, E.M. 1999, ApJ, 511, L97
Drinkwater, M. J., Phillipps, S., Jones, J. B., Gregg, M. D., Deady, J. H., Davies, J. I., Parker, Q. A., Sadler, E. M., & Smith, R. M. 2000, A&A, 355, 900
Durrell, P.R. 1997, AJ, 113, 531
Ebisuzaki, T., Makino, J., & Okumura, S.K. 1991, Nature, 354, 212
Fabbiano, G., Gioia, I.M., & Trinchieri, G. 1989, ApJ, 347, 127
Faber, S., et al. 1997, AJ, 114, 1771
Ferrarese, L., & Merritt, D. 2000, 539, L9
Ferrarese, L., & Ford, H.C. 2005, SSRv, 116, 523
Ferrarese, L., Côté, P., Jordán, A., Peng, E.W., Blakeslee, J.P., Piatek, S., Mei, S., Merritt, D., Milosavljević, M., Tonry, J.L., & West, M.J. 2006a, ApJ, in press, (astro-ph/0602297) (Paper VI)
Ferrarese, L., Côté, P., Dalla Bontà, E., Peng, E.W., Merritt, D., Jordán, A., Blakeslee, J.P., Haşegan, M., Mei, S., Piatek, S., Tonry, J.L., & West, M.J. 2006b, ApJ, submitted
Ferguson, H.C. 1989, AJ, 98, 367
Ferguson, H.C., & Sandage, A. 1989, ApJ, 346, L53
Ford, H.C., et al. 1998, Proc. SPIE, 3356, 234
Gebhardt, K., et al. 2000, ApJ, 539, L13
Graham, A.W., & Guzmán, R. 2003, AJ, 125, 2936
Graham, A.W., Erwin, P., Trujillo, I., & Asensio Ramos, A. 2003b, AJ, 125, 2951
Graham, A.W. 2004, ApJ, 613, 33
Graham, A.W., & Driver, S.P. 2005, PASA, 22, 118
Grant, N.I., Kuipers, J.A., & Phillipps, S. 2005, MNRAS, 363, 1019
Haşegan, M., Jordán, A., Côté, P., Djorgovski, S.G., McLaughlin, D.E., Blakeslee, J.P., Mei, S., West, M.J., Peng, E.W., Ferrarese, L., Milosavljević, M., Tonry, J.L., & Merritt, D. 2005, ApJ, 627, 203 (Paper VII)
Haşegan, M., et al. 2006, in preparation
Haehnelt, M.G., Natarajan, P., & Rees, M.J. 1998, MNRAS, 300, 817
Hilker, M., Infante, L., Vieira, G., Kissler-Patig, M., & Richtler, T. 1999, A&AS, 134, 75
Ho, L.C., Filippenko, A.V., & Sargent, W.L.W. 1997, ApJS, 112, 315
Ho, L.C. 1999, ApJ, 516, 672
Jedrzejewski, R.I. 1987, MNRAS, 226, 747
Jones, J.B., Drinkwater, M.J., Jurek, R., Phillipps, S., Gregg, M.D., Bekki, K., Couch, W.J., Karick, A., Parker, Q.A., & Smith, R.M. 2006, AJ, 131, 312
Jordán, A., Blakeslee, J.P., Peng, E., Mei, S., Côté, P., Ferrarese, L., Merritt, D., Milosavljević, M., Tonry, J.L., & West, M.J. 2004a, ApJS, 154, 509 (Paper II)
Jordán, A., Côté, P., Ferrarese, L., Blakeslee, J.P., Mei, S., Merritt, D., Milosavljević, M., Peng, E.W., Tonry, J.L., & West, M.J. 2005b, ApJ, 613, 279 (Paper III)
Jordán, A., Côté, P., Blakeslee, J.P., Ferrarese, L., McLaughlin, D.E., Mei, S., Peng, E.W., Tonry, J.L., Merritt, D., Milosavljević, M., Sarazin, C.L., Sivakoff, G.R., West, M.J. 2005, ApJ, 634, 1002 (Paper X)
Jordán, A., et al. 2006, in preparation
Jerjen, H., & Binggeli, B. 1997, in ASP Conf. Ser. 116, The Nature of Elliptical Galaxies, ed. M. Arnaboldi, G. S. Da Costa, & P. Saha (San Francisco: ASP), 239
Julian, W.H., Kooiman, B.L., & Sanders, W.L. 1997, PASP, 109, 297
King, I.R. 1966, AJ, 71, 64
Kleyna, J.T., Wilkinson, M.I., Gilmore, G., & Evans, N.W. 2003, ApJ, 588, L21
Kormendy, J. 1985, ApJ, 295, 73
Kormendy, J., & Richstone, D 1995, ARA&A, 33, 581
Larsen, S. 1999, A&AS, 139, 393
Lauer, T.R., et al. 1995, AJ, 110, 2622
Lauer, T.R., et al. 2005, AJ, 129, 2138
Layden, A.C., & Sarajedini, A. 2000, AJ, 119, 1760
Lotz, J.M., Telford, R., Ferguson, H.C., Miller, B.W., Stiavelli, M., & Mack, J. 2001, ApJ, 552, 572
Lotz, J.M., Miller, B.W., & Ferguson, H.C. 2004, ApJ, 613, 262
Matthews, L.D., et al. 1999, AJ, 118, 208
McConnachie, A.W., & Irwin, M.J. 2006, MNRAS, 365, 1263
Mei, S., Blakeslee, J.P., Tonry, J.L., Jordán, A., Peng, E.W., Côté, P., Ferrarese, L., Merritt, D., Milosavljević, M., & West, M.J. 2005a, ApJS, 156, 113 (Paper IV)
Mei, S., Blakeslee, J.P., Tonry, J.L., Jordán, A., Peng, E.W., Côté, P., Ferrarese, L., West, M.J., Merritt, D., & Milosavljevic, M. 2005b, ApJ, 625, 121 (Paper V)
Merritt, D., & Ferrarese, L. 2001, MNRAS, 320, 30
Merritt, D., Milosavljević, M., Favata, M., Hughes, S.A., & Holz, D.E. 2004, ApJ, 607, L9
Merritt, D., Navarro, J.F., Ludlow, A., & Jenkins, A. 2005, ApJ, 624, L85
Merritt, D., et al. 2006, in preparation
Michie, R.W. 1963, MNRAS, 125, 127
Mieske, S., Hilker, M., Infante, L., & Jordán, A. 2006, AJ, in press (astro-ph/0512474)
Mihos, J.C., & Hernquist, L. 1994, ApJ, 437, L47
Miller, R.H., & Smith, B.F. 1992, ApJ, 393, 508
Milosavljević, M., & Merritt, D. 2001, ApJ, 563, 34
Monaco, L., Bellazini, M., Ferraro, F.R., & Pancino, E. 2005, MNRAS, 356, 1396
Mori, M., & Burkert, A. 2000, ApJ, 538, 559
Moore, B., Lake, G., & Katz, N. 1998, ApJ, 495, 139
Navarro, J.F., Hayashi, E., Power, C., Jenkins, A.R., Frenk, C.S., White, S.D.M., Springel, V., Stadel, J., & Quinn, T.R 2004, MNRAS, 349, 1039
Nelder, J.A., & Mead, R. 1965, Comput.J., 7, 308
Oh, K.S., & Lin, D.N.C. 2000, ApJ, 543, 620
Oemler, A. 1974, ApJ, 194, 1
Palma, C., Majewski, S.R., Siegel, M.H., Patterson, R.J., Ostheimer, J.C., & Link, R. 2003, AJ, 125, 1352

Peng, E.W., Jordán, A., Côté, P., Blakeslee, J.P., Ferrarese, L., Mei, S., West, M.J., Merritt, D.,Milosavljevic, M., & Tonry, J.L. 2006a, ApJ, 639, 95 (Paper IX)
Peng, E.W., Côté, P., Jordán, A., Blakeslee, J.P., Ferrarese, L., Mei, S., West, M.J., Merritt, D.,Milosavljevic, M., & Tonry, J.L. 2006b, ApJ, in press (Paper XI)
Phillips, A.C., Illingworth, G.D., MacKenty, J.W., & Franx, M. 1996, AJ, 111, 1566
Phillipps, S., Drinkwater, M., Gregg, M., & Jones, J. 2001, ApJ, 560, 201
Postman, M., et al. 2005, ApJ, 623, 721
Quinlan, G.D., & Hernquist, L. 1997, NewA, 2, 533
Rangarajan, F.V.N., White, D.A., Ebeling, H., & Fabian, A.C. 1995, MNRAS, 277, 1047
Ravindranath, S., Ho, L.C., Peng, C.Y., Filippenko, A.V., & Sargent, W.L.W. 2001, AJ, 122, 653
Reaves, G. 1983, ApJS, 53, 375
Rest, A., van den Bosch, F.C., Jaffe, W., Tran, H., Tsvetanov, Z., Ford, H.C., Davies, J., & Schafer, J. 2001, AJ, 121, 2431
Sandage, A., Binggeli, B., & Tammann, G.A. 1985, AJ, 90, 1759
Sérsic, J.-L. 1968, Atlas de Galaxias Australes (Córdoba: Obs. Astron., Univ. Nac. Córdova)
Schlegel, D.J., Finkbeiner, D.P., & Davis, M. 1998, ApJ, 500, 525
Silk, J., Wyse, R.F.G., & Shields, G.A. 1987, ApJ, 332, L59
Silk, J., & Rees, M.J. 1998, A&A, 331, L1
Sirianni, M., Jee, M.J., Benítez, N., Blakeslee, J.P., Martel, A.R., Meurer, G., Clampin, M., De Marchi, G., Ford, H.C., Gilliland, R., Hartig, G.F., Illingworth, G.D., Mack, J., & McCann, W.J. 2005, PASP, 117, 1049
Smith, G.P., Treu, T., Ellis, R.S., Moran, S.M., & Dressler, A. 2004, ApJ, 620, 78
Stiavelli, M., Miller, B.W., Ferguson, H.C., Mack, J., Whitmore, B.C., & Lotz, J.M. 2001, AJ, 121, 1385
Strader, J., Brodie, J.P., Spitler, L., & Beasley, M.A. 2006, AJ, submitted (astro-ph/0508001)
Tonry, J.L., Dressler, A., Blakeslee, J.P., Ajhar, E.A., Fletcher, A.B., Luppino, G.A., Metzger, M.R., & Moore, C.B. 2001, ApJ, 546, 681
Tremaine, S.D., Ostriker, J.P., & Spitzer, L., Jr. 1975, ApJ, 196, 407
Tremaine, S.D. 1976, ApJ, 203, 72
Trujillo, I., Erwin, P., Asensio Ramos, A., & Graham, A.W. 2004, AJ, 127
Valluri, M., Ferrarese, L., Merritt, D., & Joseph, C.L. 2005, ApJ, 628, 137
van den Bergh, S. 1986, AJ, 91, 271
Walcher, C.J., van der Marel, R.P., McLaughlin, D., Rix, H.-W., Böker, T., Häring, N., Ho, L.C., Sarzi, M., & Shields, J.C 2005, ApJ, 618, 237
Weedman, D.W. 1983, ApJ, 266, 479
Wehner, E.H., & Harris, W.E. 2006, ApJ, submitted
West, M.J., Côté, P., Jones, C., Forman, W., & Marzke, R.O. 1995, ApJ, 453, L77.
Wrobel, J.M. 1991, AJ, 101, 127
Wyiethe, J.S.B., & Loeb, A. 2002, ApJ, 581, 886
Zang, T.A., & Hohl, F. 1978, ApJ, 226, 521

Table 1. Basic Data for Nuclei of Program Galaxies

ID	VCC	Other	B_T	E(B-V)	$\mu_g(1'')$	$\mu_z(1'')$	Class	Class	Mod	g_{AB}	z_{AB}	$(g-z)_{AB}$	$(g-z)^a_{AB}$	$r_{h,g}$	$r_{h,z}$	δ_n	Comments
			(mag)	(mag)	(mag □″)	(mag □″)	(VCC)	(ACS)		(mag)	(mag)	(mag)	(mag)	(″)	(″)	(″)	
(1)	(2)	(3)	(4)	(5)	(6)	(7)	(8)	(9)	(10)	(11)	(12)	(13)	(14)	(15)	(16)	(17)	(18)
1	1226	M49, N4472	9.31	0.022	16.74	15.12	N	II	cS	···	···	···	···	···	···	···	Dust. AGN?[a]
2	1316[b]	M87, N4486	9.58	0.023	17.58	15.95	N	0	cS	···	···	···	···	···	···		Dust. AGN.[c]
3	1978	M60, N4649	9.81	0.026	16.93	15.27	N	II	cS	···	···	···	···	···	···	···	AGN?[a]
4	881	M86, N4406	10.06	0.029	16.66	15.08	N	II	cS	···	···	···	···	···	···	···	Dust.
5	798	M85, N4382	10.09	0.030	16.23	14.89	N	II	cS	···	···	···	···	···	···	···	Dust:.
6	763	M84, N4374	10.26	0.041	16.47	14.88	N	0	cS	···	···	···	···	···	···		Dust. AGN.[c]
7	731	N4365	10.51	0.021	16.95	15.34	N	Ib	cS	···	···	···	···	···	···	0.014±0.008	
8	1535	N4526	10.61	0.022	···	···	N	0	···	···	···	···	···	···	···	···	Dust.
9	1903[b]	M59, N4621	10.76	0.032	16.44	14.80	N	Id	S	···	···	···	···	···	···	···	
10	1632	M89, N4552	10.78	0.041	16.34	14.68	N	II	cS	···	···	···	···	···	···	···	Dust. AGN?[a]
11	1231	N4473	11.10	0.028	16.45	14.87	N	II	S	···	···	···	···	···	···	···	
12	2095	N4762	11.18	0.022	16.76	15.25	N	Ib	S	···	···	···	···	···	···	0.009±0.009	
13	1154	N4459	11.37	0.045	16.67	15.11	N	Id	S	···	···	···	···	···	···	···	Dust.
14	1062	N4442	11.40	0.022	16.63	15.02	N	Id	S	···	···	···	···	···	···	···	
15	2092	N4754	11.51	0.032	16.77	15.15	N	Ib	S	···	···	···	···	···	···	0.027±0.008	
16	369	N4267	11.80	0.047	16.98	15.36	N	Ib	S	···	···	···	···	···	···	0.015±0.004	
17	759	N4371	11.80	0.036	17.50	15.93	N	II	S	···	···	···	···	···	···	···	Dust.
18	1692	N4570	11.82	0.022	16.65	15.06	N	Ic	S	···	···	···	···	···	···	···	
19	1030	N4435	11.84	0.029	···	···	N	0	···	···	···	···	···	···	···	···	Dust.
20	2000[b]	N4660	11.94	0.034	16.47	14.89	N	Id	S	···	···	···	···	···	···	···	
21	685	N4350	11.99	0.028	16.57	14.98	N	0	S	···	···	···	···	···	···	···	Dust.
22	1664	N4564	12.02	0.033	16.90	15.27	N	Ic	S	···	···	···	···	···	···	···	
23	654	N4340	12.03	0.026	17.45	15.95	N	Ib	S	···	···	···	···	···	···	0.025±0.007	
24	944	N4417	12.08	0.025	16.93	15.42	N	Ic	S	···	···	···	···	···	···	···	
25	1938	N4638	12.11	0.026	16.97	15.43	N	Ib	S	···	···	···	···	···	···	0.017±0.069	
26	1279	N4478	12.15	0.024	17.40	15.90	N	Id	S	···	···	···	···	···	···	···	
27	1720	N4578	12.29	0.021	17.66	16.13	N	Ia	S	18.40	16.82	1.57	1.57	0.085	0.085	0.007±0.005	
28	355	N4262	12.41	0.036	16.75	15.15	N	Id	S	···	···	···	···	···	···	···	Dust.
29	1619	N4550	12.50	0.040	17.69	16.25	N	Ia	S	17.13	15.58	1.55	1.58	0.323	0.323	0.058±0.028	Dust. AGN.[d]
30	1883	N4612	12.57	0.025	17.20	15.86	N	Ia	S	18.74	17.60	1.14	1.11	(0.024)	(0.024)	0.013±0.006	
31	1242	N4474	12.60	0.042	17.59	16.09	N	Ia	S	19.84	18.14	1.70	1.68	0.035	0.035	0.017±0.007	
32	784	N4379	12.67	0.024	17.53	16.05	N	Ia	S	18.34	16.68	1.66	1.67	0.161	0.161	0.018±0.006	
33	1537	N4528	12.70	0.046	17.30	15.82	N	Id	S	···	···	···	···	···	···	···	
34	778	N4377	12.72	0.038	16.94	15.44	N	Id	S	···	···	···	···	···	···	···	
35	1321	N4489	12.84	0.028	17.92	16.52	N	Id	S	···	···	···	···	···	···	···	
36	828	N4387	12.84	0.033	18.01	16.50	N	Ia	S	18.53	16.96	1.57	1.59	0.208	0.208	0.011±0.005	
37	1250	N4476	12.91	0.028	17.81	16.58	N	Ia	cS	19.73	18.19	1.55	1.52	0.026	0.026	0.083±0.054	Dust.
38	1630	N4551	12.91	0.039	18.00	16.46	N	Ia	S	17.39	15.72	1.68	1.71	0.501	0.501	0.014±0.007	
39	1146	N4458	12.93	0.023	18.03	16.59	N	Ia	S	15.37	13.95	1.42	1.47	0.780	0.780	0.006±0.008	
40	1025	N4434	13.06	0.022	17.48	16.00	N	Ic	S	···	···	···	···	···	···	···	
41	1303	N4483	13.10	0.020	18.00	16.50	N	Ib	S	···	···	···	···	···	···	0.016±0.008	
42	1913	N4623	13.22	0.022	18.51	17.02	N	Ia	S	17.55	15.95	1.60	1.64	0.597	0.597	0.011±0.010	
43	1327	N4486A	13.26	0.023	17.49	15.90	N	II	S	···	···	···	···	···	···	···	Dust.
44	1125	N4452	13.30	0.030	18.57	17.15	N	Ia	S	20.48	19.51	0.97	0.950	0.060	0.060	0.021±0.029	
45	1475	N4515	13.36	0.031	17.85	16.46	N	Ib	S	···	···	···	···	···	···	0.017±0.008	
46	1178	N4464	13.37	0.022	17.47	15.99	N	Ib	S	···	···	···	···	···	···	0.014±0.008	
47	1283	N4479	13.45	0.029	19.11	17.62	N	Ia	S	20.65	19.07	1.58	1.55	0.053	0.053	0.034±0.021	
48	1261	N4482	13.56	0.029	19.71	18.49	Y	Ia	S	19.50	18.28	1.22	1.25	0.041	0.036	0.028±0.018	
49	698	N4352	13.60	0.026	18.43	17.03	N	Ia	S	19.93	18.61	1.32	1.29	0.041	0.041	0.041±0.016	
50	1422	I3468	13.64	0.031	20.04	18.76	Y	Ia	S	20.22	19.00	1.22	1.26	0.038	0.035	0.038±0.018	Dust:.
51	2048	I3773	13.81	0.032	19.39	18.17	N	Ia	S	21.45	20.30	1.15	1.14	0.037	0.031	0.076±0.033	
52	1871	I3653	13.86	0.030	18.89	17.42	N	Ia	S	18.73	17.48	1.25	1.35	0.125	0.108	0.030±0.013	
53	9	I3019	13.93	0.039	22.11	20.95	Y	Ie	S	22.01	21.22	0.79	0.88	0.040	0.034	1.907±0.070	dIrr/dE.
54	575	N4318	14.14	0.025	18.38	16.96	N	Id	S	···	···	···	···	···	···	···	
55	1910	I809	14.17	0.031	20.05	18.64	Y	Ia	S	19.82	18.63	1.19	1.19	0.038	0.038	0.005±0.018	
56	1049	U7580	14.20	0.022	19.74	18.73	N	II	S	···	···	···	···	···	···	···	
57	856	I3328	14.25	0.024	20.67	19.46	Y	Ia	S	18.97	17.85	1.12	1.17	0.163	0.153	0.073±0.047	
58	140	I3065	14.30	0.037	19.60	18.37	N	Ia	S	22.09	21.19	0.91	0.93	0.030	(0.022)	0.045±0.023	
59	1355	I3442	14.31	0.034	21.84	20.59	Y	Ia	S	21.10	20.07	1.03	1.03	0.043	0.038	0.030±0.069	
60	1087	I3381	14.31	0.027	20.60	19.27	Y	Ia	S	20.22	18.89	1.33	1.33	0.027	0.027	0.012±0.032	
61	1297	N4486B	14.33	0.021	17.49	15.93	N	Id	S	···	···	···	···	···	···	···	
62	1861	I3652	14.37	0.029	20.76	19.43	Y	Ia	S	20.11	19.06	1.04	1.19	0.137	0.119	0.061±0.053	
63	543	U7436	14.39	0.031	20.56	19.29	N	Ia	cS[e]	22.56	21.20	1.36	1.19	0.157	0.196	0.056±0.034	
64	1431	I3470	14.51	0.051	19.82	18.40	Y	Ia	S	19.66	18.54	1.13	1.17	0.238	0.233	0.073±0.027	
65	1528	I3501	14.51	0.028	19.51	18.18	N	Ia	cS[e]	22.27	21.31	0.96	0.89	(0.015)	(0.018)	0.016±0.016	
66	1695	I3586	14.53	0.045	20.34	19.22	N	Ia	cS[e]	22.61	21.23	1.38	1.35	(0.022)	(0.024)	0.433±0.196	
67	1833		14.54	0.036	19.28	18.09	N	II	S	···	···	···	···	···	···	···	
68	437	U7399A	14.54	0.029	20.75	19.45	Y	Ia	S	20.00	19.01	1.00	1.03	0.089	0.083	0.032±0.029	
69	2019	I3735	14.55	0.022	20.83	19.63	Y	Ia	S	20.31	19.20	1.12	1.18	0.037	0.029	0.183±0.077	
70	33	I3032	14.67	0.037	20.79	19.75	Y	Ia	S	22.18	21.27	0.91	0.91	0.033	0.032	0.046±0.056	
71	200		14.69	0.030	20.56	19.31	Y	Ia	S	22.86	21.94	0.92	1.06	0.053	0.038	0.068±0.043	
72	571		14.74	0.022	20.12	19.11	N	0	S	···	···	···	···	···	···	···	Dust.
73	21	I3025	14.75	0.021	20.42	18.79	N	Ie	S	20.64	20.36	0.28	0.32	0.033	0.029	0.759±0.070	dIrr/dE
74	1488	I3487	14.76	0.021	20.24	19.51	N	Ia	S	23.71	22.99	0.72	0.69	0.025	0.025	0.038±0.071	
75	1779	I3612	14.83	0.028	20.45	19.62	N	Ie	S	22.41	21.58	0.83	0.85	0.021	0.024	0.542±0.191	Dust. dIrr/dE
76	1895	U7854	14.91	0.017	20.54	19.42	N	Ia	S	23.48	22.61	0.88	0.89	(0.023)	(0.021)	0.198±0.043	

Table 1. Basic Data for Nuclei of Program Galaxies— *Continued*

ID	VCC	Other	B_T	E(B-V)	$\mu_g(1'')$	$\mu_z(1'')$	Class	Class	Mod	g_{AB}	z_{AB}	$(g-z)_{AB}$	$(g-z)^a_{AB}$	$r_{h,g}$	$r_{h,z}$	δ_n	Comments
			(mag)	(mag)	(mag $\Box''$)	(mag $\Box''$)	(VCC)	(ACS)		(mag)	(mag)	(mag)	(mag)	($''$)	($''$)	($''$)	
(1)	(2)	(3)	(4)	(5)	(6)	(7)	(8)	(9)	(10)	(11)	(12)	(13)	(14)	(15)	(16)	(17)	(18)
77	1499	I3492	14.94	0.030	19.55	19.12	N	II	S	...	...	...	...	...	...	...	dIrr/dE
78	1545	I3509	14.96	0.042	19.98	18.53	N	Ia	S	21.93	20.88	1.05	1.16	0.050	0.037	0.027±0.017	
79	1192	N4467	15.04	0.023	19.05	17.53	N	Ia	S	19.09	17.90	1.19	1.22	0.120	0.121	0.007±0.013	
80	1857	I3647	15.07	0.025	22.72	21.72	Y	Ie	S	21.11	20.27	0.84	0.86	0.041	0.041	6.986±0.347	
81	1075	I3383	15.08	0.027	21.43	21.40	Y	Ia	S	21.07	20.11	0.96	0.97	0.040	0.039	0.012±0.070	
82	1948		15.10	0.025	21.59	20.57	N	Ie	S	24.30	23.21	1.09	1.04	0.041	0.054	1.426±0.057	
83	1627		15.16	0.039	19.04	17.59	N	Ia	S	18.83	17.39	1.44	1.46	0.197	0.197	0.024±0.017	
84	1440	I798	15.20	0.028	19.25	17.96	N	Ia	S	19.70	18.38	1.32	1.33	0.063	0.056	0.015±0.014	
85	230	I3101	15.20	0.028	21.14	19.91	Y	Ia	S	20.31	19.22	1.09	1.08	0.038	0.033	0.058±0.032	
86	2050	I3779	15.20	0.023	21.02	19.82	Y	Ia	S	22.38	21.41	0.97	1.08	0.073	0.066	0.037±0.039	
87	1993		15.30	0.025	20.61	19.34	N	Ib	S	...	...	...	...	...	...	0.043±0.052	
88	751	I3292	15.30	0.032	19.92	18.58	N	Ia	S	21.22	20.17	1.05	1.22	0.046	0.035	0.030±0.024	
89	1828	I3635	15.33	0.037	21.40	20.12	Y	Ia	S	21.50	20.50	1.00	1.04	0.060	0.057	0.018±0.070	
90	538	N4309A	15.40	0.020	20.14	18.98	N	Ia	S	21.27	20.15	1.13	1.13	0.033	0.030	0.028±0.016	
91	1407	I3461	15.49	0.032	20.75	19.50	Y	Ia	S	20.39	19.40	0.98	1.08	0.145	0.127	0.060±0.029	
92	1886		15.49	0.033	22.08	21.12	Y	Ia	S	22.05	21.04	1.01	0.97	0.036	0.041	0.022±0.070	
93	1199		15.50	0.022	19.56	17.97	N	Ia	S	19.75	18.39	1.36	1.45	0.075	0.063	0.040±0.036	
94	1743	I3602	15.50	0.019	21.45	20.31	N	Ib	S	...	...	...	...	...	...	0.015±0.078	
95	1539		15.68	0.032	22.01	20.86	Y	Ia	S	20.93	19.81	1.11	1.02	0.231	0.265	0.143±0.063	
96	1185		15.68	0.023	21.89	20.62	Y	Ia	S	20.86	19.91	0.95	1.00	0.057	0.050	0.004±0.069	
97	1826	I3633	15.70	0.017	20.52	19.34	Y	Ia	S	20.10	18.91	1.19	1.17	(0.024)	(0.025)	0.043±0.028	
98	1512		15.73	0.050	20.27	19.42	N	II	cS	...	...	...	...	...	...	...	dIrr/dE
99	1489	I3490	15.89	0.034	22.03	20.98	Y	Ia	S	22.38	21.51	0.87	0.83	0.051	0.058	0.021±0.070	
100	1661		15.97	0.020	22.57	21.34	Y	Ia	S	20.30	19.25	1.05	1.02	0.079	0.082	0.027±0.069	

Key to Columns:
(1) identification number;
(2) Virgo Cluster Catalog (VCC) number (Binggeli, Sandage & Tammann (1987);
(3) alternative names in the Messier, NGC, UGC or IC catalogs;
(4) total blue magnitude from VCC;
(5) extinction from Schlegel, Finkbeiner & Davis (1998);
(6-7) g- and z-band surface brightness measured at a geometric radius of $0\farcs1$
(8) nuclear classification in VCC;
(9) nuclear classification (see Table 2);
(10) model used fit the galaxy brightness profile: (cS) = core-Sérsic; (S) = Sérsic;
(11-12) g- and z-band magnitudes for nucleus;
(13) integrated color of nucleus;
(14) nucleus color within a 4-pixel aperture;
(15-16) King model half-light radii in the g- and z-bands. Radii in parantheses indicate that the nucleus is formally unresolved in our images;
(17) offset from galaxy photocenter in arcseconds;
(18) comments on galaxy morphology, AGN and dust properties. Magnitudes and colors in this table have not been corrected for extinction.
[a] Low-level radio emission detected by Wrobel (1991) and/or Ho et al. (1997).
[b] Central $\lesssim 0.3''$saturated in F475W images.
[c] Fr I radio galaxy (e.g., Ho 1999; Chiaberge et al. 1999).
[d] LINER galaxy according to Ho et al. (1997).
[e] Galaxy classified as Sérsic in Paper VI.

TABLE 2. NUCLEAR CLASSIFICATIONS FOR THE ACS VIRGO CLUSTER SURVEY.

Classification	Number
No Classification Possible (Type 0)	
Dust	4
AGN	2
Total	**6**
Nucleated (Type I)	
fitted nucleus (Ia)	51
no fit possible (Ib)	11
Total	**62**
Non-Nucleated (Type II)	**12**
Uncertain (Type I)	
likely nucleated (Ic)	4
possibly nucleated (Id)	11
possible offset nucleus (Ie)	5
Total	**20**
All Galaxies	**100**

Table 3. Comparison of Nuclear Classifications from Previous *HST* Studies.

VCC	Other	M_B (mag)	Rest et al. (2001)	Ravindranath et al. (2001)	Lauer et al. (2005)	Lotz et al. (2004)	ACSVCS
1226	NGC4472	-21.87	···	no	yes	···	no (II)
1978	NGC4649	-21.39	···	···	no	···	no (II)
881	NGC4406	-21.15	···	no	yes	···	no (II)
798	NGC4382	-21.13	···	···	···	···	no (II)
763	NGC4374	-21.01	···	yes	···	···	AGN (O)
731	NGC4365	-20.67	no	···	yes	···	yes (Ib)
1632	NGC4552	-20.49	···	···	yes	···	no (II)
1903	NGC4621	-20.47	no	···	no	···	possibly (Id)
1231	NGC4473	-20.11	···	···	no	···	no (II)
2000	NGC4660	-19.30	···	···	no	···	possibly (Id)
1664	NGC4564	-19.21	no	···	···	···	probably (Ic)
944	NGC4417	-19.12	···	no	···	···	probably (Ic)
1279	NGC4478	-19.04	no	···	yes	···	possibly (Id)
1242	NGC4474	-18.67	yes (II)	···	···	···	yes (Ia)
1146	NGC4458	-18.26	···	···	no	···	yes (Ia)
1261	NGC4482	-17.65	yes (III)	···	···	···	yes (Ia)
9	IC3019	-17.33	···	···	···	no	possible offset (Ie)
1297	NGC4486B	-16.85	···	···	no	···	possibly (Id)
543	UGC7436	-16.93	···	···	···	no	yes (Ia)
1948	IC3693	-16.10	···	···	···	no	possible offset (Ie)

Note: Classifications from Rest et al. (2001) vary from I (weakly nucleated) to III (strongly nucleated).

TABLE 4. LUMINOSITY FUNCTION PARAMETERS.

	A_n	$\overline{m}_n^0$ (mag)	σ_n (mag)	$\overline{M}_n^{0\,a}$ (mag)
g	12.3±1.1	20.35±0.18	1.47±0.16	–10.74±0.23
z	11.5±0.9	19.12±0.19	1.77±0.15	–11.97±0.24

TABLE 5. GLOBAL PROPERTIES OF NUCLEI AND ULTRA COMPACT DWARFS.

Parameter	Nuclei	UCDs
r_h (pc)	≤2–62 4.2±3.8 (med.)	25.9±9.1
$\langle\mu_{h,g}\rangle$ (mag arcsec^{-2})	16.5±1.5	19.2±0.5
$\langle\mu_{h,z}\rangle$ (mag arcsec^{-2})	15.2±1.6	18.5±0.6
$\langle M_g\rangle$ (mag)	−10.9±1.7	−11.2±0.6
$\langle M_z\rangle$ (mag)	−12.0±1.9	−12.2±0.6
$\langle(g-z)_{AB}\rangle$ (mag)	0.67–1.61 1.13±0.25	1.03±0.06

TABLE 6. MEAN METALLICITIES FOR GALACTIC NUCLEI.

$(g-z)_0$-[Fe/H]	τ (Gyr)	$\langle$[Fe/H]$\rangle$ (dex)
Bruzual & Charlot (2003)	1	+0.82±0.52
	2	+0.04±0.64
	5	−0.54±0.65
	10	−0.90±0.71
Peng et al. (2006)[a]	···	−0.88±0.79

[a] Adopted Virgo distance: 16.52±0.22 (random) ±1.14 (systematic) Mpc.
[a] Broken linear relation based on gz photometry and spectroscopic metallicities for 95 globular clusters in the Milky Way, M49 and M87 (Peng et al. 2006 = Paper IX).

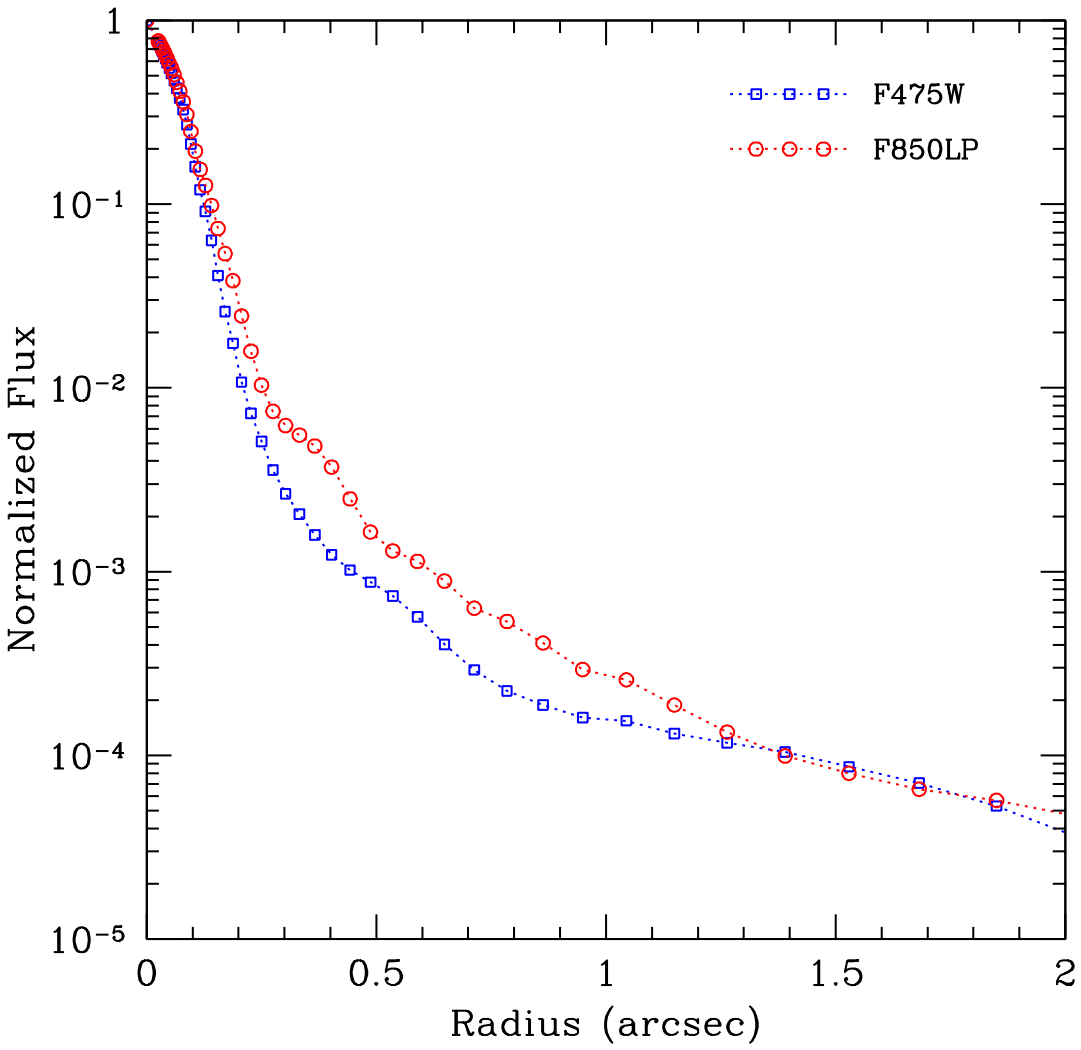

FIG. 1.— Azimuthally-averaged point spread functions for the nucleus of VCC1303, the galaxy closest to the mean position of the centers for the full sample of galaxies. The profiles for F475W and F850LP are shown as squares and circles, respectively. The profiles have been normalized to the same central intensities.

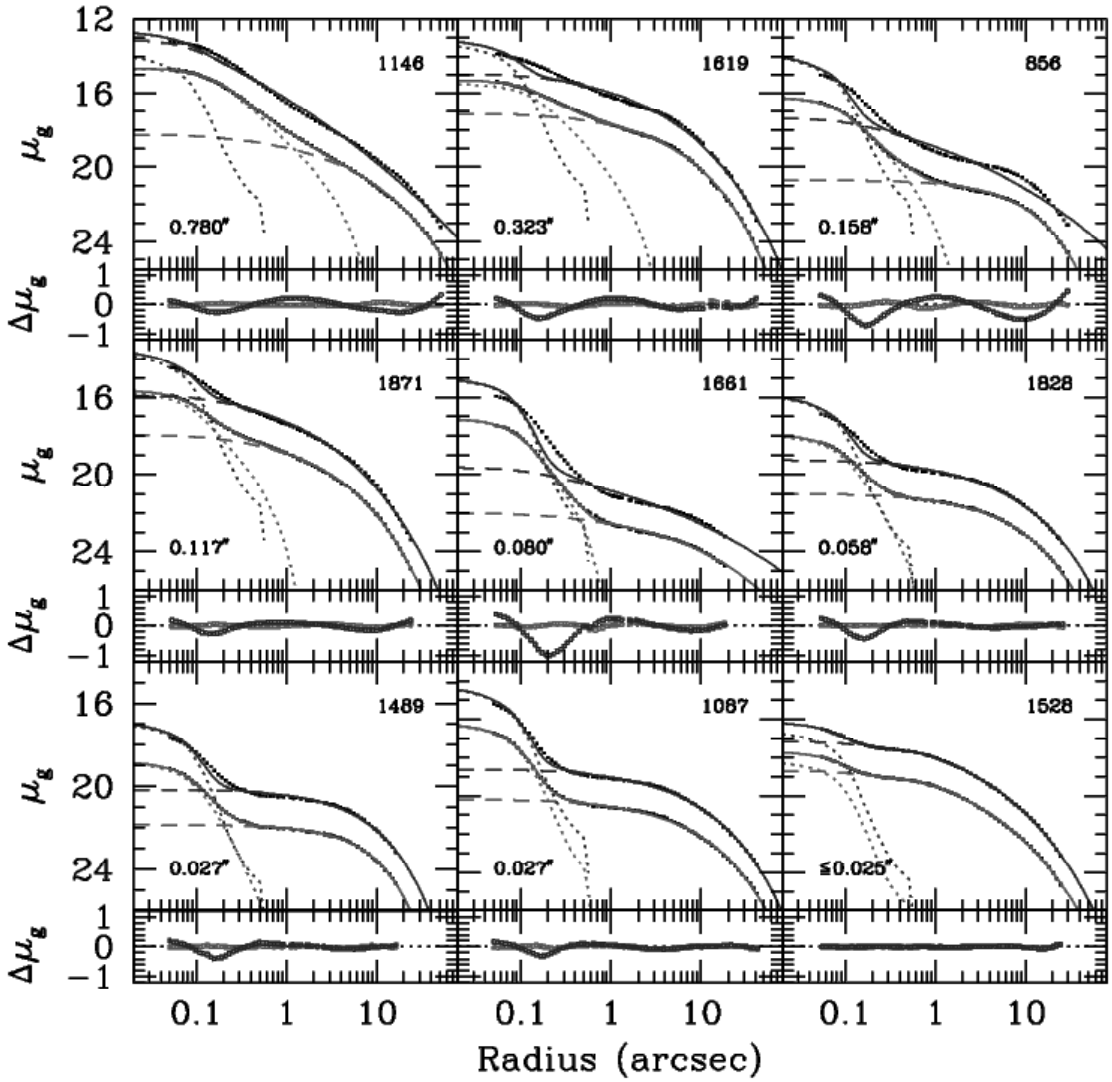

FIG. 2.— Surface brightness profiles for nine Type Ia galaxies whose nuclei span the full range in half-light radius. In each panel, we show the azimuthally-averaged brightness profile in the g band (small squares) along with the fitted models. The respective components for the nucleus and galaxy (a Sersic model in all cases except for VCC1528, where a core-Sésic model was used) are shown as the dotted and short dashed curves. Two different assumptions for the nucleus component are shown for each galaxy — red curves show the results obtained for a King model while blue curves show the results obtained by fitting a central point source. In the latter case, both the data and model have been shifted upwards by 1.5 mag for clarity. Residuals about the fitted relations, $\Delta\mu_g$, are shown below in each panel. For VCC1528, the best-fit half-light radius of $r_{h,g} = 0\farcs015$ falls below the resolution limit of $0\farcs025$, meaning that the nucleus is formally unresolved in this case. In the eight remaining cases, a point-source nucleus provides an inadequate representation of the measured brightness profiles. The median half-light radii measured for the sample of Type Ia galaxies (see §4.1) are $0\farcs051$ (g band) and $0\farcs048$ (z band).

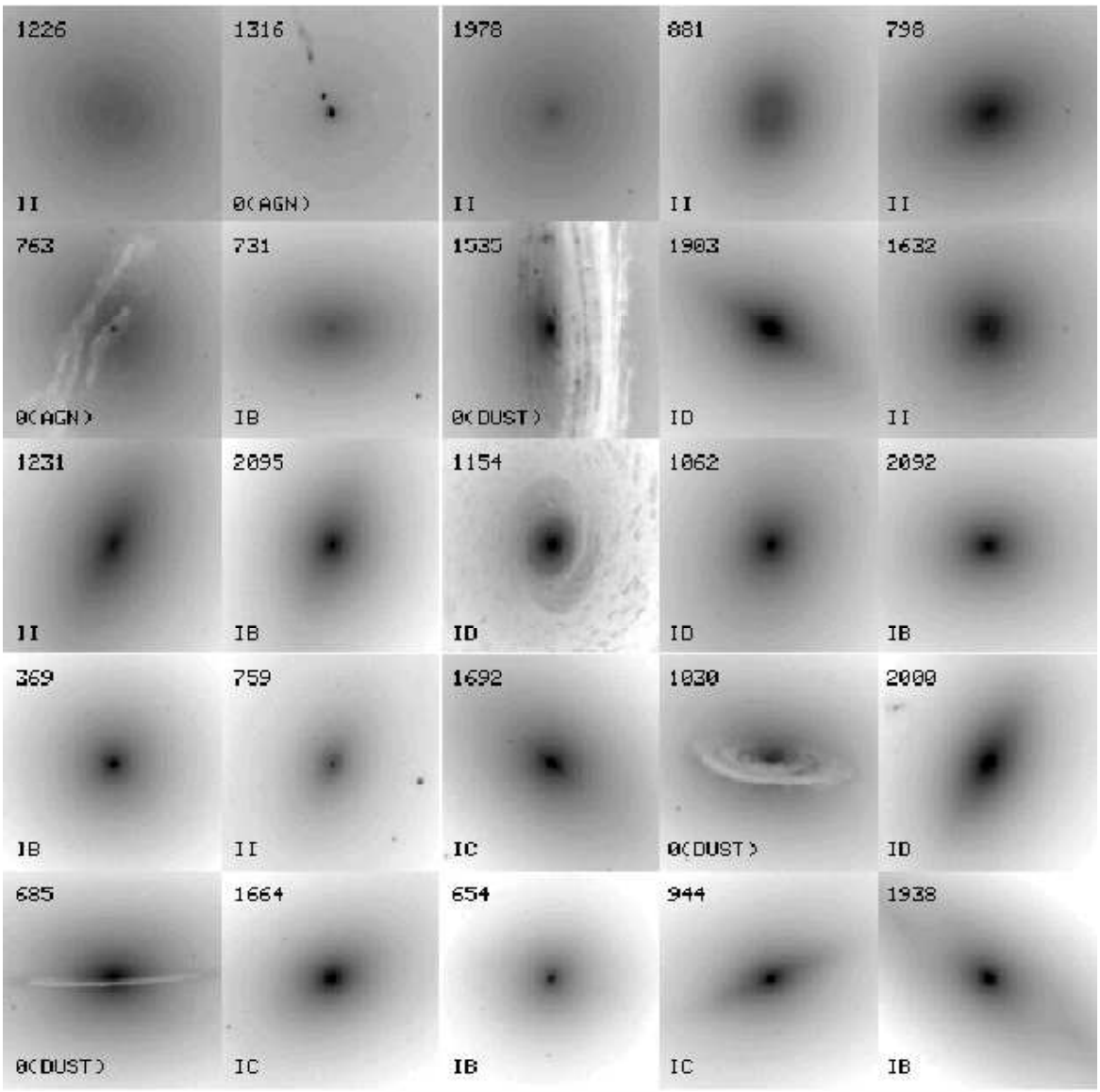

FIG. 3.— F475W (g) images for galaxies from the ACS Virgo Cluster Survey. Panels show the inner $10'' \times 10''$ ($\approx 800 \times 800$ pc) of each galaxy. Galaxies are rank ordered by blue magnitude, which increases from left to right and from top to bottom (i.e., decreasing luminosity). Classifications from Table 1 are reported in the lower left corner of each panel. The classification scheme itself is summarized in Table 2. For those galaxies with possible offset nuclei (Type Ie galaxies), the arrow shows the presumed nucleus while the cross indicates the galaxy photocenter. Only the brightest 25 galaxies are included in this submission; images for the remaining galaxies can be found in the version posted on the ACSVCS webpage: http://www.cadc.hia.nrc.gc.ca/community/ACSVCS/publications.html#acsvcs8.

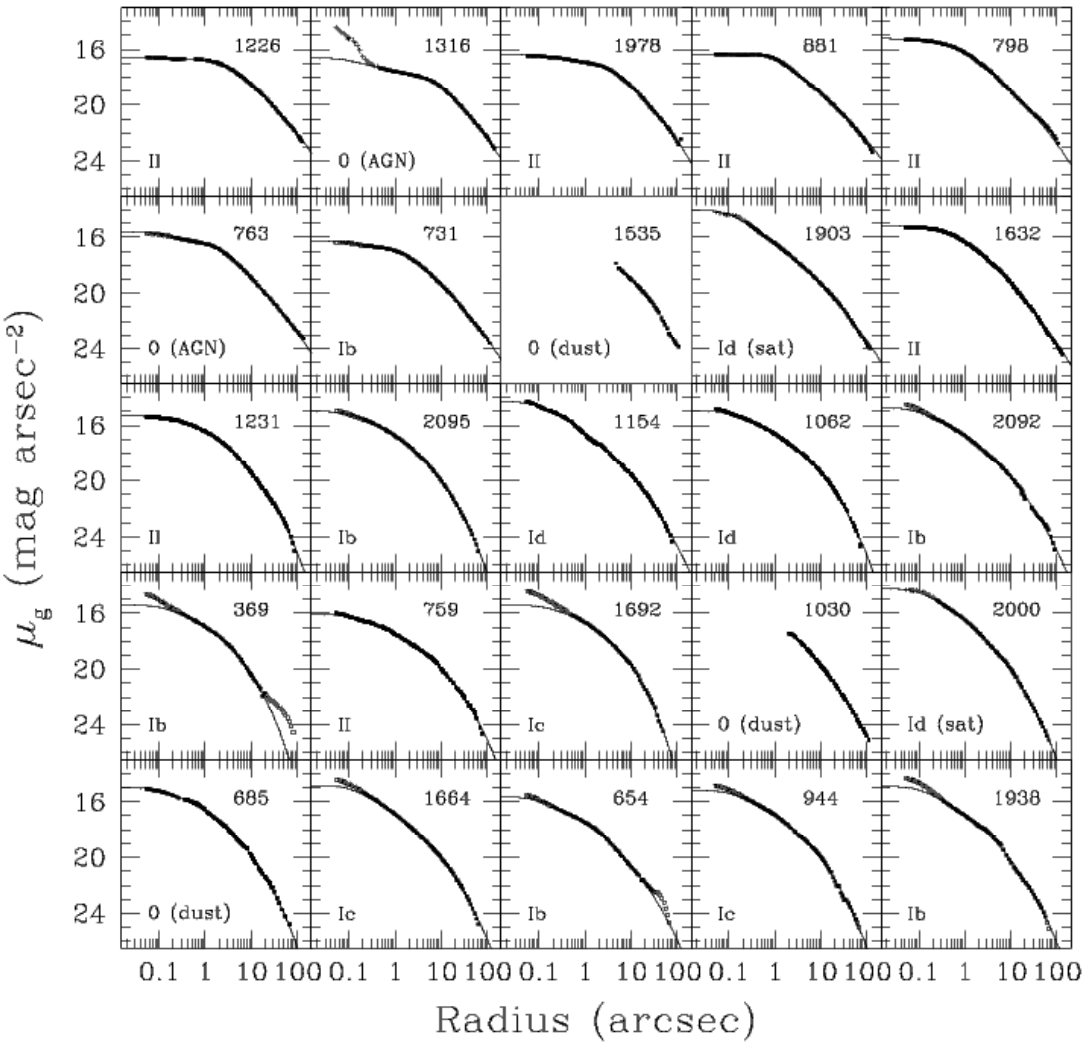

FIG. 4.— Azimuthally-averaged g-band surface brightness profiles for the galaxies from the ACS Virgo Cluster Survey (see Figure 3). The galaxies are rank ordered by blue magnitude, which decreases from left to right and from top to bottom. Classifications from Table 1 are reported in the lower left corner of each panel. The classification scheme itself is summarized in Table 2. In each panel, the solid curve shows the best-fit galaxy model; open symbols show datapoints that were excluded during the fitting of the models. For Type Ia galaxies, dashed and dotted curves show the respective models for the galaxy and the nucleus. The fitted models for galaxies with possible offset nuclei (the Type Ie galaxies) do not include components for the nuclei. For VCC1316, VCC1903 and VCC2000, the crosses show regions affected by saturation of the F475W images; these regions were excluded when fitting models to the brightness profiles. The brightness profiles for two galaxies (VCC1192 and VCC1199) flatten outside of $\approx 10'$ due to contamination from the halo of VCC1226 (M49), which is $\lesssim 5'$ away in both cases. These outer points have been excluded in the fits.

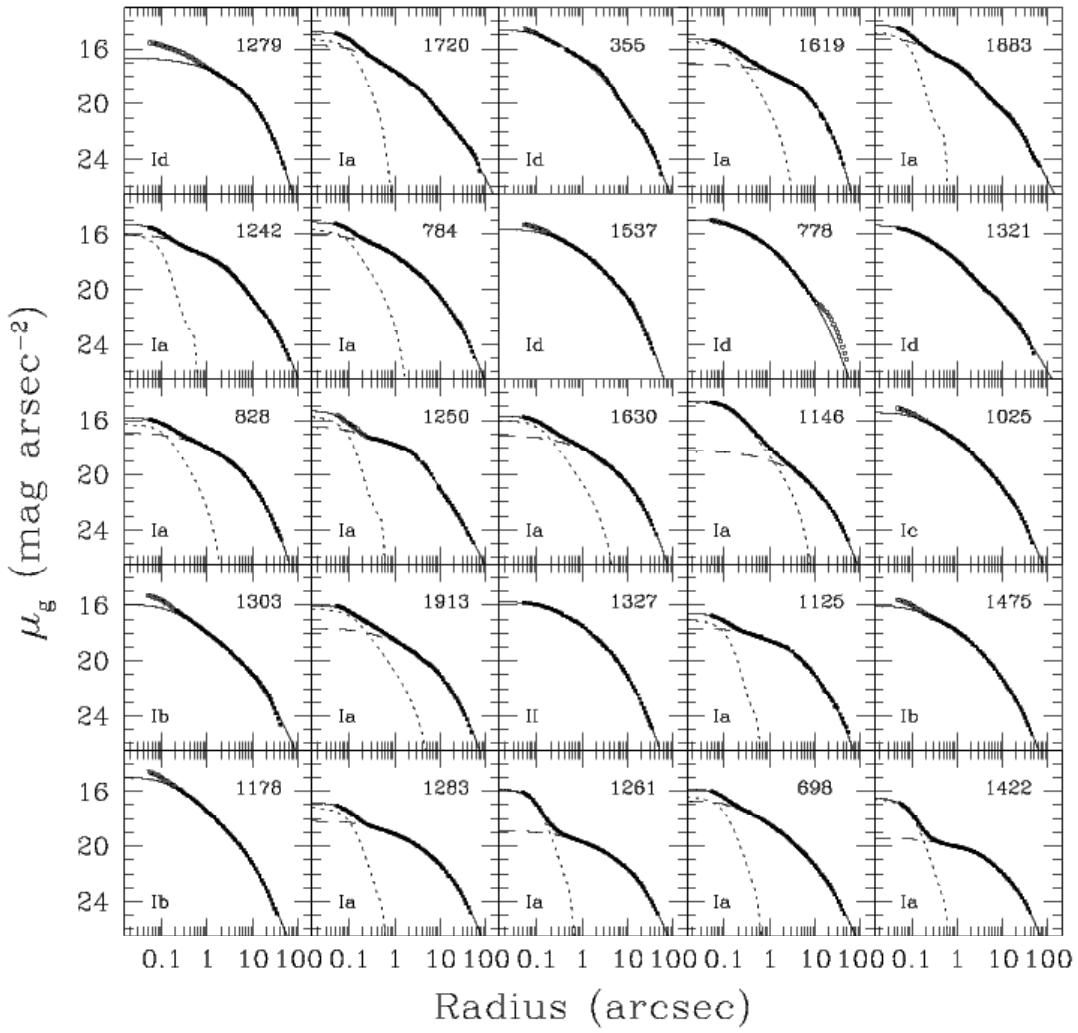

FIG. 4.— Azimuthally-averaged g-band surface brightness profiles for the galaxies from the ACS Virgo Cluster Survey (see Figure 3). The galaxies are rank ordered by blue magnitude, which decreases from left to right and from top to bottom. Classifications from Table 1 are reported in the lower left corner of each panel. The classification scheme itself is summarized in Table 2. In each panel, the solid curve shows the best-fit galaxy model; open symbols show datapoints that were excluded during the fitting of the models. For Type Ia galaxies, dashed and dotted curves show the respective models for the galaxy and the nucleus. The fitted models for galaxies with possible offset nuclei (the Type Ie galaxies) do not include components for the nuclei. For VCC1316, VCC1903 and VCC2000, the crosses show regions affected by saturation of the F475W images; these regions were excluded when fitting models to the brightness profiles. The brightness profiles for two galaxies (VCC1192 and VCC1199) flatten outside of $\approx 10'$ due to contamination from the halo of VCC1226 (M49), which is $\lesssim 5'$ away in both cases. These outer points have been excluded in the fits.

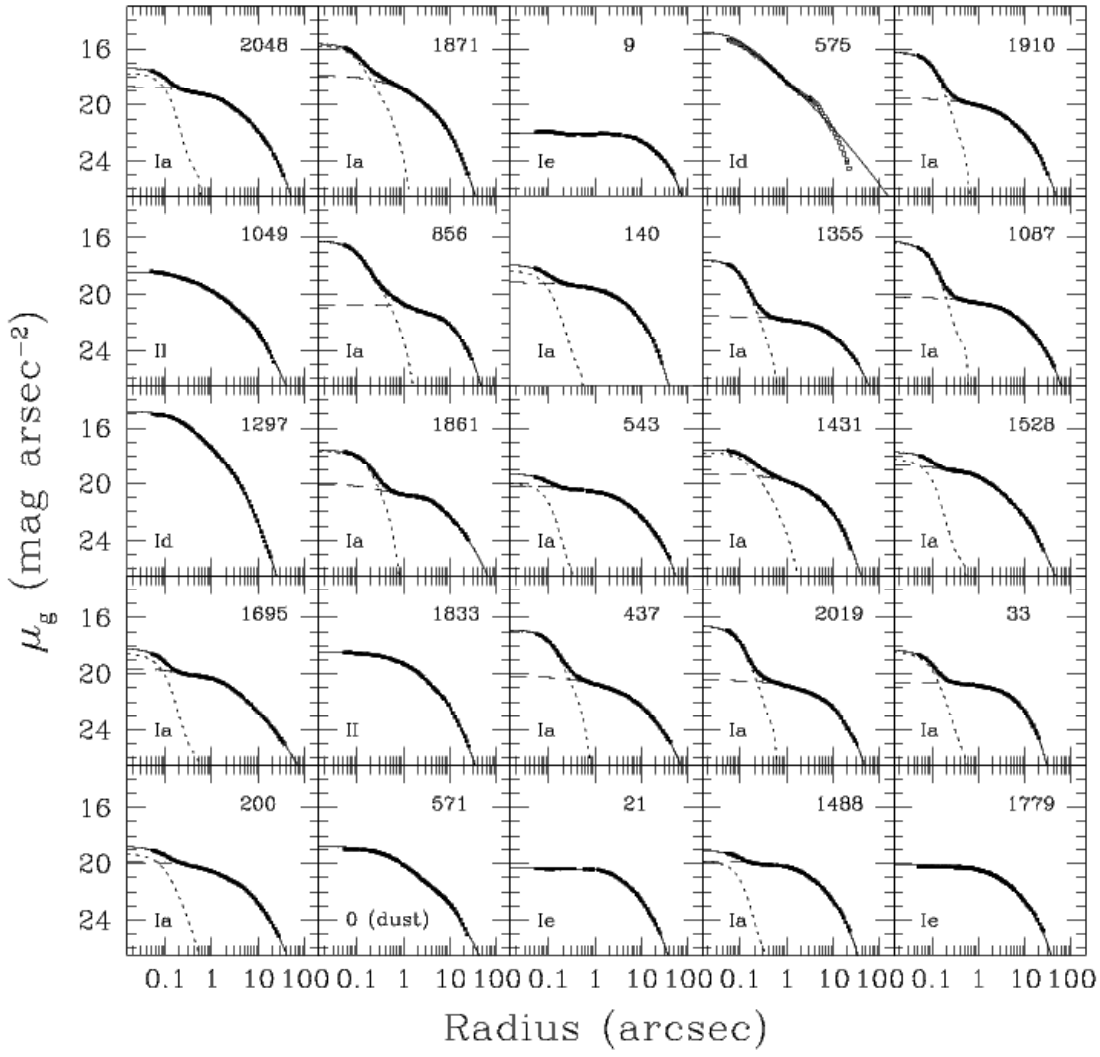

FIG. 4.— Azimuthally-averaged g-band surface brightness profiles for the galaxies from the ACS Virgo Cluster Survey (see Figure 3). The galaxies are rank ordered by blue magnitude, which decreases from left to right and from top to bottom. Classifications from Table 1 are reported in the lower left corner of each panel. The classification scheme itself is summarized in Table 2. In each panel, the solid curve shows the best-fit galaxy model; open symbols show datapoints that were excluded during the fitting of the models. For Type Ia galaxies, dashed and dotted curves show the respective models for the galaxy and the nucleus. The fitted models for galaxies with possible offset nuclei (the Type Ie galaxies) do not include components for the nuclei. For VCC1316, VCC1903 and VCC2000, the crosses show regions affected by saturation of the F475W images; these regions were excluded when fitting models to the brightness profiles. The brightness profiles for two galaxies (VCC1192 and VCC1199) flatten outside of $\approx 10'$ due to contamination from the halo of VCC1226 (M49), which is $\lesssim 5'$ away in both cases. These outer points have been excluded in the fits.

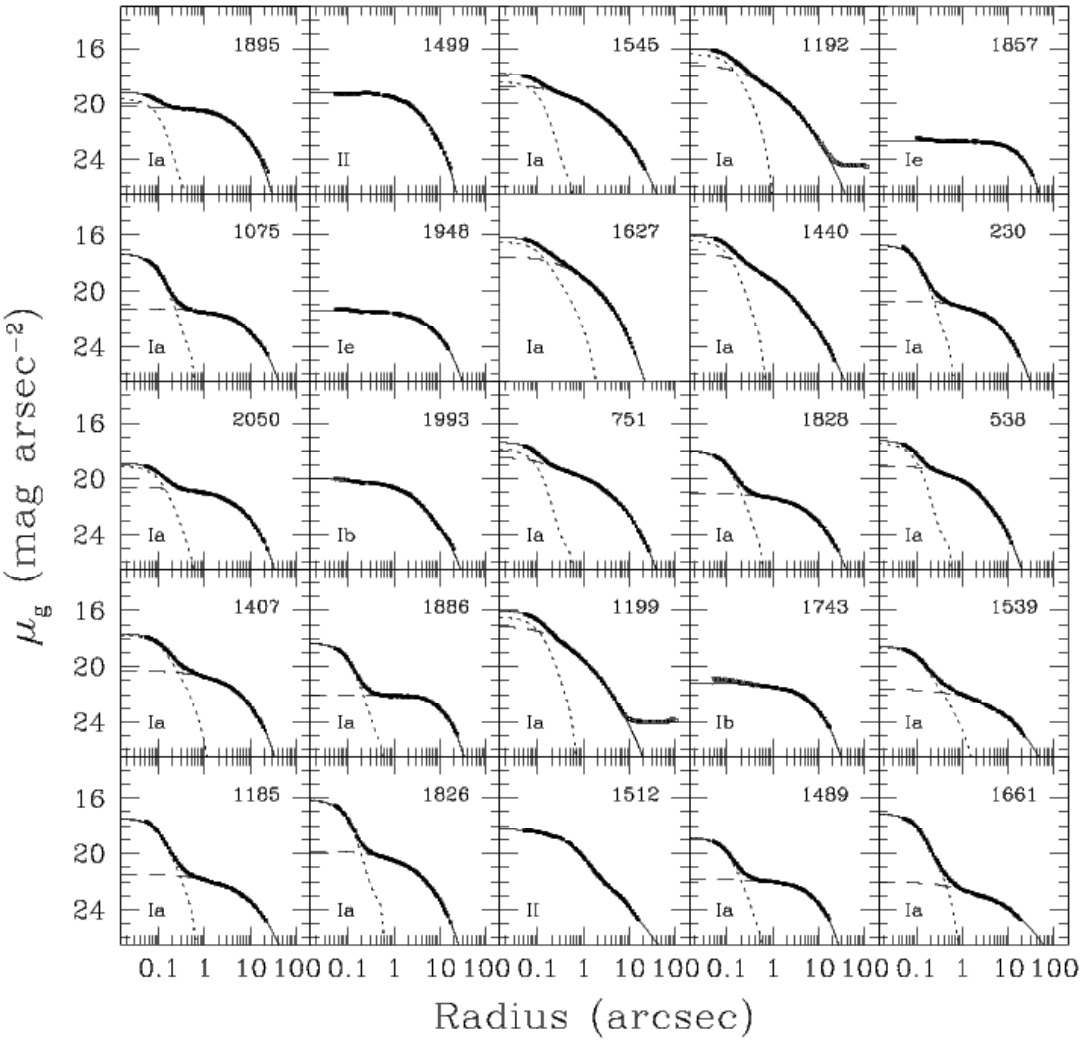

FIG. 4.— Azimuthally-averaged g-band surface brightness profiles for the galaxies from the ACS Virgo Cluster Survey (see Figure 3). The galaxies are rank ordered by blue magnitude, which decreases from left to right and from top to bottom. Classifications from Table 1 are reported in the lower left corner of each panel. The classification scheme itself is summarized in Table 2. In each panel, the solid curve shows the best-fit galaxy model; open symbols show datapoints that were excluded during the fitting of the models. For Type Ia galaxies, dashed and dotted curves show the respective models for the galaxy and the nucleus. The fitted models for galaxies with possible offset nuclei (the Type Ie galaxies) do not include components for the nuclei. For VCC1316, VCC1903 and VCC2000, the crosses show regions affected by saturation of the F475W images; these regions were excluded when fitting models to the brightness profiles. The brightness profiles for two galaxies (VCC1192 and VCC1199) flatten outside of $\approx 10'$ due to contamination from the halo of VCC1226 (M49), which is $\lesssim 5'$ away in both cases. These outer points have been excluded in the fits.

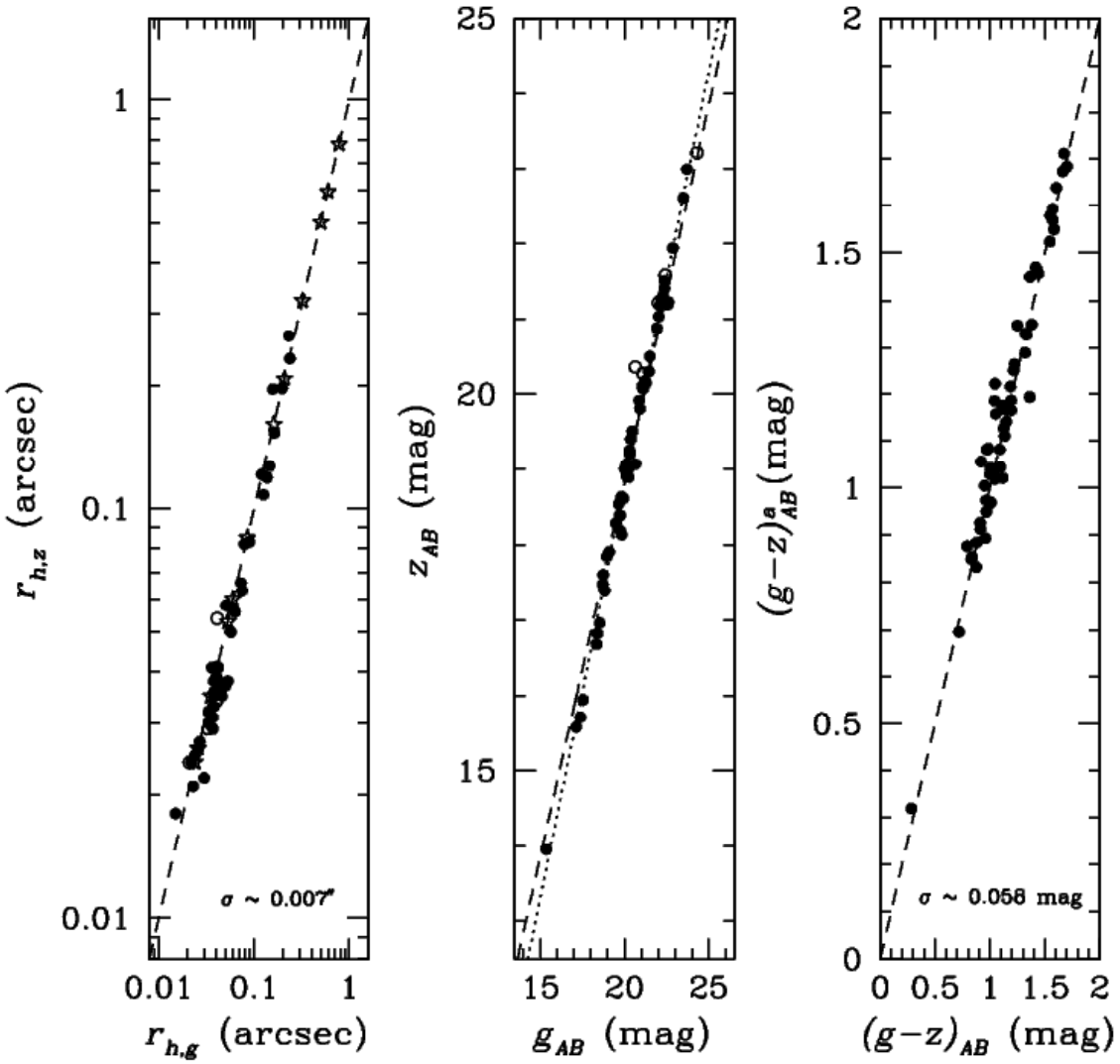

FIG. 5.— *(Left Panel)*: Comparison of the King model half-light radii, r_h, measured for the nuclei in the F850LP (z) and F475W (g) filters (filled circles). The 51 nuclei with reliable photometric and structural measurements are shown by the filled circles and open stars. The latter symbols indicate the 11 galaxies with $B_T \leq 13.5$, for which the half-light radii were constrained to be the same in the two bandpasses. The five galaxies with possible offset nuclei are shown as open circles. The dashed line shows the one-to-one relation. *(Middle Panel)*: Comparison of the measured z- and g-band magnitudes for the nuclei. The dotted line shows the least-squares line of best fit. The dashed line shows the relation corresponding to the mean color of the nuclei: $\langle (g-z) \rangle = 1.15$ mag. *(Right Panel)*: Comparison of the nuclei colors obtained by direct integration of the best-fit model, $(g-z)_{AB}$, with those from 4-pixel aperture measurements, $(g-z)^a_{AB}$. The dashed line shows the one-to-one relation.

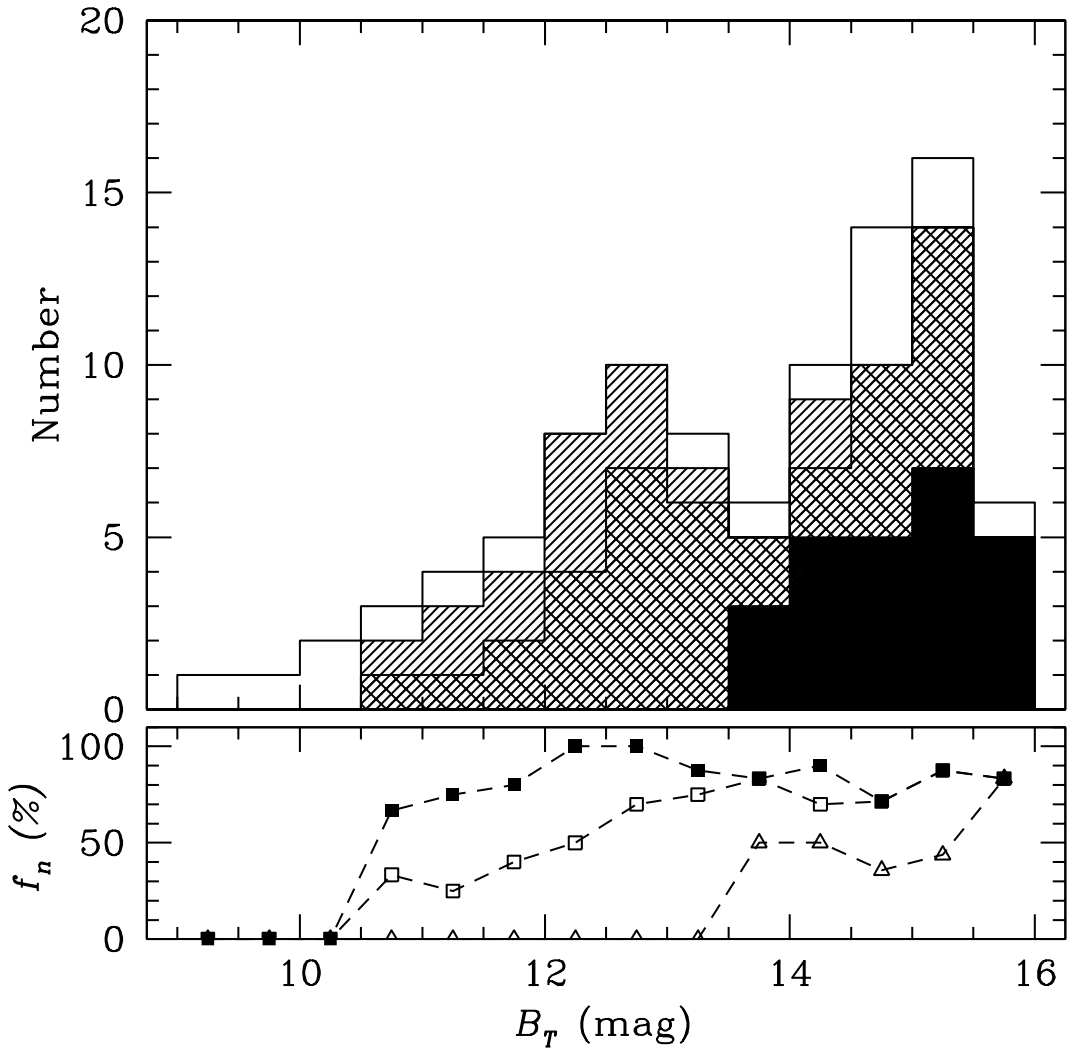

FIG. 6.— *(Upper Panel)* Luminosity distribution of the 94 program galaxies for which a classification as nucleated or non-nucleated is possible from our ACS images (open histogram). The double-hatched histogram shows the luminosity distribution for the 62 galaxies which we classify unambiguously as nucleated (i.e., Types Ia and Ib). The hatched histogram shows this same sample plus the 15 galaxies which *may* have central nuclei (i.e., Types Ia and Ib, plus Types Ic and Id). The solid histogram shows the 25 galaxies in our survey which were classified as nucleated in the Virgo Cluster Catalog (Binggeli, Sandage & Tammann 1985). *(Lower Panel)* Percentage of nucleated galaxies, f_n, as a function of blue magnitude. Open and filled squares show the frequency of nucleation for Types Ia and Ib (62 galaxies) and Types Ia, Ib, Ic and Id (77 galaxies). Open triangles show results found using the classifications of Binggeli, Sandage & Tammann (1985).

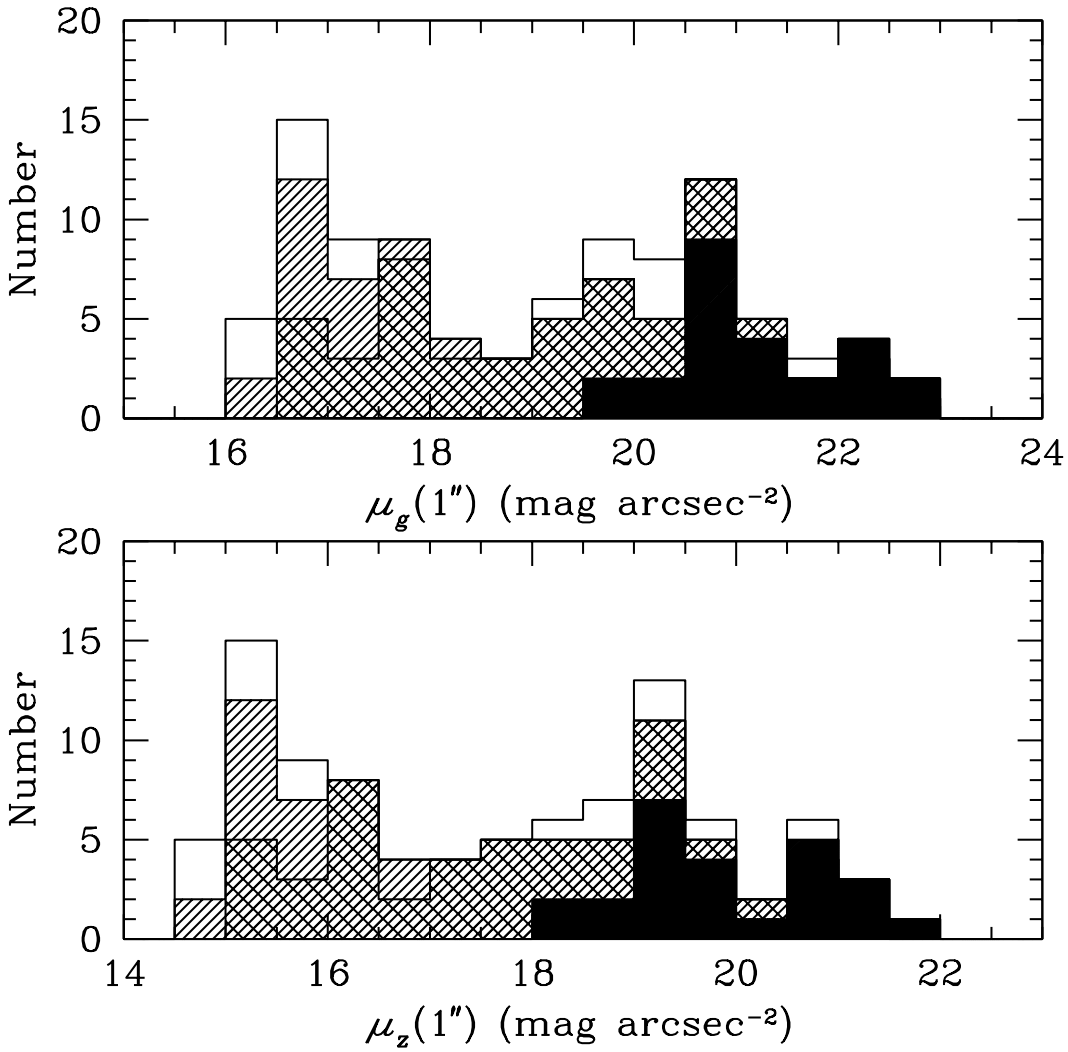

FIG. 7.— *(Upper Panel)* Distribution of g-band surface brightnesses, measured at a geometric mean radius of $1''$, for the 94 galaxies from the ACS Virgo Cluster Survey for which a classification as nucleated or non-nucleated is possible (open histogram). The hatched histogram shows the luminosity distribution for the 62 galaxies which we classify unambiguously as nucleated (i.e., Types Ia and Ib). The double-hatched histogram shows this same sample plus the 15 galaxies which *may* have central nuclei (i.e., Types Ia, Ib, Ic or Id). The 25 ACS Virgo Cluster Survey galaxies classified as nucleated in Binggeli, Sandage & Tammann (1985) are shown by the filled histogram. *(Lower Panel)* Same as above, except for the z band.

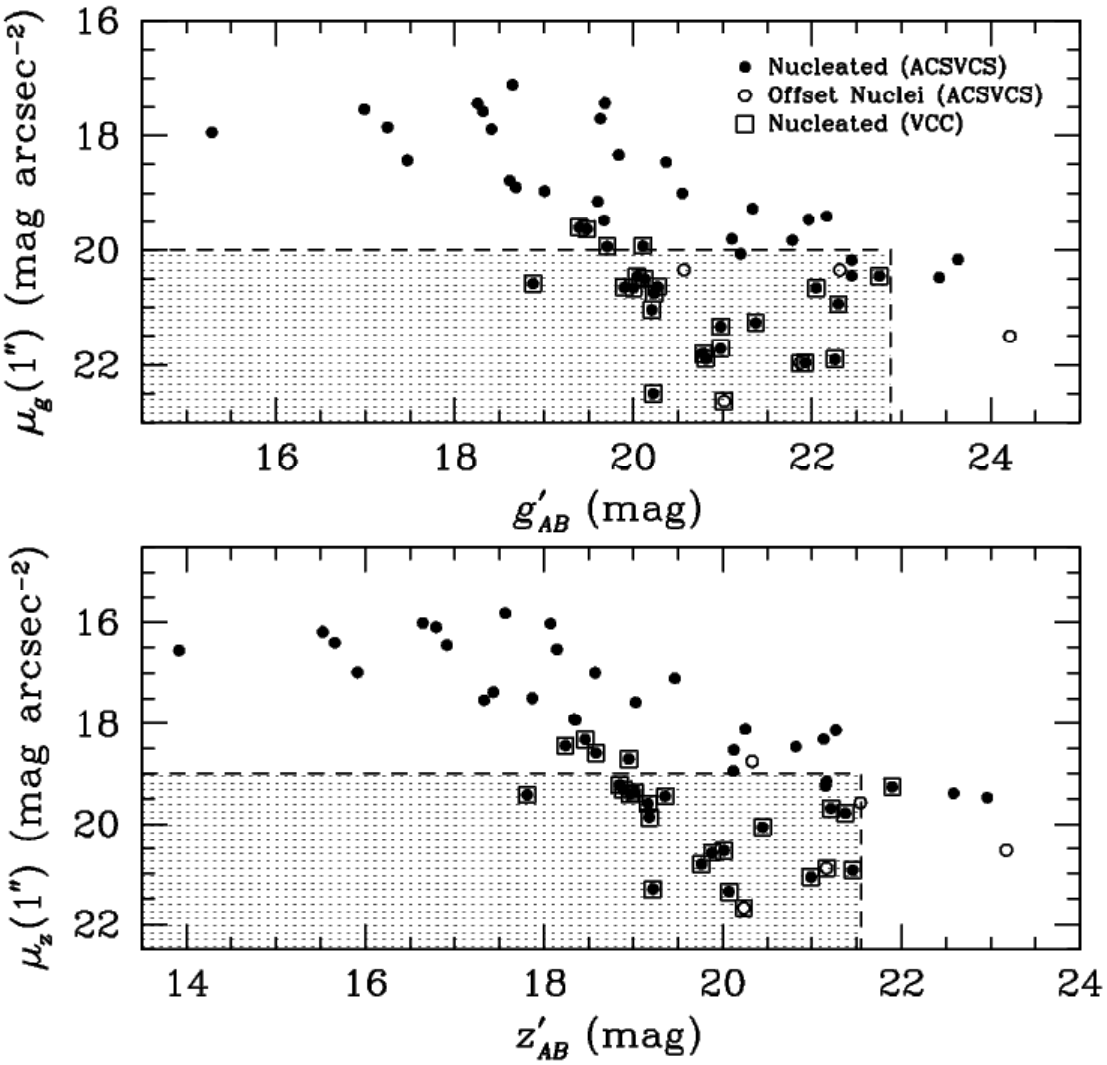

FIG. 8.— *(Upper Panel)*: Galaxy g-band surface brightness, measured at a geometric mean radius of $1''$, plotted against the dereddened magnitude of the nucleus. Filled circles represent the 51 galaxies in our survey which show unambiguous evidence for a nucleus at or near their photocenters, and for which we are able to measure reliable photometric and structural parameters (i.e., Type Ia galaxies). Open circles show the five galaxies with possible offset nuclei (i.e., Type Ie galaxies). Open squares show the 25 galaxies classified as nucleated by Binggeli, Sandage & Tammann (1985). The shaded region shows the approximate region of the magnitude vs. surface brightness plane where selection effects were relatively unimportant in the survey of Binggeli, Tammann & Sandage (1987). *(Lower Panel)*: Same as above, except for the z band.

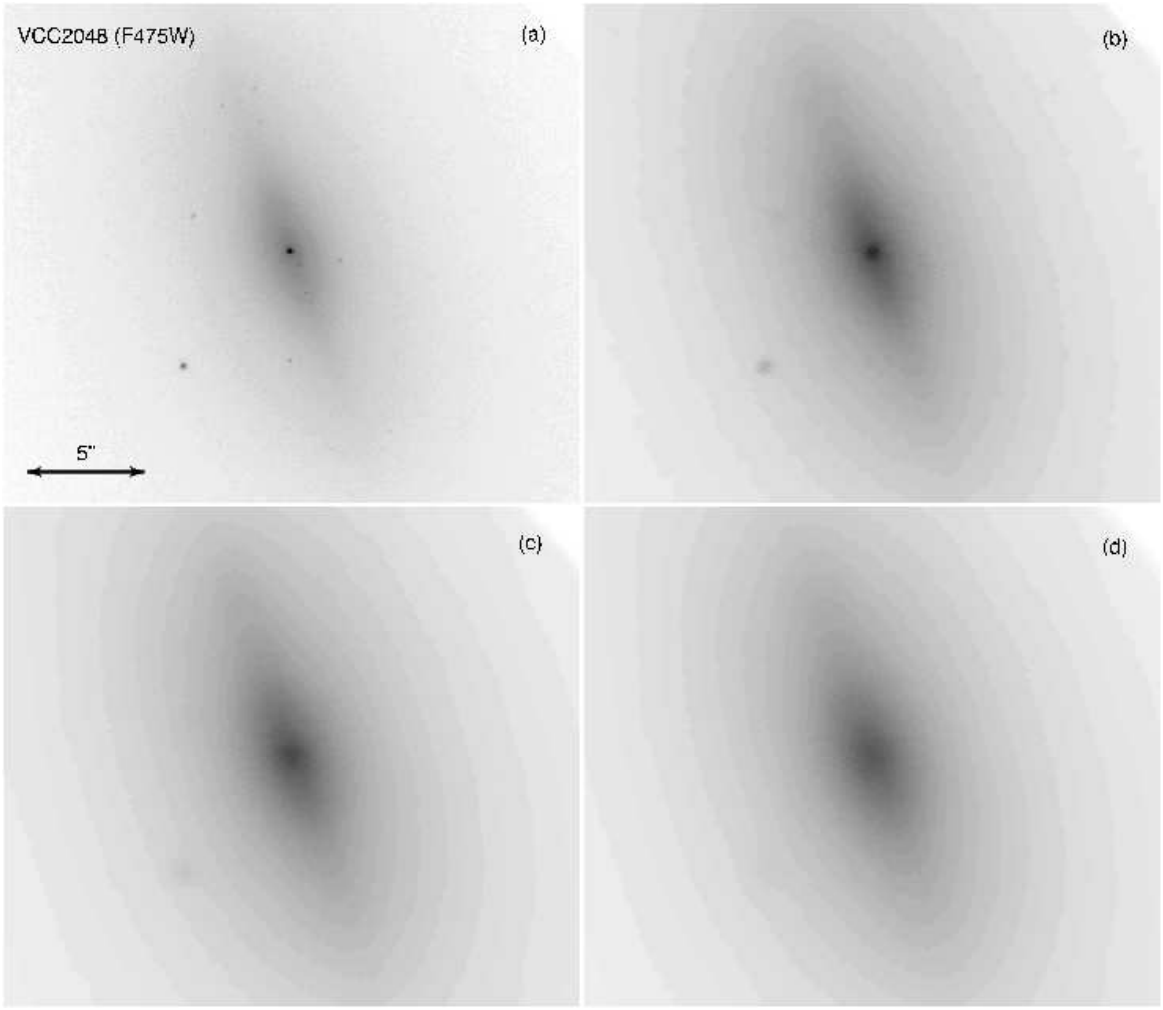

FIG. 9.— *(Panel a)*: A magnified view of the F475W image of VCC2048 (IC3773). This is the brightest dwarf galaxy in our sample according to the morphological classifications of Binggeli, Sandage and Tamman (1985). It is classified as non-nucleated in the Virgo Cluster Catalog, with type d:S0(9). *(Panels b–d)*: The same image, after binning 4×4 pixels and convolving with Gaussians of FWHM = 0.″5, 0.″9 and 1.″4, respectively.

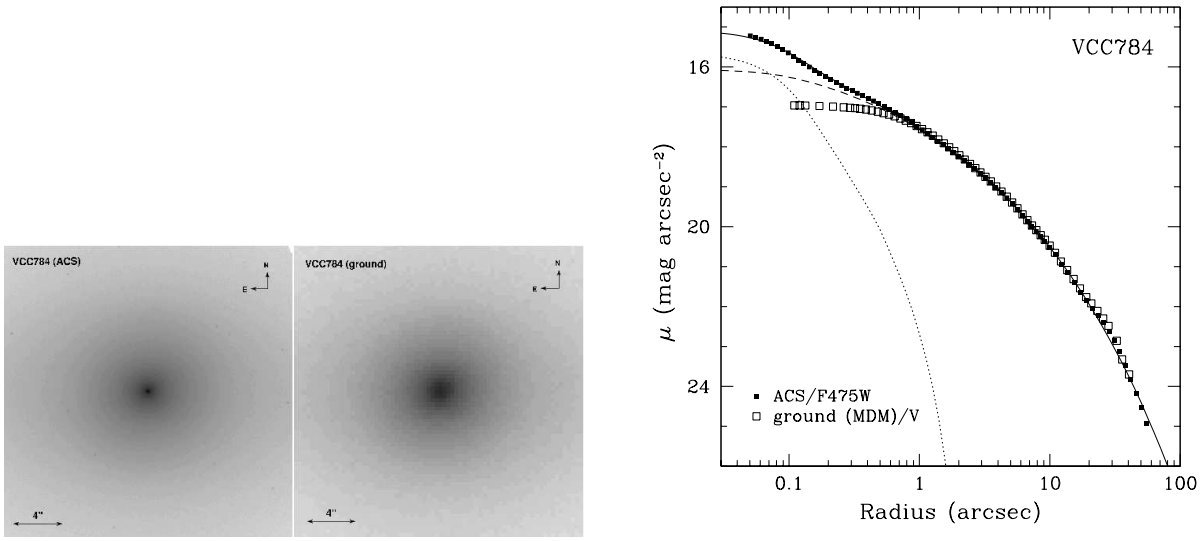

FIG. 10.— *(First Panel)* F475W (g) image for VCC784 (NGC4379), one of the brightest Type Ia galaxies in our survey. *(Second Panel)* Ground-based V-band image of VCC784, taken with the 2.4m Hiltner telescope (FWHM = $1\farcs14$). *(Third Panel)* Comparison of surface brightness profiles measured for VCC784 using the ACS (filled squares) and ground-based images (open squares). To aid in the comparison, the V-band profile has been matched to the ACS profile at a radius of $1''$. The best-fit two-component model for the galaxy and nucleus based on the ACS profile are shown by the dashed and dotted curves. The solid curve shows the combined profile.

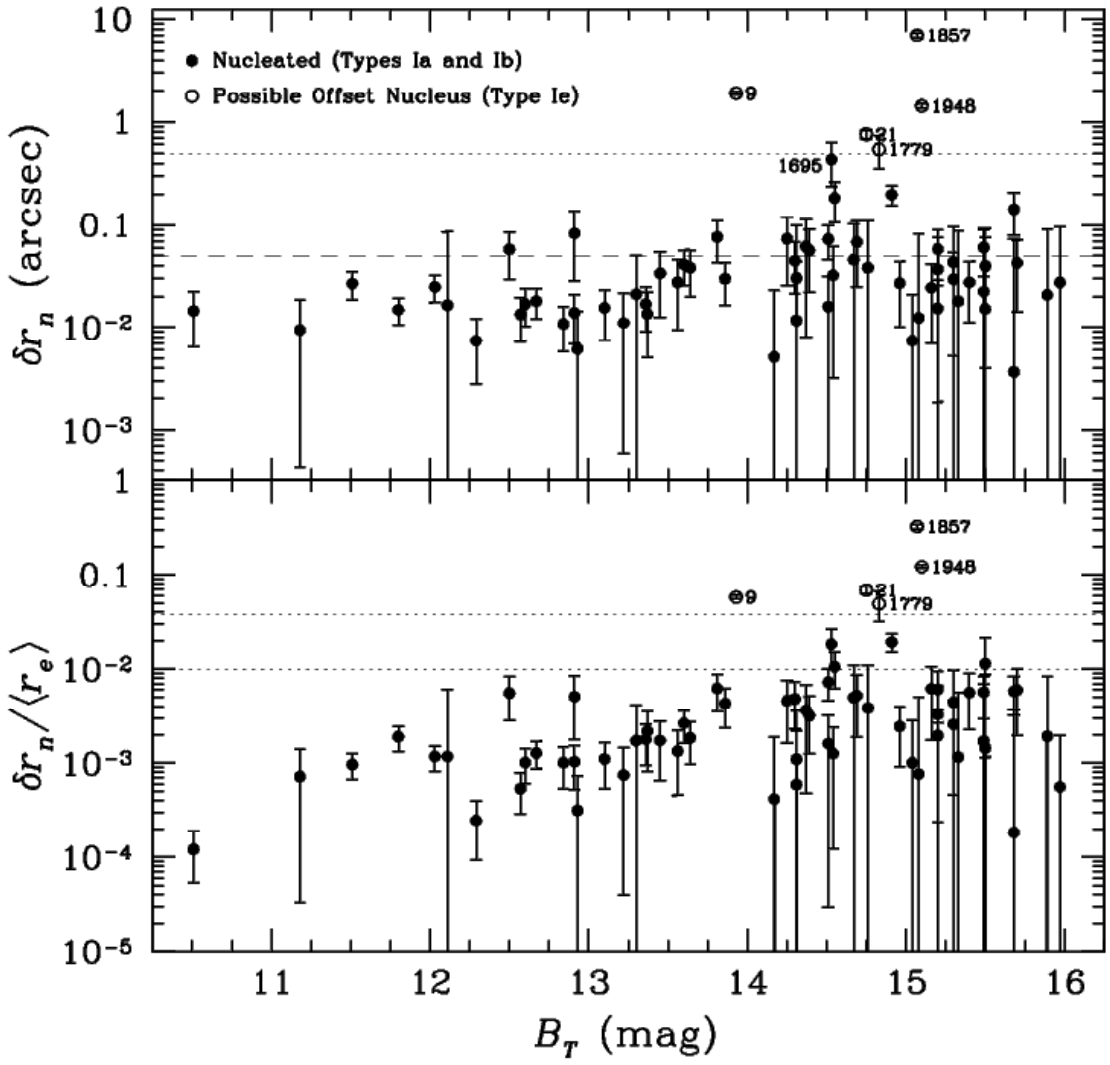

FIG. 11.— *(Upper Panel)*: Projected offset, δr_n, between the position of the galaxy center and that of the nucleus, plotted as a function of galaxy magnitude. Filled circles show 62 galaxies of Types Ia and Ib. Open circles indicate the five galaxies in our sample which may have offset nuclei (Type Ie). The dotted line shows an offset of $\delta r_n = 0\farcs5$, or ten ACS/WFC pixels; a single pixel is represented by the lower, dashed line. *(Lower Panel)* Ratio of the offset to the mean effective radius, $\langle r_e \rangle$, of the host galaxy in the two bands, plotted as a function of galaxy magnitude. The symbols are the same as in the previous panel. The upper dotted line in this case is drawn at $\delta r_n/\langle r_e \rangle = 0\farcs5/13\farcs13 \approx 0.038$, where $\langle r_e \rangle = 13\farcs13$ is the mean effective radius of Type Ia galaxies. The lower dotted line is drawn at a fractional offset of 1% the effective radius. A total of nine galaxies lie above this lower line.

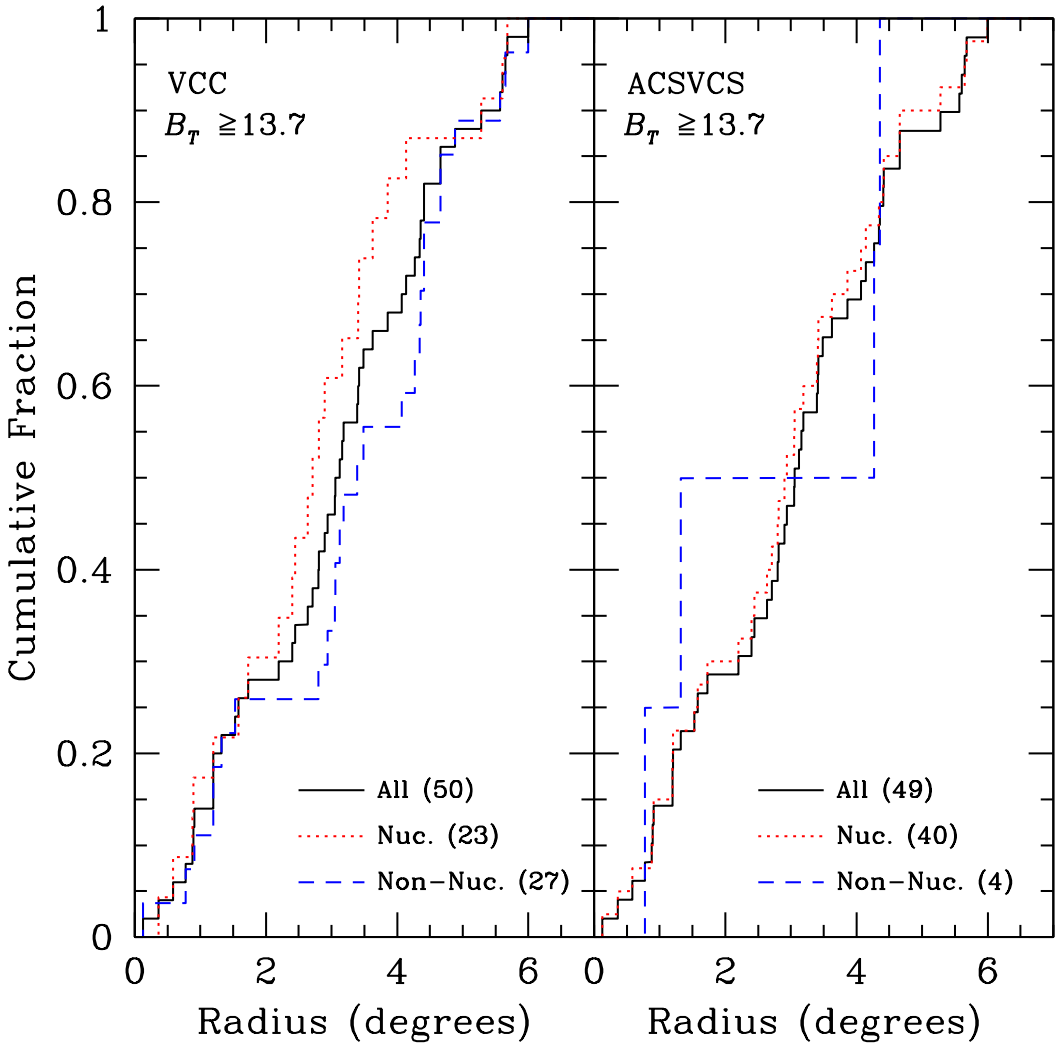

FIG. 12.— *(Left Panel)*: Cumulative distribution of Virgocentric radii for the 50 galaxies from the ACS Virgo Cluster Survey fainter than $B_T = 13.7$. Using the morphological classifications from Binggeli, Sandage & Tammann (1985), this sample is sub-divided into 23 nucleated and 27 non-nucleated galaxies. The dotted and dashed curves show the cumulative distributions for these two samples. *(Right Panel)* Cumulative distribution of Virgocentric radii for the 49 galaxies from the ACS Virgo Cluster Survey fainter than $B_T = 13.7$ for which a classification as nucleated or non-nucleated is possible from our ACS images. (One galaxy in this magnitude range, VCC571, cannot be classified due to the presence of dust.) This sample is shown sub-divided into 40 nucleated (Type Ia and Ib) and 4 non-nucleated (Type II) galaxies (dotted and dashed curves, respectively). The five galaxies with possible offset nuclei have been excluded from the analysis.

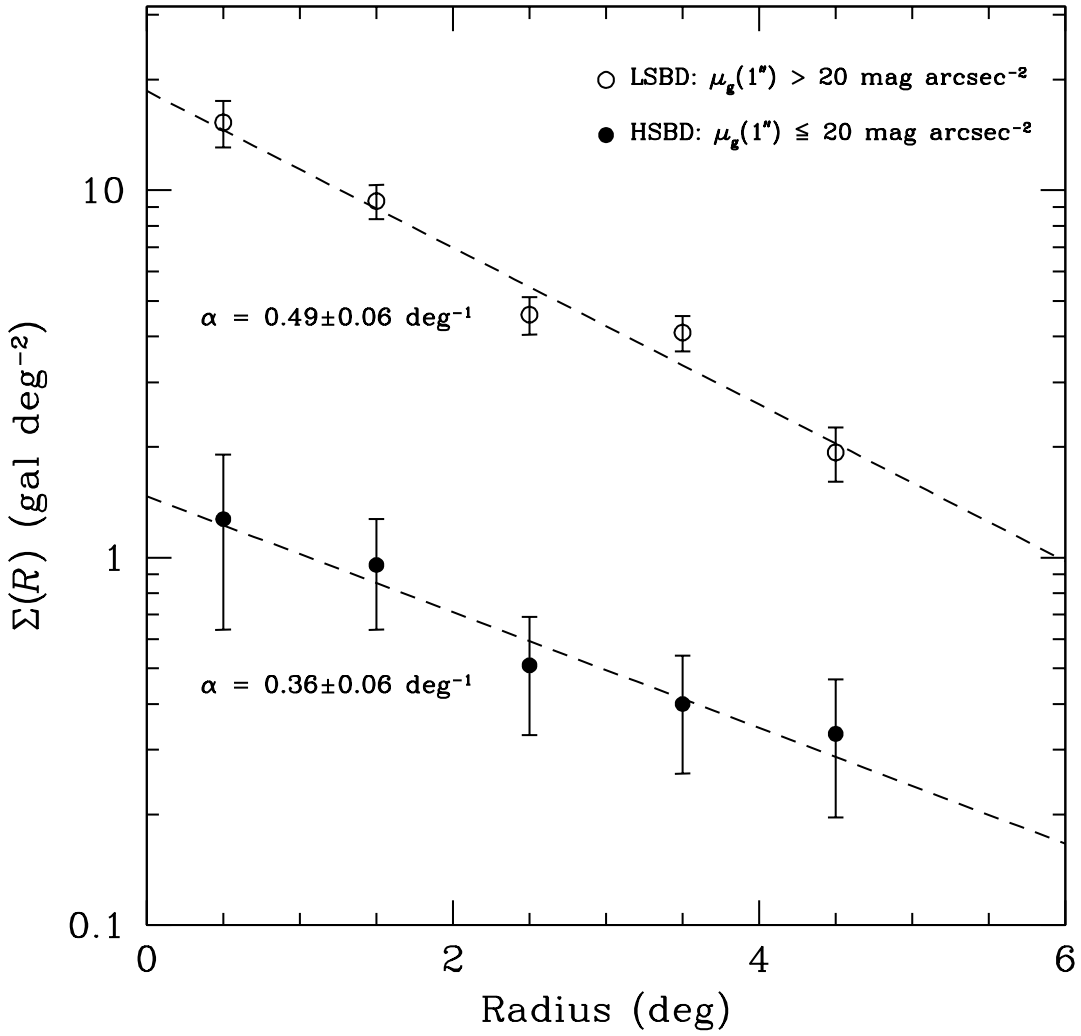

FIG. 13.— Surface density profile for early-type, low-surface-brightness dwarf (LSBD) galaxies in the Virgo Cluster (open circles). These galaxies have blue magnitudes in the range $14.55 < B_T \leq 18.0$, which correspond to central g-band surface brightnesses of $\mu_g(1'') \gtrsim 20$ mag arcsec^{-2}. High-surface-brightness dwarfs (HSBDs) are defined as early-type galaxies with $13.7 \leq B_T \leq 14.55$ and $\mu_g(1'') \lesssim 20$ mag arcsec^{-2} (filled circles). Nuclei in the HSBDs were preferentially missed in the survey of Binggeli, Tamman & Sandage (1987), which may explain their observation that the non-nucleated dwarfs in Virgo have a more extended distribution within the cluster than the nucleated dwarfs.

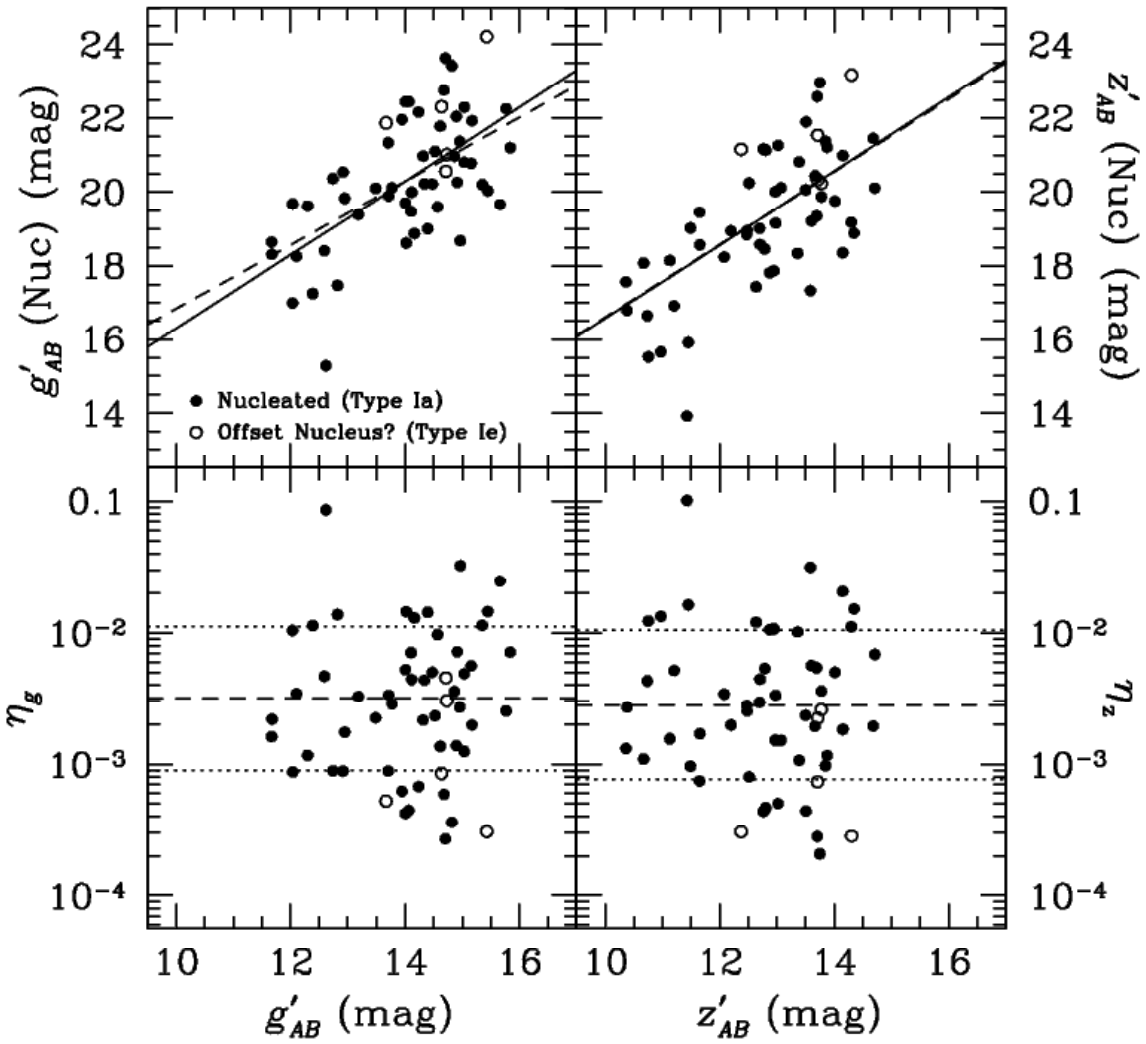

FIG. 14.— *(Upper Panels)*: Nucleus magnitude plotted against against that of the host galaxy. Results for the g and z bands are shown in the left and right panels, respectively. Filled circles show the 51 galaxies of Type Ia. Open circles indicate the five galaxies in our sample which may have offset nuclei (Type Ie). The dashed line shows the best-fit linear relation while the best-fit relation with unity slope is shown by the solid line. *(Lower Panels)*: Ratio of nucleus luminosity to that of the host galaxy, η, plotted against galaxy magnitude. Results for the g and z bands are shown in the left and right panels, respectively. Filled circles show the 51 galaxies of Types Ia. Open circles indicate the five galaxies in our sample which may have offset nuclei (Type Ie). The dashed and dotted lines show the mean and $\pm 1\sigma$ limits for the sample of Type Ia galaxies.

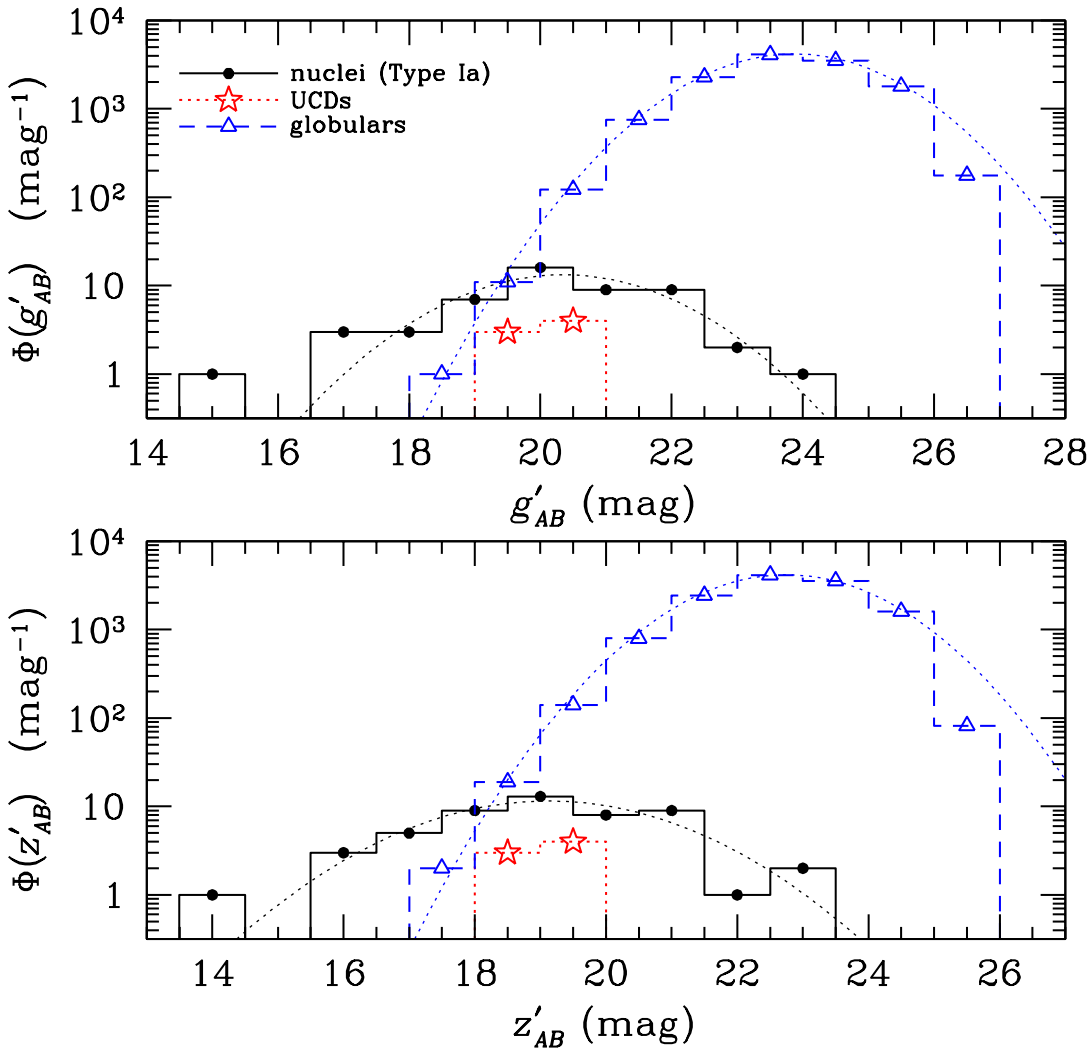

FIG. 15.— *(Upper Panel)*: Luminosity function, measured in the g band, for the nuclei of the 51 galaxies classified as Type Ia. For comparison, we also show Virgo globular cluster candidates from Jordán et al. (2006) and seven probable ultra-compact dwarf galaxies (UCDs) from Haşegan et al. (2005; 2006). *(Lower Panel)*: Same as above, except for the z band.

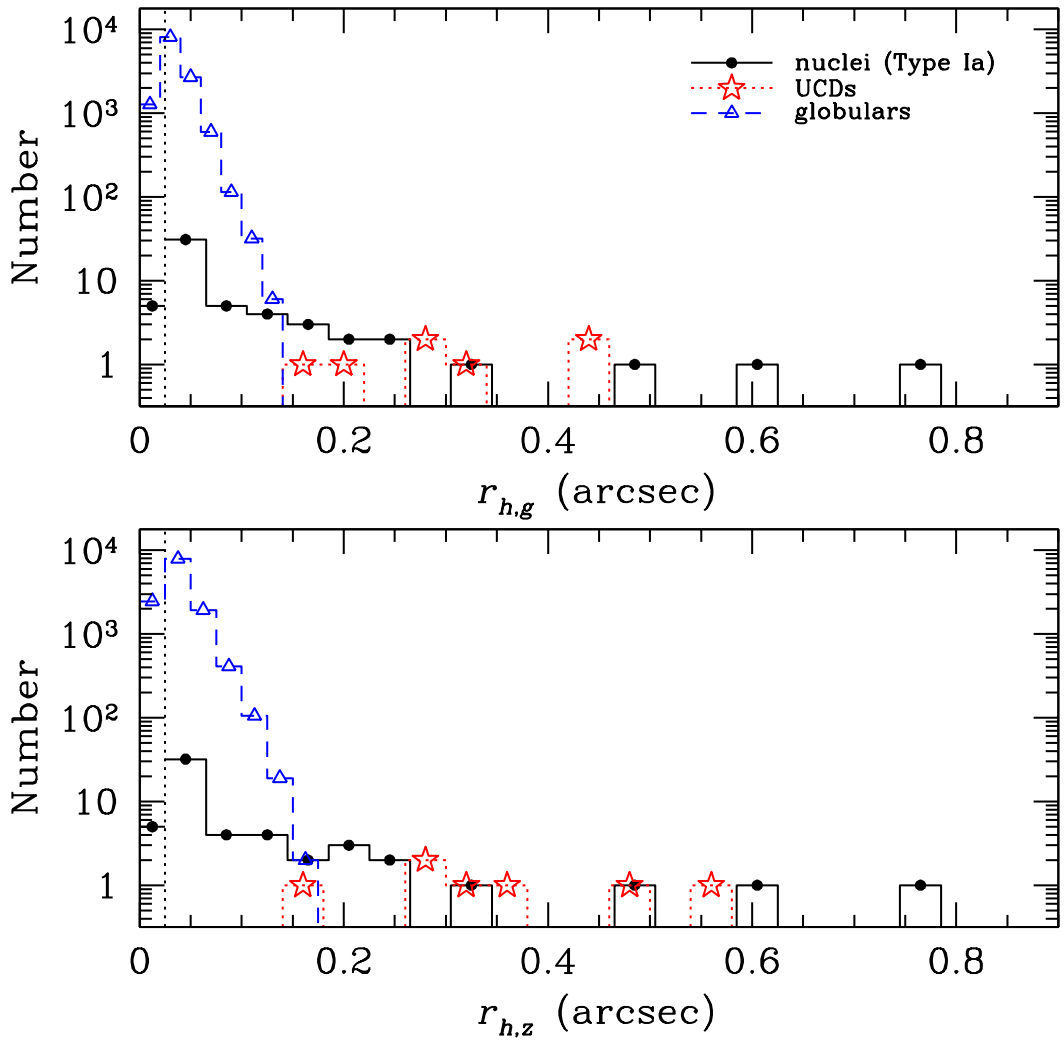

FIG. 16.— *(Upper Panel)*: Distribution of half-light radii, measured in the g-band, for the nuclei of the 51 galaxies classified as Type Ia. Also shown are seven probable ultra-compact dwarf galaxies (UCDs) from Haşegan et al. (2005; 2006) and a sample of Virgo globular cluster candidates from Jordán et al. (2006). The vertical dotted line shows the approximate resolution limit for the ACS images drizzled using a *Gaussian* interpolation kernel. *(Lower Panel)*: Same as above, except for the z band.

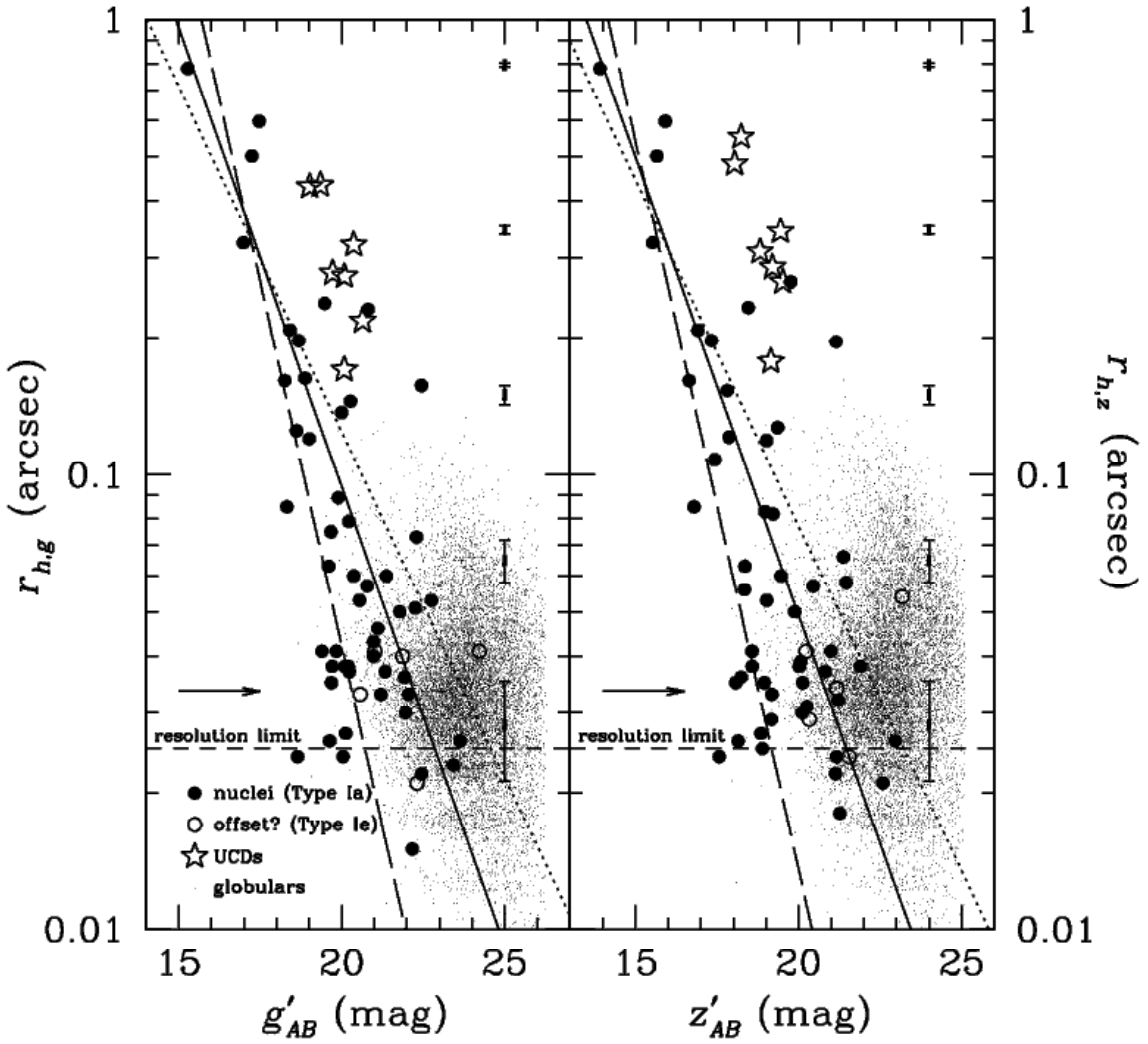

FIG. 17.— *(Left Panel)*: The size-magnitude relation, in the g band, for the nuclei of the 51 galaxies classified as Type Ia (filled circles). Open circles indicate the five galaxies which may have offset nuclei (Type Ie). Typical errorbars for the nuclei are shown in the right had side of the panel. Also shown are seven probable ultra-compact dwarf galaxies (UCDs) from Haşegan et al. (2005; 2006) and a sample of globular clusters from Jordán et al. (2006). The arrow shows the "universal" half-light radius of $\langle r_h \rangle = 0\farcs033 \approx 2.7$ pc for globular clusters in Virgo (Jordán et al. 2005), while the dashed line shows a conservative estimate for the resolution limit of those ACS images which were drizzled using a Gaussian interpolation kernel (rather than a Lanczos kernel). The diagonal lines shows relations of the form $r_h \propto \mathcal{L}^{\beta}$. The long-dashed line shows the extrapolation of the size-luminosity relation for giant galaxies, from Equation (11) of Haşegan et al. (2005). See text for details. *(Right Panel)*: Same as the left panel, except for the z band.

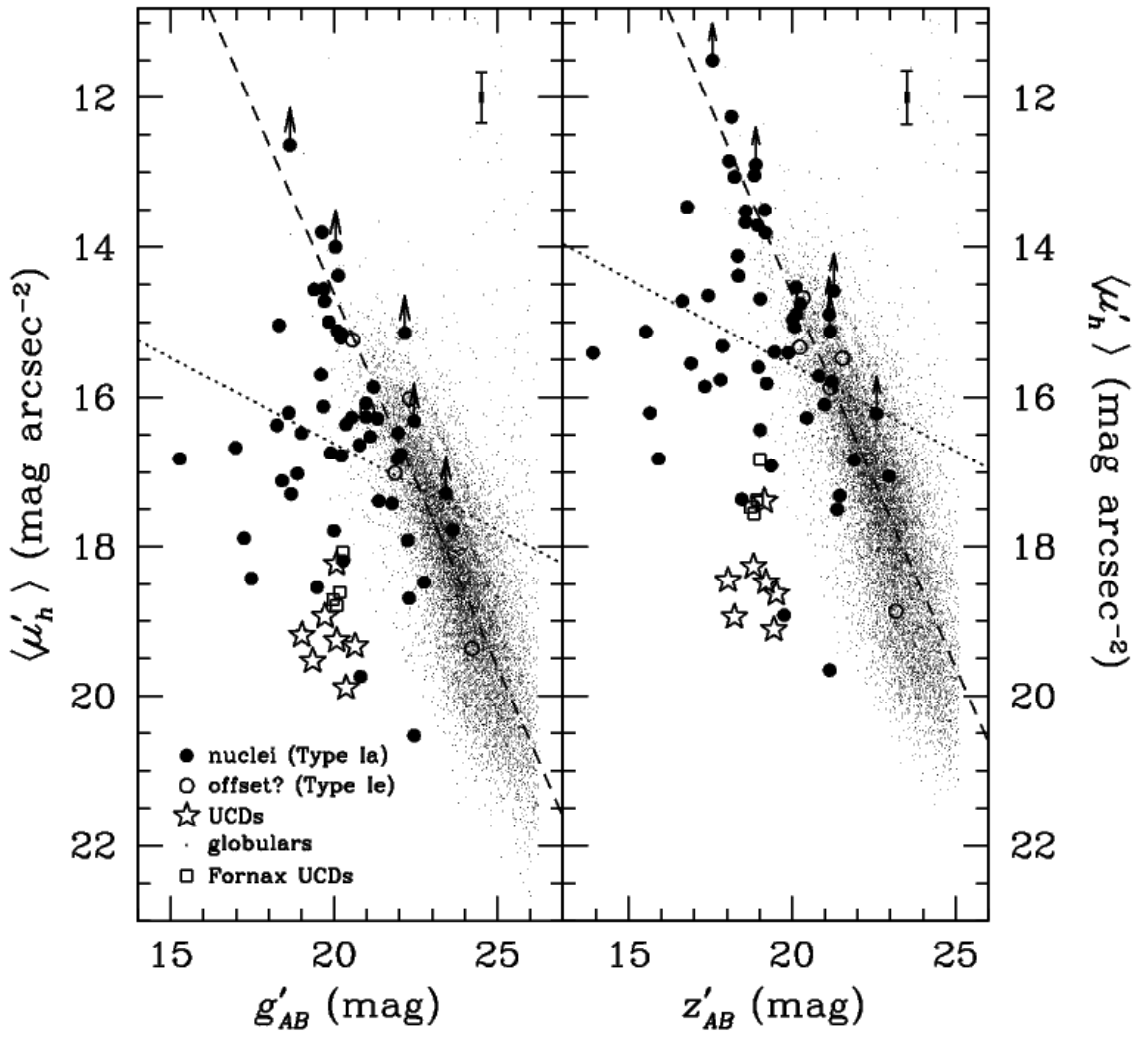

FIG. 18.— *(Left Panel)*: Average surface brightness within the half-light radius plotted against magnitude for the nuclei of the 51 galaxies classified as Type Ia (filled circles). Open circles indicate the five galaxies which may have offset nuclei (Type Ie). Both the magnitude and surface brightness measurements refer to the g band. Also shown are seven probable ultra-compact dwarf galaxies (UCDs) from Haşegan et al. (2005; 2006), a sample of Virgo globular clusters candidates from Jordán et al. (2006) and four UCDs in the Fornax Cluster studied by de Propris et al. (2005). The dashed line shows the relation expected for globular clusters if they have a "universal" half-light radius of $\langle r_h \rangle = 0\farcs033 \approx 2.7$ pc (Jordán et al. 2005). The dotted line shows the predicted scaling relation for nuclei formed by the mergers of globular clusters (Bekki et al. 2004). Arrows indicate lower limits on the surface brightness for unresolved nuclei. *(Right Panel)*: Same as the left panel, except for the z band.

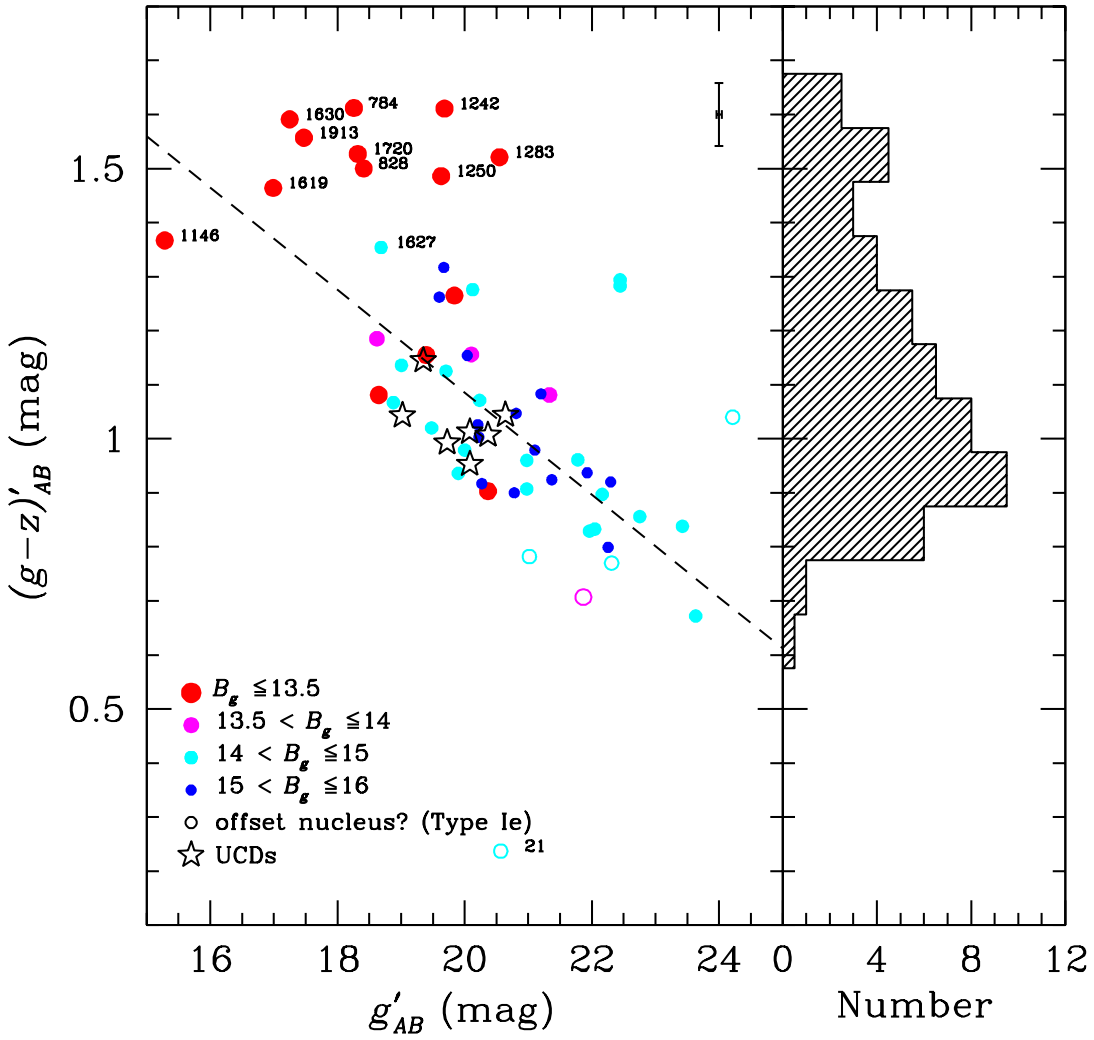

FIG. 19.— *(Left Panel)* Color-magnitude diagram for the nuclei of the 51 galaxies classified as Type Ia (filled circles). Open circles indicate the five galaxies which may have offset nuclei (Type Ie). Magnitudes and colors have been corrected for extinction and reddening. The size of the symbol for the nuclei is proportional to the magnitude of the host galaxy. Galaxies with unusually blue or red nuclei are labelled. For comparison, we show seven probable ultra-compact dwarf galaxies from Haşegan et al. (2005; 2006). The short-dashed line shows the best-fit relation for the nuclei of galaxies fainter than $B_T = 13.5$ (see §4.9). The dashed line shows the the best-fit relation for the nuclei of galaxies fainter than $B_T = 13.5$ (see §4.9). *(Right Panel)* Histogram of de-reddened nuclei colors.

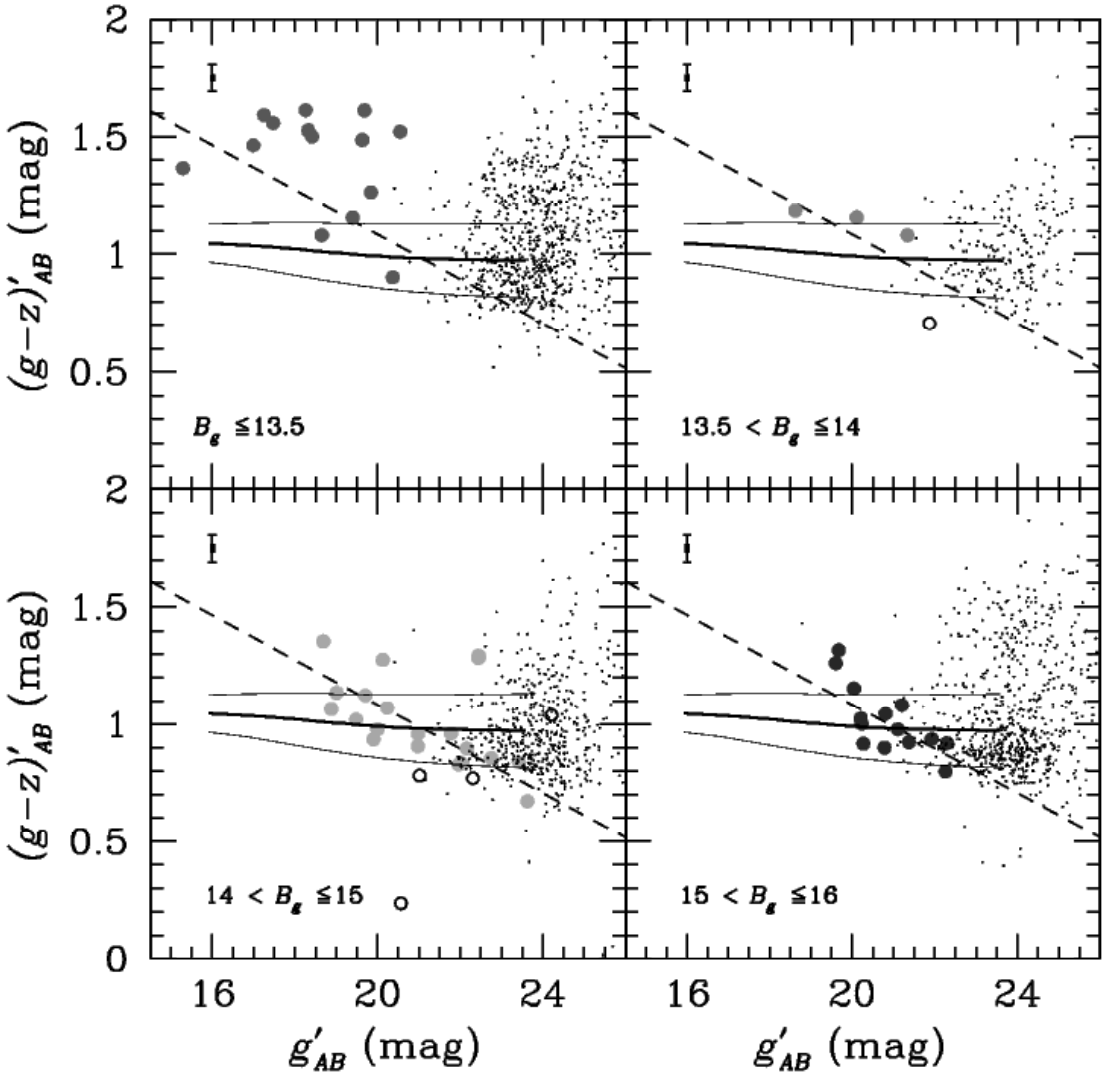

FIG. 20.— Comparison of the color magnitude diagrams for the nuclei of the 51 galaxies classified as Type Ia (filled circles) with those of the globular clusters belonging to our program galaxies (points). Possible offset nuclei are shown as open circles (i.e., Type Ie galaxies). The samples have been divided into four panels based on the blue luminosity of the host galaxy. The dashed line in each panel shows the best-fit relation for the nuclei of galaxies fainter than $B_T = 13.5$ (see §4.9). The heavy solid curve shows the color magnitude relation predicted by Monte-Carlo experiments in which the nuclei are assembled from globular cluster mergers; the thin solid curves show the 95% confidence limits (see §5.2 for details).

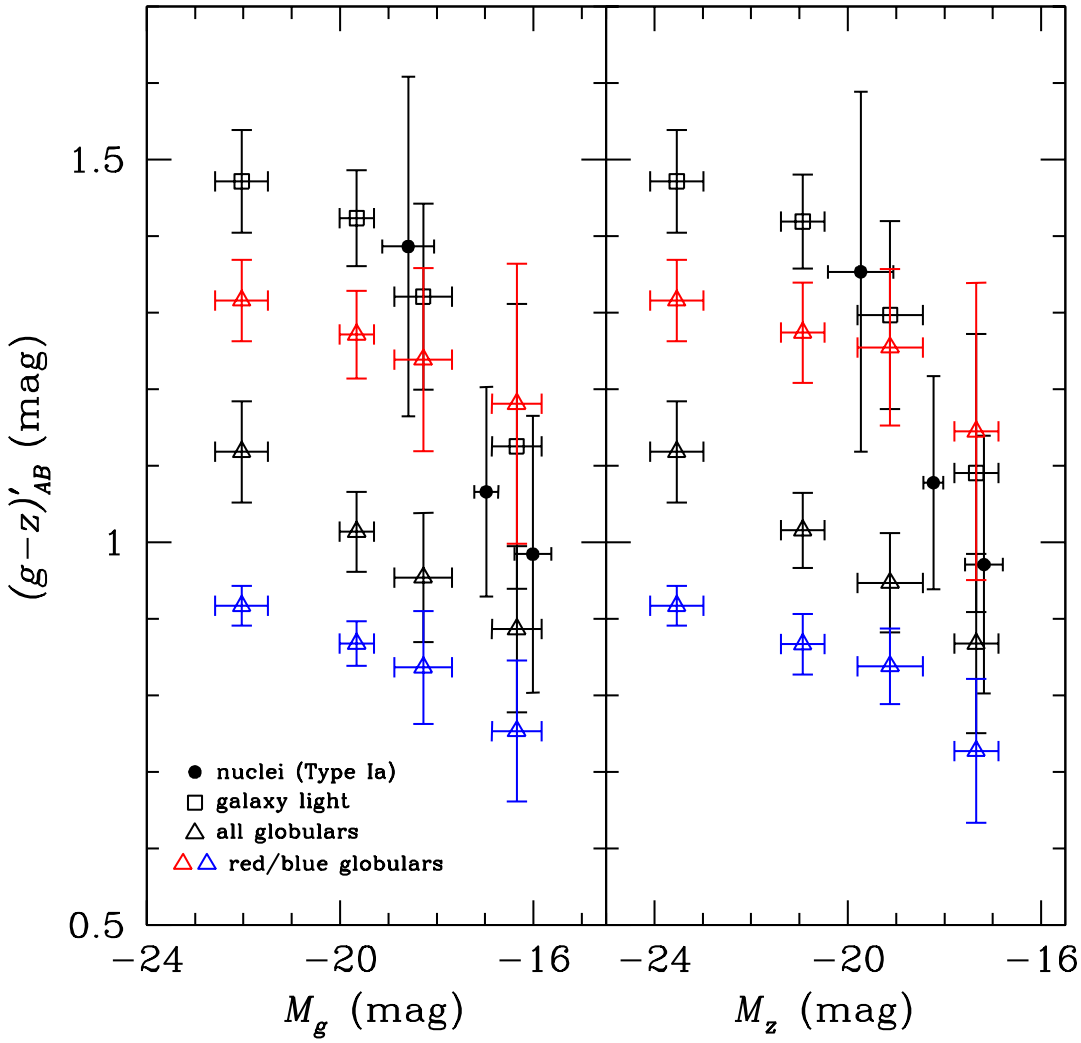

FIG. 21.— *(Left Panel)* Comparison of the M_g vs. $(g-z)'_{AB}$ color magnitude relation for nuclei (filled circles), globular clusters (open triangles) and galaxies (open squares) from the ACS Virgo Cluster Survey. The galaxies have been divided into four bins in absolute magnitude. The globular clusters have been further divided into red and blue subcomponents as described in Peng et al. (2006a). The nuclei of the 51 Type Ia galaxies have been divided into three magnitude bins containing roughly equal numbers of nuclei. *(Right Panel)* M_z vs. $(g-z)'_{AB}$ color magnitude relation for nuclei, globular clusters and galaxies.

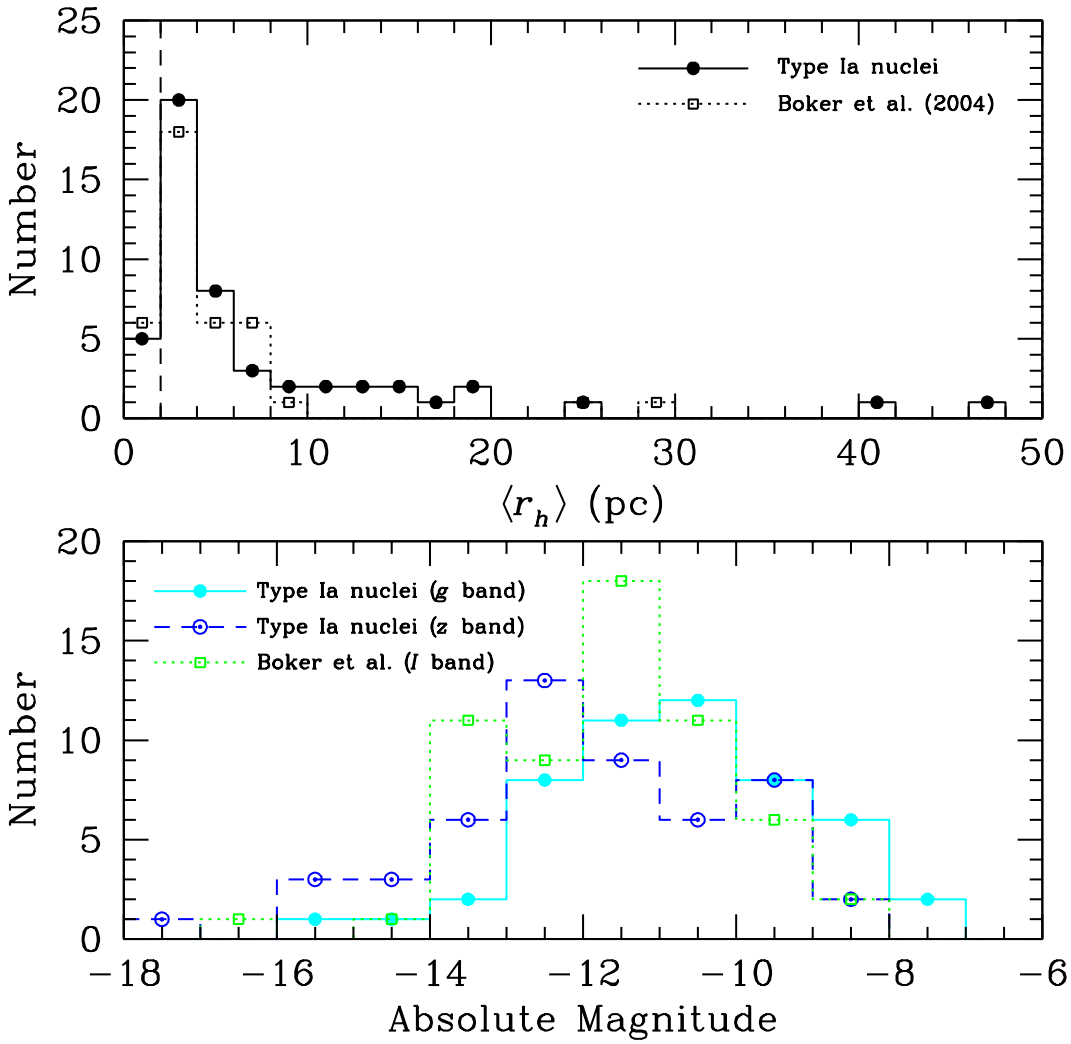

FIG. 22.— *(Upper Panel)* Distribution of half-light radii for the nuclei of early-type galaxies from the ACS Virgo Cluster Survey, compared to those of late-type galaxies from Böker et al. (2004). The plotted half-light radii for the early-type galaxies are averages of the measurements in the g and z bands. *(Lower Panel)* Distribution of absolute magnitudes for the nuclei of early-type galaxies from the ACS Virgo Cluster Survey, compared to those of late-type galaxies from Böker et al. (2004). Results in both the g and z bands are shown for the early-type galaxies, while those for the late-type galaxies refer to the I band.

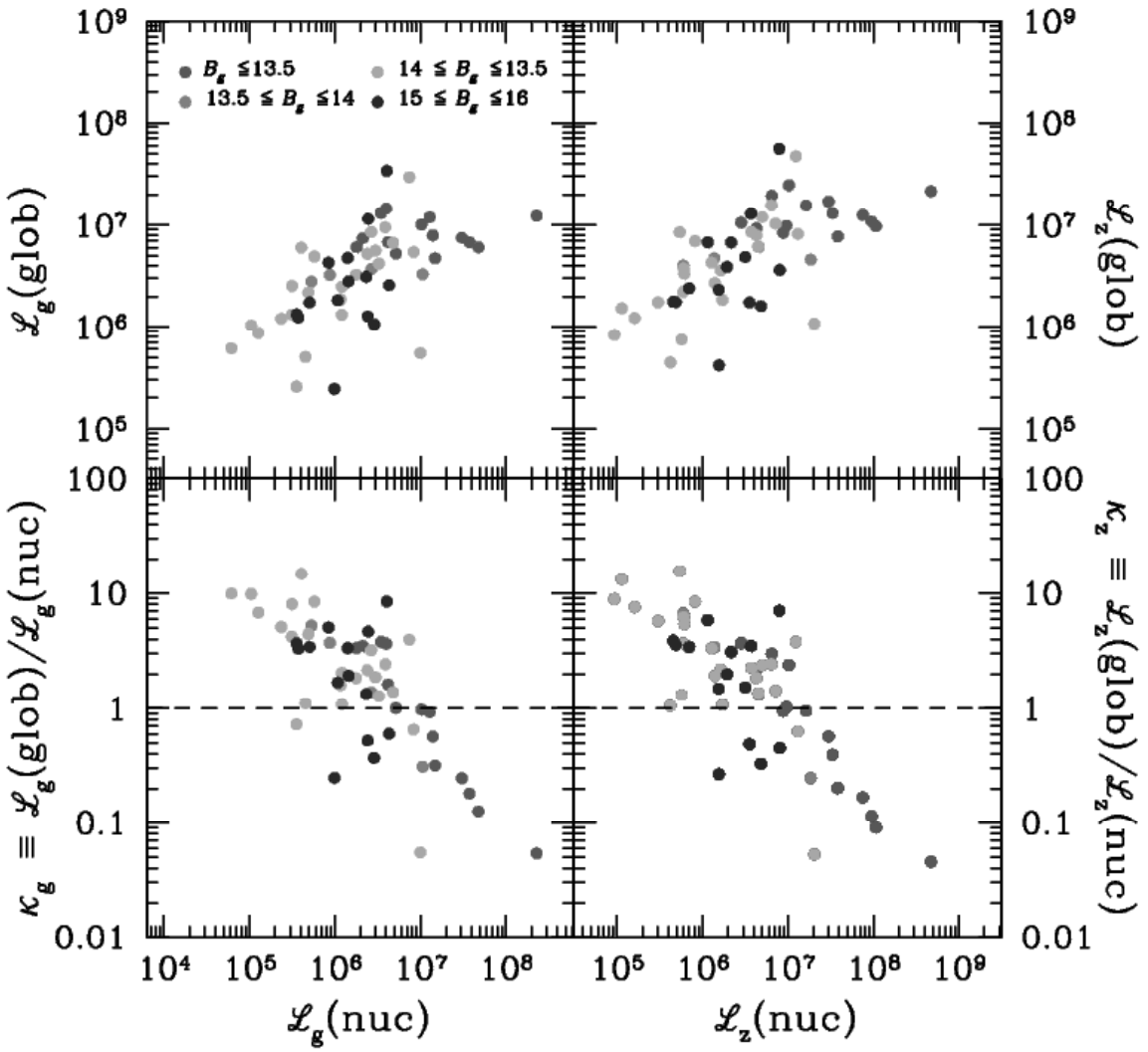

FIG. 23.— *(Upper Left Panel)* Total g-band luminosity of globular clusters belonging to 51 nucleated (Type Ia) galaxies, plotted against g-band nucleus luminosity. Symbols are color coded according to the blue magnitude of host galaxy. *(Lower Left Panel)* Ratio of total g-band luminosity in globular clusters to that contained in the nucleus. The dashed line corresponds to $\kappa_g = 1$. *(Right Panels)* As before, except for the z band.

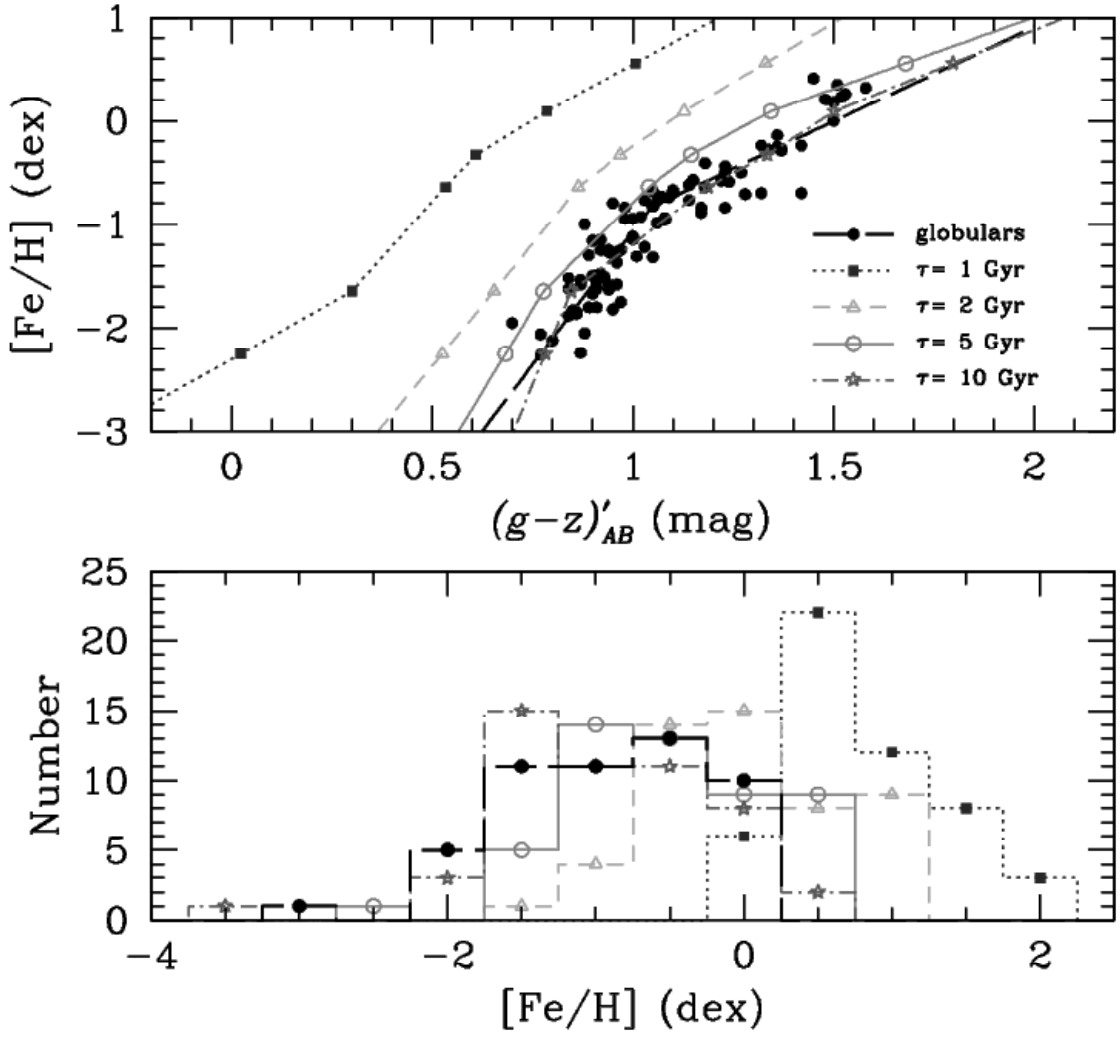

FIG. 24.— *(Upper Panel)* Color-metallicity relations for old stellar populations. The long-dashed (broken linear) relation shows the empirical metallicity relation of Peng et al. (2006 = Paper IX) which is based on 95 globular clusters (asterisks) in the Milky Way, M49 (NGC4472 = VCC1226) and M87 (NGC4486 = VCC1316). The remaining relations show theoretical predictions based on the models of Bruzual & Charlot (2003) which assume simple stellar populations with a Chabrier (2003) initial mass function and ages of $\tau = 1$, 2, 5 and 10 Gyr. The curves show linear interpolations of the models. *(Lower Panel)* Histograms of metallicities for the 51 Type Ia nuclei in our sample, based on the color metallicity relations shown in the upper panel. The symbols are the same as above.

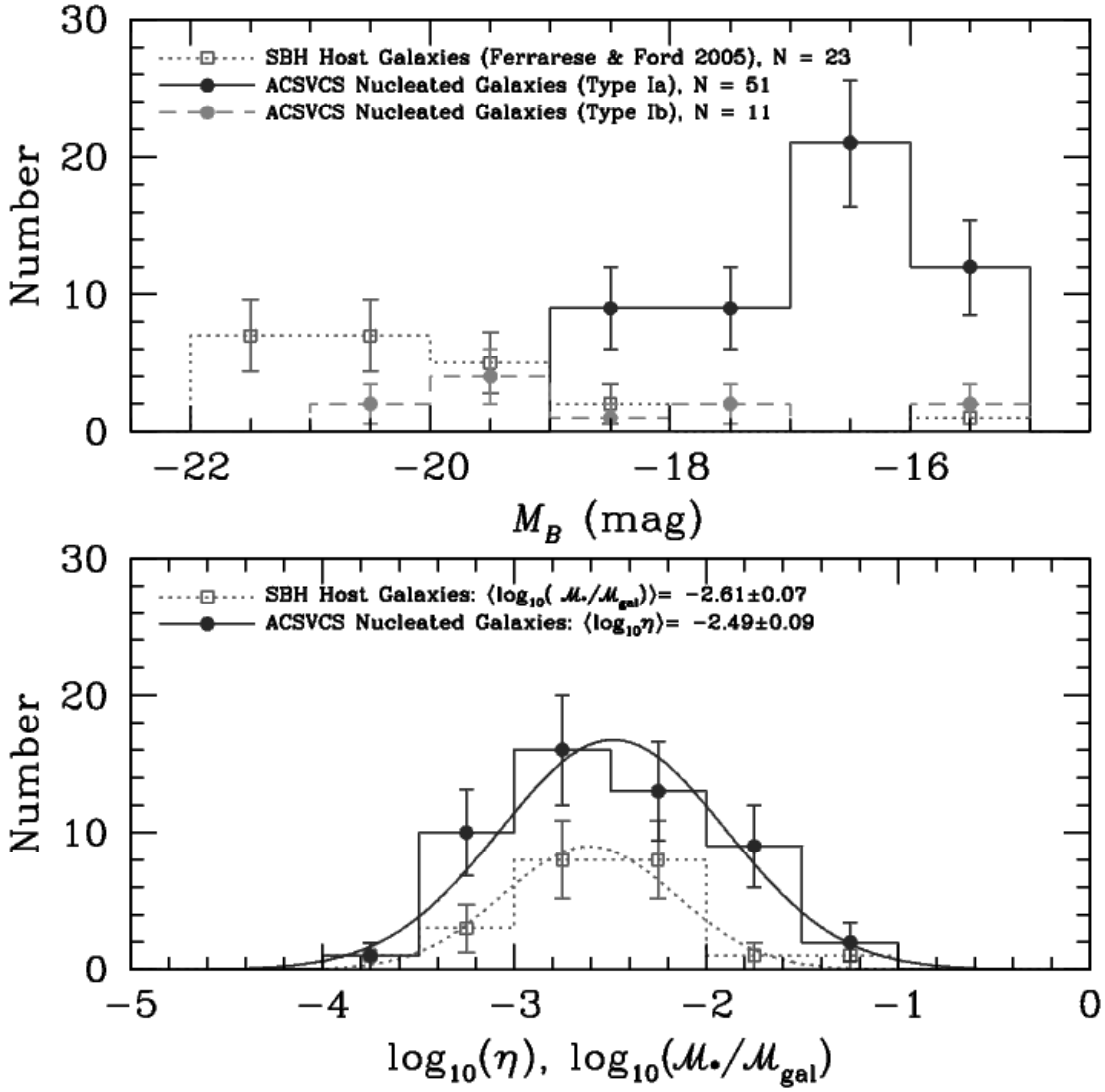

FIG. 25.— *(Upper Panel)* Distribution of absolute blue magnitudes for 23 early-type galaxies with supermassive black holes (SBHs) taken from the compilation of Ferrarese & Ford (2005) (open squares). The distribution of 51 nucleated (Type Ia) galaxies in the ACS Virgo Cluster Survey is shown by the solid histogram; 11 galaxies with Type Ib nuclei are shown by the dashed histogram. *(Lower Panel)* Distribution of the mass fraction, η, for early-type galaxies containing supermassive black holes (SBHs) with that for nucleated galaxies (Type Ia) in the ACS Virgo Cluster Survey. In the former case, $\mathcal{M}_\bullet/\mathcal{M}_{gal}$ measures the dynamical mass of the SBH relative to host galaxy's bulge mass. For the nucleated galaxies, η is the ratio of the nucleus and galaxy luminosities, averaged in the g and z bandpasses. The smooth curves show the best-fit Gaussians.

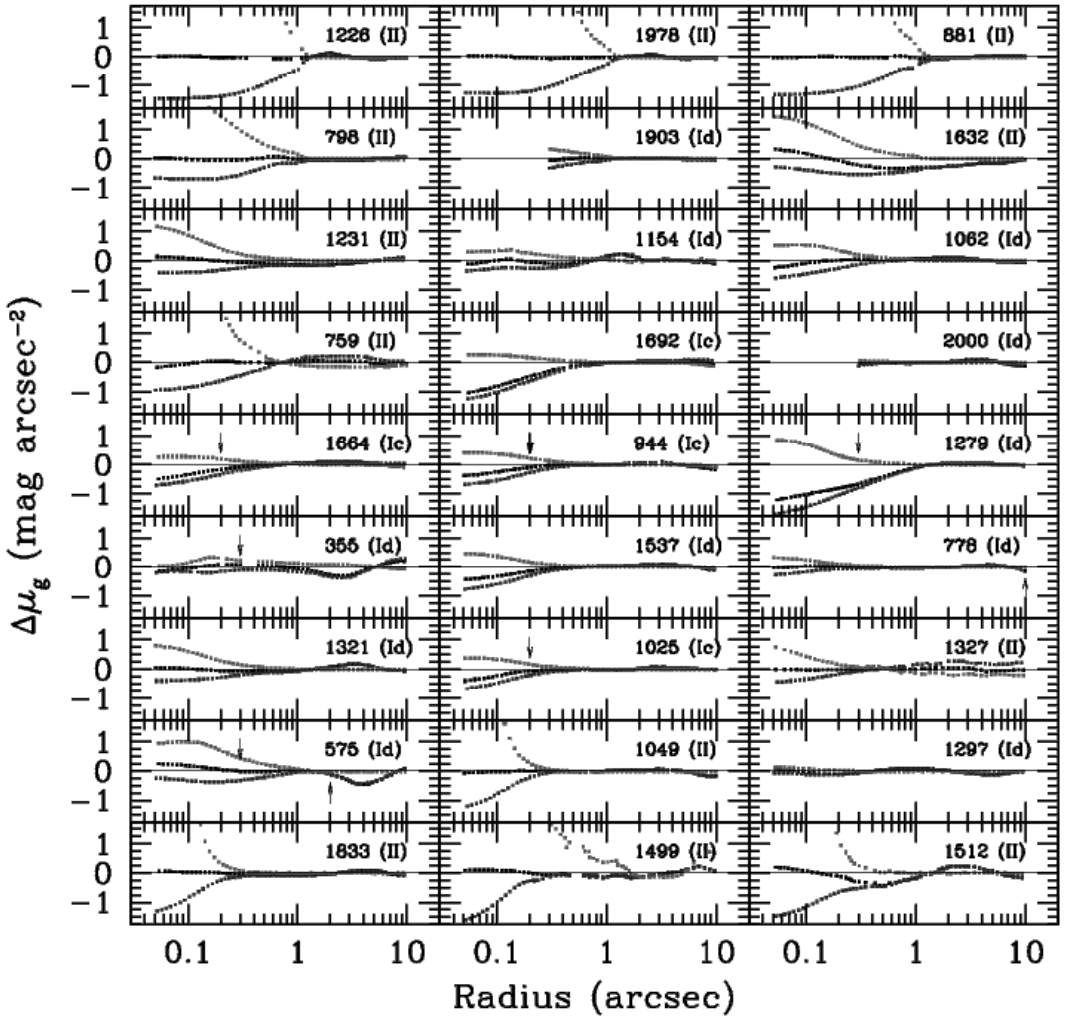

FIG. 26.— The 27 galaxies from the ACS Virgo Cluster Survey which are classified as non-nucleated, or having uncertain classifications, in Tables 1 and 2. Galaxies are ordered according to blue luminosity, which decreases left to right and top to bottom. Galaxy names and nuclear classifications from Table 2 are given in the upper right corner of each panel. In each panel, we plot the difference, $\Delta\mu_g$, between the fitted model surface brightness profile and: (1) the observed profile (black squares); (2) the profile obtained after *adding* a central nucleus to the observed profile (blue squares); and (3) the profile obtained after *subtracting* a central nucleus from the observed profile (red squares). In the interests of clarity, residuals are shown for the inner $10''$ only. For VCC1903 (M59 = NGC4621) and VCC2000 (NGC4660), no data are plotted with $\lesssim 0\farcs3$ since their g-band profiles are saturated inside this point.

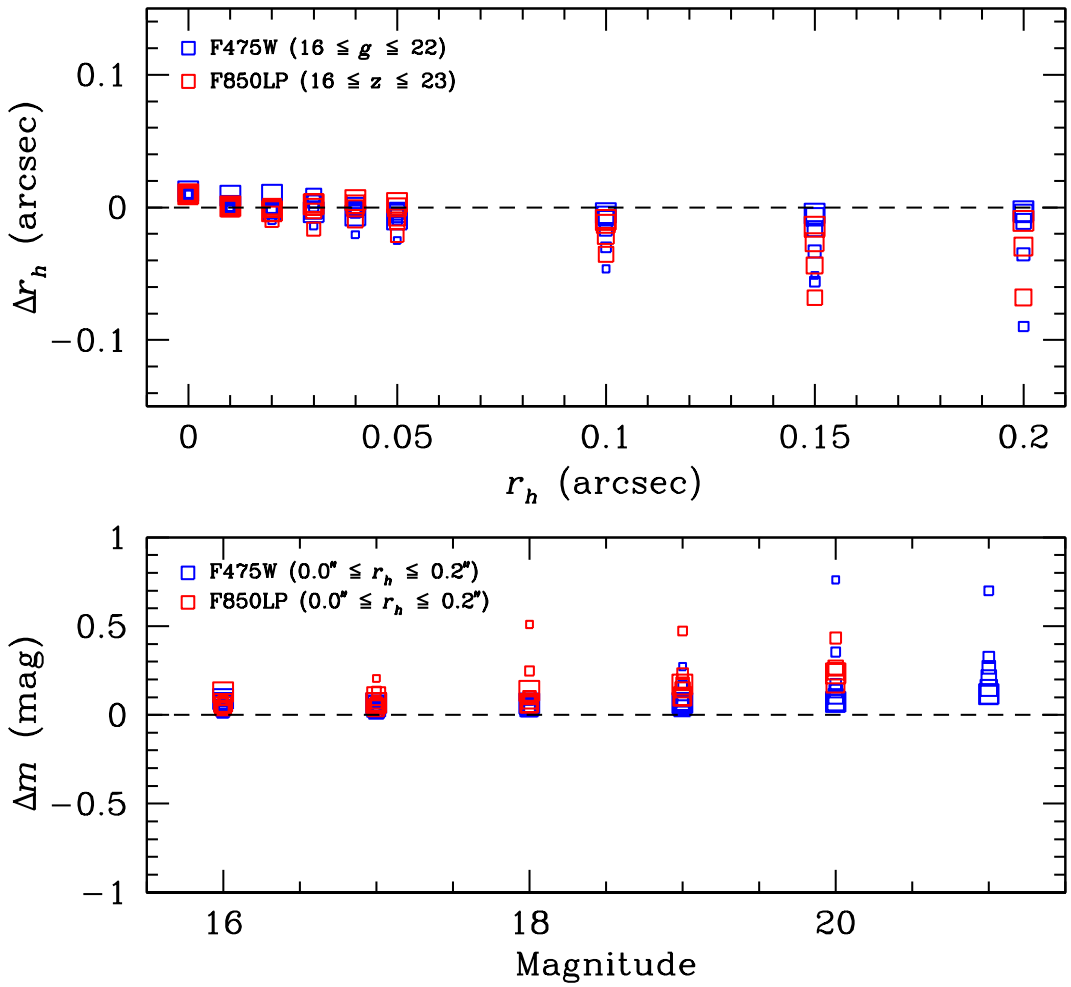

FIG. 27.— *(Upper Panel)* Difference between the recovered and input half-light radii, Δr_h, for simulated nuclei added to VCC1833, the faintest non-nucleated galaxy in our survey (excluding two dIrr/dE transition objects). The central surface brightness of this galaxy is $\mu_g(1'') \approx 19.3$ and $\mu_z(1'') \approx 18.1$ mag arcsec^{-2}, near the average for our sample galaxies. The blue and red squares show the respective results for the F475W and F850LP images, where the symbol size is proportional to the input magnitude (in the sense that brighter nuclei are plotted with larger symbols). *(Lower Panel)* Difference between the recovered and input magnitude Δm, for simulated nuclei added to VCC1833. In this case, the symbol size is proportional to input radius: i.e., the most compact nuclei are plotted with the largest symbols.

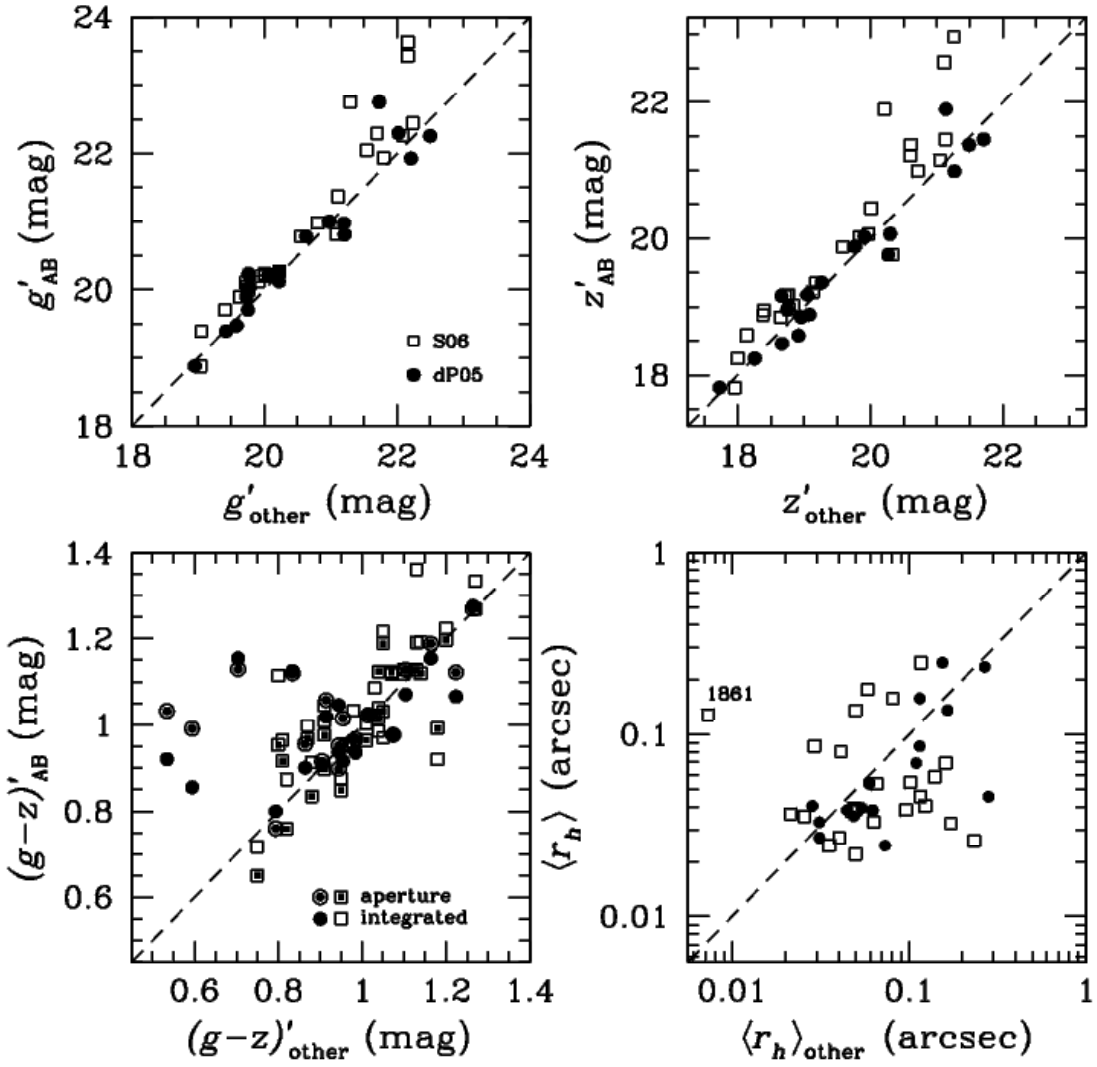

FIG. 28.— Comparison of photometric and structural parameters for nuclei in common with the studies of de Propris et al. (2005; dP06) and Strader et al. (2006; S06). *(Upper Left Panel)* Comparison of g-band magnitudes, on the AB system, for 18 and 25 nuclei from dP06 and S06 (open squares and filled circles, respectively). *(Upper Right Panel)* Comparison of z-band magnitudes, on the AB system. *(Lower Left Panel)* Integrated $(g-z)$ colors, on the AB system (filled circles and open squares). Circled symbols show our *aperture* measurements for the nuclei colors. *(Lower Right Panel)* Comparison of measured half-light radii in arcseconds. Our measurements refer to unweighted averages from the two bandpasses. VCC1861 (IC3652) has been labelled since the half-light radius reported by Strader et al. (2006), $r_h = 0\farcs007$, is $\sim 4\times$ below the ACS resolution limit.